

Development and Evaluation of Testing Protocols for Fatigue Damage and Crack-Healing of Bituminous Mixtures

by

Dandi Zhao

A thesis

presented to the University of Waterloo

in fulfillment of the

thesis requirement for the degree of

Doctor of Philosophy

in

Civil Engineering

Waterloo, Ontario, Canada, 2023

© Dandi Zhao 2023

Examining Committee Membership

The following served on the Examining Committee for this thesis. The decision of the Examining Committee is by majority vote.

External Examiner	Dr. Bernhard Hofko Institute of Transportation, Vienna University of Technology (TU Wien)
Supervisor	Dr. Hassan Baaj Civil and Environmental Engineering, University of Waterloo
Supervisor	Dr. Pejoohan Tavassoti Civil and Environmental Engineering, University of Waterloo
Internal Member	Dr. Giovanni Cascante Civil and Environmental Engineering, University of Waterloo
Internal Member	Dr. Shunde Yin Civil and Environmental Engineering, University of Waterloo
Internal-external Member	Dr. Kaan Inal Mechanical and Mechatronics Engineering, University of Waterloo

Author's Declaration

This thesis consists of material all of which I authored or co-authored: see Statement of Contributions included in the thesis. This is a true copy of the thesis, including any required final revisions, as accepted by my examiners.

I understand that my thesis may be made electronically available to the public.

Statement of Contributions

This thesis is partially the product of co-authored publications as follows:

Chapter 3

- Dandi Zhao, Hassan Baaj, and Pejoochan Tavassoti. Validation of Polymer Modified Binder Characterization through Ultrasonic Pulse Propagation and Indirect Tensile Testing of Asphalt Concrete Specimens (under revision)

Chapter 4

- Dandi Zhao, Hassan Baaj, Pejoochan Tavassoti, and Giovanni Cascante. Dynamic High-Frequency Healing with Rest Period (D2HRP) as a New Test Protocol for Determination of Intrinsic Healing Rates of Bituminous Mixtures (under revision)

Chapter 5

- Dandi Zhao, Hassan Baaj, and Pejoochan Tavassoti. Indirect Measurement of Fatigue and Healing of Asphalt Mixtures Using Ultrasonic Wave Propagation Approach (under revision)

Abstract

Fatigue testing is a very important performance test for asphalt concrete mixtures and has been studied for many years with varying levels of success. However, there are several imperfections in the commonly used fatigue tests. Furthermore, there is currently no universal standard to define fatigue failure in these tests, as fatigue damage cannot be effectively quantified due to the presence of bias effects. Researchers have used modified fatigue tests to study the self-healing capability of bituminous material. The healing capability of the material is typically quantified by comparing the modulus change with and without rest periods. However, the presence of reversible phenomena makes it even harder to quantify the healing effects. This research aims to improve the laboratory asphalt concrete fatigue damage and crack-healing tests by combining Non-destructive testing (NDT) methods.

This study was conducted on polymer-modified asphalt concretes. The properties of the material used has been well studied in previous research and were used to compare with the results from this research. An ultrasonic pulse propagation test (UPPT) was conducted on undamaged specimens, specimens under monotonic loading and cyclic loading conditions, and during the healing processes. Two experimental protocols that combine traditional asphalt fatigue or cracking tests with UPPT to quantify and evaluate the damage and self-healing property of asphalt concrete were proposed. Several signal processing techniques were applied to study the performance of the test material.

The results indicate that the UPPT method is sensitive to the microstructure, viscosity, elasticity, damage level and healing properties of asphalt concrete. The proposed Dynamic High-frequency Healing with Rest Period (D2HRP) test protocol successfully distinguishes changes in healing between stiffer and more aged binders. The combination of ultrasonic pulse propagation tests and tension-compression tests provides an indirect observation of changes of material property during the test, and the proportion of the bias effects were successfully quantified. The improved laboratory cracking and fatigue tests can promote sustainability in pavement materials and designs. Furthermore, this project will also contribute to a better understanding of crack initiation and propagation processes in pavement materials, which can improve the existing state of pavement rehabilitation and maintenance techniques as well as pavement condition prediction models.

Acknowledgements

I would like to express my deepest appreciation to my supervisors, Dr. Hassan Baaj and Dr. Pejooan Tavassoti for their unwavering support, guidance, encouragement, and mentoring during my study at the University of Waterloo. Prof. Baaj gave me many opportunities to work in the lab starting from my undergrad study. Both of my supervisors have inspired me a lot during this journey. I would also like to thank Dr. Giovanni Cascante for his assistance in the nondestructive testing and signal processing part of the study. He is like a third supervisor to me, and I enjoyed very much being his teaching assistant during my grad study. I would like to extend my sincere thanks to my thesis committee members, Dr. Bernhard Hofko, Dr. Giovanni Cascante, Dr. Shunde Yin, and Dr. Kaan A. Inal.

This study was funded by the Natural Science and Engineering Research Council of Canada (NSERC) and Yellowline Asphalt Products Ltd. I would like to thank Mike Aurilio for his useful feedback and support.

My gratitude also goes to the Civil and Environmental Engineering Department's technical staff: Peter Volcic, Robert Kaptein, Richard Morrison, and Victor Lewis for their outstanding support in the laboratory.

I am particularly thankful for my colleagues, and co-op students from the CPATT and iNDT groups, Rob Aurilio, Dr. Haya Almutairi, Ali Qabur, Aditi Sharma, Cristobal Lara, Aiman Khan, Camden Naylor, Zahra Miri, Dr. Ju Huyan, Dr. Tamanna Kabir, Tianshu Zhang, Peggie Wang, Luis Diego Zumbado, Dr. Eskedil Melese, Dr. Abimbola Grace Oyeyi, Mahshad Omidi, Yifei Yang, Dr. Frank Mi-Way Ni, Dr. Shenglin Wang, Dr. Luke Zhao, Dr. Daniel Liao, Jonathan Zingaro, Adam Schneider, Dr. Peter Mikhailenko, Dr. Jessica Achebe, Dr. Yahsar Azimi Alamdary, Dr. Seyedata Nahidi, Dr. Hawraa Kadhim, Dr. Taher Baghaee Maghaddam, Dr. Saeid Salehiashani, Dr. Abdulrhman Hamid, and Dr. Taha Younes for their help and support.

I am very grateful to my friends and family: Zi Yang, Marilyn Wang, Yiran Liu, Dr. G. Wayne Brodland and his wife Heather, Olivia Xu, my brother Jason Zhao, my mom Yu Li, and my church family for their encouragement and emotional support in this journey.

Financial support from the Ontario Graduate Scholarship (OGS) program and the Irene Marguerite McLeod Postgraduate Scholarship, is greatly appreciated as well.

Last but not least, I would like to thank my LORD Jesus Christ for enabling me to carry out this study and have this life experience to work with the people in my research group. I have learned more than just the research itself. I think I've become a better person.

Table of Contents

Examining Committee Membership.....	ii
Author’s Declaration	iii
Abstract.....	v
Acknowledgements.....	vi
List of Figures.....	xi
List of Tables	xiii
List of Abbreviation.....	xiv
Chapter 1 Introduction.....	1
1.1 Problem Statement.....	1
1.2 Research Hypothesis.....	2
1.3 Research Objective	3
1.4 Research Methodology	3
1.5 Thesis Organization.....	4
Chapter 2 Literature Review.....	6
2.1 Asphalt Mixture Fundamental	6
2.1.1 Asphalt Concrete Composites.....	6
2.1.2 Asphalt Mixture Behavior	6
2.1.3 Flexible Pavement Structure.....	8
2.2 Asphalt Fatigue.....	9
2.2.1 Fatigue Fundamental	9
2.2.2 Fatigue Tests.....	9
2.2.3 Bias Effects.....	11

2.2.4 Asphalt Fatigue Models and Failure Criteria.....	12
2.3 Self-healing of Asphalt.....	16
2.3.1 Self-healing Mechanisms.....	16
2.3.2 Common Healing Tests	18
2.4 Non-destructive Testing for Asphalt Mixtures	19
2.4.1 Current NDT Methods on Bituminous Material.....	19
2.4.2 Device Setting in This Research.....	21
Chapter 3 Validation of Polymer Modified Binder Characterization through Ultrasonic Pulse Propagation and Indirect Tensile Testing of Asphalt Concrete Specimens	23
3.1 Introduction.....	24
3.1.1 Theoretical Background of Cracking Test Indices	26
3.2 Thoracal Background of Signal Processing.....	28
3.2.1 Wave Velocity Equations	28
3.2.2 Fourier Transformation.....	28
3.2.3 Wave Attenuation	29
3.3 Materials and Methods	29
3.3.1 Materials Selection and Volumetric Design	29
3.3.2 Methodology	30
3.3.3 Indirect Tensile Asphalt Cracking Test (IDEAL-CT) Procedure.....	31
3.3.4 Ultrasonic Pulse Propagation Test (UPPT) Procedure	32
3.4 Results and Discussion	35
3.4.1 IDEAL-CT Verification.....	35
3.4.2 Wave Attenuation Analysis	40
3.4.3 IDEAL-CT and LAS Test Results.....	45

3.4.4 Mix UPPT and Binder MSCR Test Results	46
3.5 Conclusions and Recommendations	48
Chapter 4 Dynamic High-Frequency Healing with Rest Period (D2HRP) as a New Test Protocol for Determination of Intrinsic Healing Rates of Bituminous Mixtures.....	50
4.1 Introduction.....	50
4.2 Theoretical Background.....	53
4.2.1 Indirect Tensile Test	53
4.2.2 Fast Fourier Transformation (FFT)	53
4.2.3 Continuous Wavelet Transform (CWT)	54
4.2.4 Wavelet Synchro Squeezed Transform (WSST)	54
4.3 Experimental Program	55
4.3.1 Materials Used.....	55
4.3.2 Proposed Hybrid Test Setup	57
4.4 Analysis	60
4.4.1 Mechanical Test Data Analysis	60
4.4.2 NDT Data Analysis.....	62
4.4.3 D2HRP Data Analysis	67
4.5 Results and Discussion	69
4.6 Conclusions and Future Work	70
Chapter 5 Indirect Measurement of Fatigue and Healing of Asphalt Mixtures Using Ultrasonic Wave Propagation Approach	72
5.1 Introduction.....	72
5.2 Theoretical Background.....	78
5.2.1 Signal Energy Comparison	78

5.2.2 Time Cross-Correlation	78
5.2.3 Dynamic Time Warping	79
5.3 Materials and Methods	80
5.3.1 Materials and Sample Preparation	80
5.3.2 Test Equipment Setup.....	81
5.4 Proposed Test Protocol.....	82
5.4.1 Bias Effects, Fatigue Damage, and Healing Estimation.....	86
5.5 Results and Discussion	87
5.5.1 Signal Energy Evolution.....	90
5.5.2 Time Signals Comparison.....	91
5.5.3 Using Signal Similarity to Evaluate Fatigue Damage of Asphalt Mixture	92
5.6 Summary and Conclusions	94
Chapter 6 Conclusions, Contributions, Recommendations and Future Work.....	96
6.1 General Summary	96
6.2 Significant Contributions.....	97
6.3 Recommendations and Future Works.....	98
References.....	99

List of Figures

Figure 2-1. Typical behaviors for asphalt cement [16]	7
Figure 2-2. Typical behaviors for asphalt concrete [17]	7
Figure 2-3. (a) Master curve construction [18] and (b) Analogy of “2S2P1D” model [19]	8
Figure 2-4. Sketch of fatigue cracking in asphalt concrete [21]	9
Figure 2-5. Stiffness evolution curve during a fatigue test [20].....	11
Figure 2-6. Wöhler curve determination of ϵ_6 [26]	12
Figure 2-7. RDEC plot [31]	14
Figure 2-8. Interval in "DGCB" model (a) stiffness evolution, (b) dissipated energy evolution [33] ..	14
Figure 2-9. VECD explanation	15
Figure 2-10. Scheme of capillary healing model [40].....	17
Figure 2-11. FM images of the crack healing process of SBS modified asphalt [42]	18
Figure 2-12. Schematic test setup for UPV test (ASTM C597).....	20
Figure 2-13. Schematic of Impact Resonant Test [50].....	21
Figure 2-14. Schematic of Input Signal	22
Figure 3-1. Flow chat of the methodology	31
Figure 3-2. Photo of UPPT setup	33
Figure 3-3. Schematic UPPT test setup.....	33
Figure 3-4. Example of (a)input and output signals (b) travel time	33
Figure 3-5. Schematic of wave propagation and windowed signal.....	34
Figure 3-6. (a) CT_{index} , (b)FI, (c)CRI, and (d) FST comparison plots.....	38
Figure 3-7. (a) Peak Load, (b) Displacement at Peak Load, and (c) Fracture Energy till Fracture Point comparison plots	39
Figure 3-8. FFT Area for full output signals.....	41
Figure 3-9. Frequency spectra of the windowed waveforms (a) first arrivals, (b) the tail parts.....	44
Figure 3-10. Amplitude ratio of windowed and unwindowed dominant frequency	45
Figure 3-11. Fracture Energy values.....	45
Figure 3-12. Comparison between Indirect Tensile Test and the Linear Amplitude Sweep (LAS) test results	46
Figure 3-13. J_{nr} vs. Percent polymer [66].....	47

Figure 3-14. Wave attenuation vs. J_{nr}	47
Figure 4-1. Comparison of FFT, CWT, WSST.....	55
Figure 4-2. Photograph and schematic of test setup.....	58
Figure 4-3. D2HRP Test Protocol.....	58
Figure 4-4. Extensometer Readings for M2 PG 58-28 Control Specimen	62
Figure 4-5. Time Signal for M2 PG 58-28 Control Specimen.....	63
Figure 4-6. (a) FFT and (b) CWT for signals collected from M2 PG58-28 Control specimen	64
Figure 4-7. WSST for M2 PG58-28 Control specimen	64
Figure 4-8. Time signal plot of original signal and (a)windowed time signal, (b) convolution of filter and original signal, and (c) reconstructed signal from filtered WSST.....	65
Figure 4-9. Frequency Spectra of original signal and (a)windowed time signal, (b) convolution signal, and (c) reconstructed signal.....	66
Figure 4-10. Filtered Fourier Transformation for M2 PG 58-28 Control Specimen	67
Figure 4-11. D2HRP Data Analysis for M2 PG 58-28 Control Specimen	68
Figure 4-12. Healing Rate Calculation for M2 PG 58-28 Control Specimen.....	69
Figure 5-1. Stiffness evolution curve during a fatigue test [89].....	73
Figure 5-2. Soltani and Anderson’s research [49].....	75
Figure 5-3. Schematic representation of different effects during cyclic loading [4].	76
Figure 5-4. Schematic of asphalt mixture self-healing process [83].....	76
Figure 5-5. (a) Euclidean Matching (b) Dynamic Time Warping Matching [97].....	79
Figure 5-6. Experimental Setup	82
Figure 5-7. Schematic representation of proposed test procedure	84
Figure 5-8. (a) Temperature, (b) Modulus, (c) Phase Angle, (d) Dissipated Energy, and (e) Signal Energy with respect to time during the entire test.....	89
Figure 5-9. Signal Energy Plot.....	90
Figure 5-10. Time signal comparison between (a) ‘a’& ‘c’, (b) ‘c’& ‘d’, and (c) ‘e’& ‘f’	92
Figure 5-11. Data comparison using (a) Dynamic Time Warping and (b) Time Cross-Correlation	93

List of Tables

Table 2-1. General categories of the test methodologies [1][2][22]	10
Table 2-2. Coefficient C_i in "DGCB" approach [22]	15
Table 3-1. Superpave 12.5 FC2 Asphalt Mix Design	30
Table 3-2. ANOVA Table for CT_{index} and CRI.....	37
Table 3-3. Summary of Specimen Properties.....	42
Table 4-1. Volumetric properties of tested asphalt mixtures	56
Table 4-2. Ending Point of First Loading Phase	59
Table 4-3. Work of Fracture Comparison	61
Table 4-4. Summary of D2HRP Analysis.....	70
Table 5-1. Superpave 12.5 FC2 Asphalt Mix Design used in this study	80
Table 5-2. Ending Point of Stage II Determination	85
Table 5-3. Reference Points	87
Table 5-4. Fatigue Damage Rate Comparison	94

List of Abbreviation

2S2P1D	Two Springs, Two Parabolic Elements, One Dashpot
AASHTO	American Association of State Highway and Transportation Officials
AFM	Atomic Force Microscope
ASTM	American Society for Testing and Material
COV	Coefficient of Variation
CPATT	Centre for Pavement and Transportation Technology
CRI	Cracking Resistance Index
CT	Computed Tomography
CT _{index}	Cracking Test Index
CWT	Continuous Wavelet Transformation
D2HRP	Dynamic High-frequency Healing with Rest Period
DCT	Disk-Shaped Compact Tension
DGCB	Département Génie Civil et Bâtiment
DTW	Dynamic Time Warping
FFT	Fast Fourier Transform
FI	Flexibility Index
FM	Fluorescence Microscopy
FST	Fracture Strain Tolerance
FTIR	Fourier Transform Infrared Spectroscopy
FWD	Falling Weight Deflectometer
GPR	Ground Penetrating Rader
HMA	Hot Mix Asphalt
IDEAL-CT	Indirect Tensile Asphalt Cracking Test
IDT	Indirect Tensile
IE	Impact Echo
IR	Impact Resonant
IRT	Infrared Thermography
L1	First Loading Phase

L2	Second Loading Phase
LAS	Linear Amplitude Sweep
LVE	Linear ViscoElastic
MMHC	Methylene-to-Methyl-Hydrocarbon
MSCR	Multiple Stress Creep Recovery
MTS	Material Testing Systems
NDT	Non-Destructive Testing
NCHRP	National Cooperative Highway Research Program
PMB	Polymer-Modified Binders
RDEC	Ratio of Dissipated Energy Change
ROC	Rate of Change
RP	Rest Period
SASW	Spectral Analysis of Surface Waves
SBR	Styrene-Butadiene Rubber
SBS	Styrene-Butadiene-Styrene
SCB	Semicircular Bending
SEM	Scanning Electron Microscopy
SPt	Softening Point
T/C	Tension-Compression
TOF	Time-of-Flight
UPPT	Ultrasonic Pulse Propagation Test
UPV	Ultrasonic Pulse Velocity
VECD	Viscoelastic Continuum Damage
VFA	Voids Filled with Asphalt
VMA	Voids in Mineral Aggregate
WSST	Wavelet Synchro Squeezed Transformation

Chapter 1

Introduction

1.1 Problem Statement

The study of asphalt fatigue has attracted the attention of civil engineers for many years. Different types of tests have been deployed to investigate this phenomenon [1][2]. In laboratory, accelerated fatigue damage can be induced in asphalt specimens, where various analysis methods and models have been developed in order to predict the fatigue life of the asphalt concrete. The conventional fatigue tests are conducted at intermediate temperatures to simulate real-life conditions. However, prediction of the fatigue life of bituminous mixes is challenging due to the presence of some bias effects, such as intrinsic healing, thixotropy, local heating and non-linearity[3]. These effects occur with fatigue simultaneously, and some of these effects make it quite difficult to characterize the true fatigue resistance of asphalt concrete [4]. Furthermore, the separation of these bias effects from the actual fatigue test is nearly impossible. Therefore, in order to characterize the healing behavior, it is important to improve our understanding of asphalt mixture fatigue behavior by adequately evaluating the bias effects.

Other challenges of conventional fatigue tests include, but not limited to: the high cost of the test equipment and the time consuming nature of the cyclic loading process [2][5]. An indirect tensile asphalt cracking test (IDEAL-CT) has been developed in 2017 [5]. The IDEAL-CT is a simple, practical, and efficient test that have been compared with cement tests [6] and other types of fracture tests [7]. The results from the literature indicate the test has a great protentional to be used as an efficient and economical tool for asphalt mixtures quality control. However, the test has not been validated with the elastomer modified asphalt yet.

Researchers have used modified fatigue tests to study the self-healing capability of bituminous material in macroscale [8][9][10]. Healing capability of the material is typically quantified by comparing the modulus change with and without rest periods [11]. However, the existence of reversible phenomena makes it even harder to quantify the healing effects. It should be noted that healing is not simply crack closure or recovery, the recovery and healing are components of restoration, which have not been distinguished clearly in previous research [12]. Therefore, the visualization tools, such as computed tomography (CT) Scanner that has been used to study the recovery of asphalt mixture cracking in microscale and mesoscale, may not be good enough for capturing the healing property [13]. Another approach is needed to property characterize the self-healing property of asphalt concrete. Therefore,

coming up with a proper self-healing characterization method which is supported by strong theoretical and experimental evidence is deemed necessary in the proposed research.

Non-destructive testing (NDT) methods can offer great benefits, especially with respect to studying the recovery of material properties [14]. The use of wave propagation-based methods can be instrumental to study the location and characteristics of the induced damage during the fatigue characterization. Such techniques are also unique as they can provide engineering measures of the materials without the need of mechanical loading application, which is of high importance during the rest periods application in a modified fatigue test. Some researchers use ultrasonic wave velocity to predict the modulus of asphalt concrete, with varying success [15]. However, there has been little research that utilizes wave attenuation to evaluate damage in asphalt concrete. Wave attenuation can be used as an indication of the level of fracturing of a medium [15], and many analysis methods have been developed such as Fourier transformation, wavelet transformation, etc. The technique will provide means of quantifying the damage and healing.

1.2 Research Hypothesis

The main hypotheses for this research are as follows:

- Fatigue is one of the main failure modes of pavement structures. The asphalt mixture cracking process can be better understood by adequately evaluating the laboratory fracture test and the bias effects in fatigue tests.
- Self-healing is an intrinsic property of bituminous material. It could be understood better if no mechanical loadings were applied during the rest periods.
- Non-destructive testing (NDT) methods are efficient and economical for material property evaluation. When the signal with the same energy propagates through the asphalt specimen, the energy of the received signal correlates with the damage that accumulates in the specimen.
- IDELA-CT test, as a simple and fast test, has been reported in the literature. If validated with a fatigue test, it can be used as a good tool for asphalt mixture quality control.

1.3 Research Objective

This research aims to improve the laboratory asphalt concrete fatigue and self-healing tests by combining NDT methods so that the mechanical performance of asphalt can be better understood. The new understanding will lead to more effective and sustainable use of bituminous material. Furthermore, this project will also contribute to a better understanding of crack initiation and propagation processes in pavement materials, which can improve the existing state of pavement rehabilitation and maintenance techniques as well as pavement condition prediction models.

The key objectives of this research are:

- To provide a fundamental understanding of wave propagation in viscoelastic materials.
- To develop a non-destructive testing technique and quantify the damage and healing characteristics of asphalt mixtures undergoing monotonic and cyclic loadings.
- To validate existing fatigue models for tension/compression fatigue test with wave attenuation approach.
- To develop and validate experimental protocols by adopting and modifying existing fatigue and cracking tests to assess the self-healing ability of bituminous materials.
- To compare a newly developed asphalt fracture test (IDEAL-CT) with the existing results and evaluate its sensitivity for characterizing polymer-modified asphalt.

1.4 Research Methodology

The objectives of this thesis were achieved through a three-stage comprehensive laboratory testing at the Centre for Pavement and Transportation Technology (CPATT) at the University of Waterloo. Ultrasonic pulse propagation test (UPPT) was conducted on three groups of specimens: 1) undamaged, 2) damaged with monotonic loading, and 3) damaged with cyclic loading processes. Several signal-processing techniques were applied to understand the mechanical behaviour of this viscoelastic material. A brief summary of these three stages is listed below:

Stage 1: UPPT on Undamaged Specimen (Chapter 3)

This stage is the foundation of the other stages. The UPPT was first applied to the elastomer-modified asphalt mixtures, then the specimens were tested under monotonic loading with the IDEAL-CT

procedure. A correlation between the wave attenuation analysis and the mechanical loading test results is drawn. The results were also compared with the binder test results from the previous study.

Stage 2: UPPT during Fracture Healing Test (Chapter 4)

An indirect tensile test has been selected for this stage as it predetermines the crack location. A loading, resting and the reloading process was applied to the asphalt concrete specimen, and an ultrasonic pulse-receiver device was used to monitor the whole test process. The damage and healing of the asphalt specimens were studied by comparing the changes in the ultrasonic signals and the measured physical and mechanical properties of the specimen.

Stage 3: UPPT during Fatigue Healing Test (Chapter 5)

A modified uniaxial tension-compression fatigue test was used for this stage. The specimen is fatigue damaged to a certain level and then a rest period was applied so that both fatigue and healing processes can be studied. Ultrasonic transmitters were mounted to the specimen to conduct UPPT. The specimen was conditioned in a chamber to meet the test condition. The temperature change process was also monitored with the UPPT, and the data were used to quantify the bias effects of the cyclic loading by comparing the property of the specimen with and without loading at the same temperature level.

Detailed explanations of the signal processing techniques and the research methodology used in each stage are provided in Chapters 3 to 5 of this thesis.

1.5 Thesis Organization

This thesis is organized as follows:

Chapter 1: Introduction – This chapter provides the general scope and overall objectives of the research.

Chapter 2: Background – This chapter provides background information on asphalt mixture fundamentals, asphalt fatigue and self-healing mechanisms and existing tests, and a brief summary of non-destructive tests on asphalt mixtures.

Chapter 3: Validation of Polymer Modified Binder Characterization through Ultrasonic Pulse Propagation and Indirect Tensile Testing of Asphalt Concrete Specimens – This chapter

is presented as a paper. It investigates the feasibility of using the ultrasonic pulse propagation test and the indirect tensile test to characterize asphalt mixtures.

Chapter 4: Dynamic High-Frequency Healing with Rest Period (D2HRP) as a New Test Protocol for Determination of Intrinsic Healing Rates of Bituminous Mixtures – This chapter is presented as a paper. It introduces and evaluates a new test protocol that combines an indirect tensile test with an ultrasonic pulse propagation test.

Chapter 5: Indirect Measurement of Fatigue and Healing of Asphalt Mixtures Using Ultrasonic Wave Propagation Approach – This chapter is presented as a paper. A new test configuration combines the asphalt fatigue test with the ultrasonic pulse propagation test. The effects of bias effects in the fatigue test can be indirectly quantified.

Chapter 6: Conclusions, Recommendations and Contributions are presented.

Chapter 2

Literature Review

2.1 Asphalt Mixture Fundamental

2.1.1 Asphalt Concrete Composites

Asphalt concrete is a composite material, and it mainly consists of aggregates, asphalt cement, and air voids. Additives such as fillers, fibres and modifiers that can enhance specific aspects of asphalt concrete may be used in some designs as well.

Asphalt cement is manufactured from crude oil, which varies in both physical and chemical properties. When manufacturing asphalt mixtures, asphalt cement is used as a lubricant. After the mixture being mixed and compacted, asphalt cement functions as a glue to bind aggregates and additives in hot mix asphalt. It is the most expensive component in the asphalt mixture [3]. The asphalt cement selection for a design depends on the temperature range, traffic volume, and loading situation at the designated location. Aggregates make up 90 to 95 percent of the mixture by weight, and they form the skeleton of the asphalt concrete [3]. Aggregates may have different reactions with asphalt cement because of the minerals it contains, and the gradation of aggregates also plays an important role in the hot mix asphalt. Air voids are the percentage of void spaces in asphalt concrete. A conventional asphalt layer in pavement are initially constructed with 6 to 8 percent air voids which will be compacted in the future due to traffic loading [3]. Sufficient voids should provide adequate allowance for asphalt expansion due to temperature increases, without causing bleeding or loss of stability.

There is a general agreement that the properties of asphalt concrete are highly variable due to the resources and manufacturing processes of each constituents, and the mixture manufacture processes. Therefore, it is very important to conduct performance tests to ensure the quality of the material.

2.1.2 Asphalt Mixture Behavior

Asphalt can be assumed as a viscoelastic material, whose mechanical properties depend on time and temperature. The behavior of asphalt cement can be illustrated using strain amplitude (ϵ) and temperature (T), as presented in Figure 2-1 [16]. Similarly, the behavior of asphalt concrete can be identified with strain amplitude and the number of applied cyclic loadings (N) (Figure 2-2)[17]. When studying asphalt concrete, the applied strain amplitude is always relatively small so that it can simulate

the material experience in real world. At low temperature, asphalt behaves elastic and may have brittle failure. At intermediate temperature, asphalt has viscoelastic behavior and it may fail due to repetitive loading. At high temperature, asphalt cement behaves more viscous and might lead to rutting. Asphalt behavior also depends on the loading rate, briefly explained in the next session.

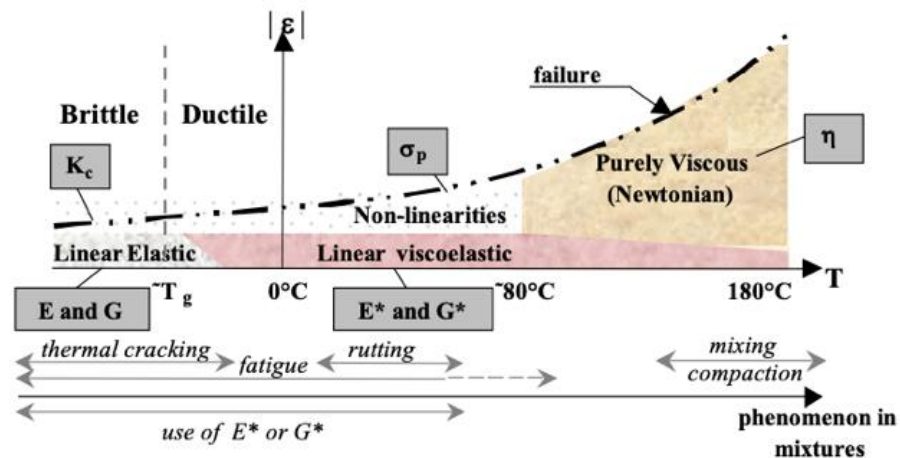


Figure 2-1. Typical behaviors for asphalt cement [16]

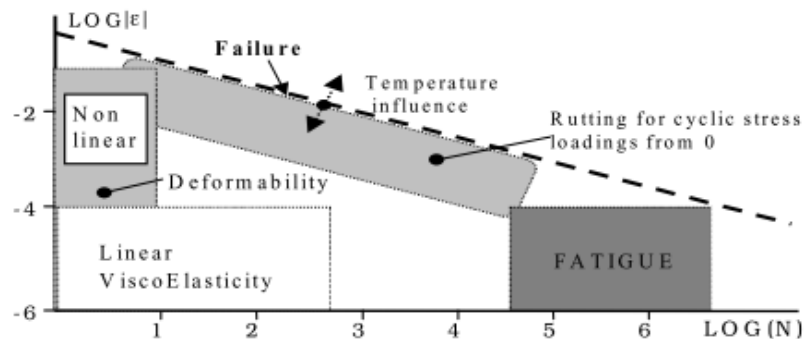


Figure 2-2. Typical behaviors for asphalt concrete [17]

2.1.2.1 “2S2P1D” model

In the linear viscoelastic region, the rheological properties of both asphalt cement and asphalt concrete can be expressed in terms of the norm of complex modulus ($|E^*|$) and the phase angle (δ) master curves [18]. A master curve (Figure 2-3a) describes frequency dependent mechanical properties of the viscoelastic material at a reference temperature. It can be constructed with time temperature superposition principle.

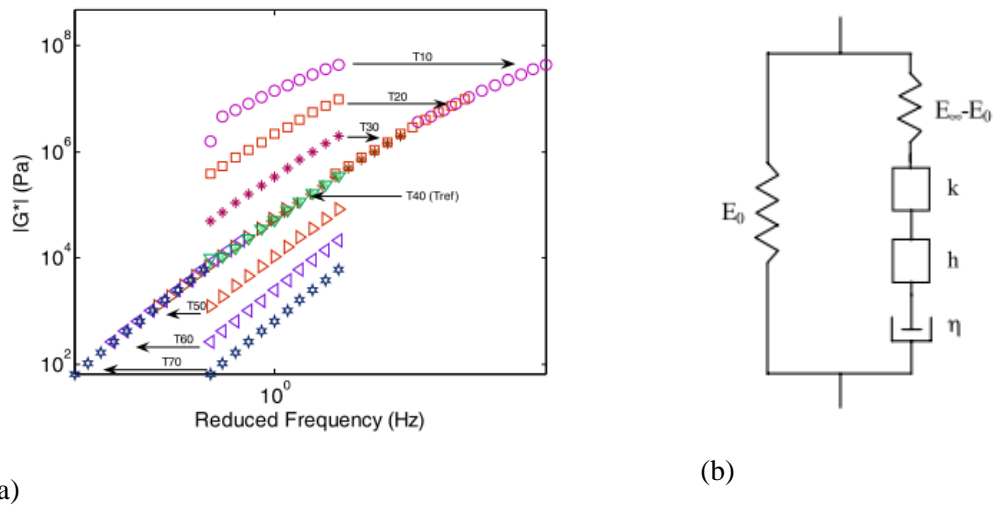


Figure 2-3. (a) Master curve construction [18] and (b) Analogy of “2S2P1D” model [19]

There are many existing models to express the master curve [18]. Among all the models, the “2S2P1D” model (Figure 2-3b) appears to be the most precise one [19]. It uses combinations of 2 springs (2S, elastic element), 2 parabolic elements (2P, an analogical model with a parabolic creep function and consequently a stiffness complex modulus), and 1 linear dashpot (1D, Newtonian viscous element). This model can describe both asphalt cements and mixes. To construct this model, a complex modulus test needs to be conducted. The results can be plot in a Cole-Cole plane and a black-space diagrams to examine the thermo-rheological behavior of materials [20]. The constants in the model can be identified by analyzing the data. The damping ratio of asphalt mixtures generally increases with an increase in temperature, usually varying from 2 to 7 % [21].

2.1.3 Flexible Pavement Structure

Typical flexible pavement structures are composed of multiple layers of engineering materials. Conventionally, the surface layer is composed of hot mix asphalt (HMA) in order to better distribute the stress induced by the traffic. The base layer, underlying the HMA materials, then further distributes the load and facilitates drainage. Typically, this layer is made of crushed and graded mineral aggregates. The subbase course functions as the final structural layer. Subbase is usually composed of lower quality crushed aggregates or engineering fill materials. The entire pavement structure is laid on subgrade soil. The thickness of each layers and the material selection for each layers will depend on the traffic and climate in which pavement is built [20]. Pavement might fail in many ways, including rutting, fatigue

cracking, and thermal cracking. Unlike other materials, the distresses such as fracture or elastic deformation cannot be accurately predicted for asphalt pavements. Therefore, when designing pavement, a mechanistic-empirical method that considers performance criteria, material characterization and field data is needed. Typically, rutting and fatigue are the two performance criteria for pavement design.

2.2 Asphalt Fatigue

2.2.1 Fatigue Fundamental

Asphalt concrete fatigue cracking, a.k.a. alligator cracking, is the dominant pavement distress type at the intermediate temperatures. If left unattended, they will result in the formation of potholes which are costly and difficult to repair [20]. The repeated loading induces tensile stress and strain at the bottom of HMA layers in both tangential and transverse directions, which forms microcracks [19]. Microcracks then propagate and forms macrocracks. The fatigue cracking process is sketched in Figure 2-4.

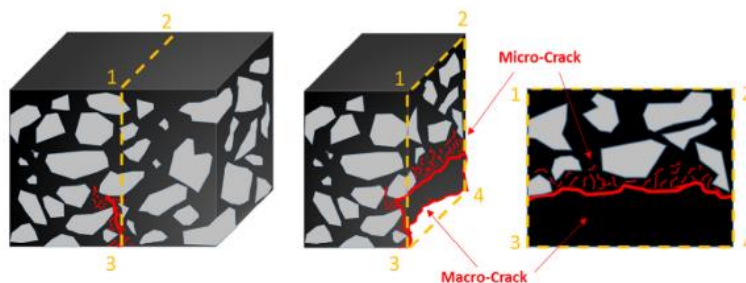





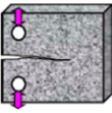
Figure 2-4. Sketch of fatigue cracking in asphalt concrete [22]

2.2.2 Fatigue Tests

Various test methods have been developed to simulate the fatigue behavior of asphalt concrete. Tangella et al. [1] and National Cooperative Highway Research Program (NCHRP) 9-44 [2] have summarized the general categories of the test methodologies, include: uniaxial, triaxial, diametral, flexure, fracture, and full-scale tests. In laboratory, the most commonly used tests for fatigue property evaluation are the uniaxial tension/compression test, the bending tests, indirect tensile test, and the semicircular bending test. The test setups are summarized in Table 2-1 [1] [2] [23], where full-scale test is not present as they are not in laboratory scale.

None of the aforementioned tests is perfect[1][23]. Most of the fatigue tests are non-homogeneous tests, which means their stress and strain cannot be directly measured. The bending tests are based on flexural mechanics and they usually predominate the failure points. This type of test is misguided because it assumes the tested material has elastic behavior, which is not the case for asphalt. The failure of indirect tensile test may not only be due to fractures, but also permanent deformation at the loading location. The semicircular bending test requires sawing a notch in the specimen so that the notch tip can localize the maximum stress location. However, in some cases, the notch may cut through aggregates and in other cases, the cut may majorly through the mastic phase, which can strongly affect the results interpretation. Both indirect tensile test and fracture test use high level of strain where the material behaves non-linearly so that they may not be the best candidates to study fatigue precisely. The only homogeneous test is the uniaxial test, which does not need behavior law and can measure stress and strain directly from the test setup. Even though the test setup is better than the other tests, the existence of bias effects due to the application of cyclic loading make it harder to analyze the fatigue behavior of asphalt concrete. Even though the tests are not perfect, they can provide insights into the characterization of material so that the fatigue life of the material can be estimated.

Table 2-1. General categories of the test methodologies [1][2][23]

Test Type	Common Tests	Sample Test Geometry	Loading Conditions
Uniaxial	Complex modulus test Tension-Compression (T/C) Fatigue test		Cyclic loads, with or without stress reversal
Triaxial	Resilient modulus test Permanent deformation	Uniaxial testing with confinement	Cyclic load
Diametral	Indirect tensile (IDT) test Indirect tensile asphalt cracking test (IDEAL-CT)		Monotonic load
Flexure	2-, 3-, 4-Point bending (2-, 3-, 4-PB) test		Cyclic load with varying magnitudes.
Fracture	Semicircular bending (SCB) test Disk-Shaped Compact Tension (DCT) Test		Varies with loading configuration.

2.2.3 Bias Effects

During cyclic fatigue tests on asphalt concrete, the norm of the complex modulus, or the stiffness, decreases with the number of cycles. Several studies have been done to qualify and quantify the cause of decreases [4][23][24][22]. Dr. Di Benedetto [4] divided the fatigue process into three phases (Figure 2-5). Although a fatigue test is conducted, damage from fatigue is not the only factor that leads to a decrease in stiffness of bituminous material. During cyclic loading, various effects that occur in conjunction with damage are the main contributors to the complex modulus degradation in each phase.

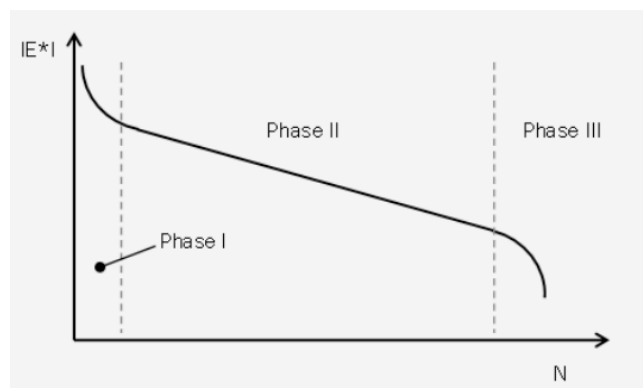


Figure 2-5. Stiffness evolution curve during a fatigue test [20]

Phase I is characterized by a rapid drop of the modulus. It is mainly due to dominant asphalt cement viscosity decrease and other reversible phenomena. The non-fatigue effects in the fatigue test are called bias effects and have been studied intensively. Phase II is typically a quasi-stationary stage where fatigue damage is dominant and microcracks are formed. Bias effects also exist in this phase; however, they have a relatively lower impact than fatigue damage. Phase III has a rapid decrease of modulus, which leads to unpredictable behavior. At this stage, microcracks grow into macrocracks. Therefore, most studies focus on the first two phases, and laboratory predicted fatigue life is usually located in Phase II to deduct the risk of insufficient design.

Nonlinearity occurs at the first cycle, the sudden drop of norm of complex modulus is partly due to nonlinearity. The effect of nonlinearity decreases when the strain amplitude moves towards zero. At rather small strain level, it is reversible [4], [25]. During Phase I, the rapid degradation is mainly due to temperature increase in the specimen and thixotropy. Thixotropy is a reversible phenomenon in asphalt cement. During the whole loading process, thixotropy causes dissociation and deformation of inter-and intra-molecular bonds in asphalt cement until it reaches a sol structure [22], which reduces

the viscosity and the modulus of the material. The effect gradually vanishes when material is at rest. The other bias effect is heating. Heating is caused by viscous dissipated energy (molecular friction) during loading. It reduces the modulus by separating the secondary intermolecular bonds due to thermal expansion. This is also a reversible phenomenon. When loading disappears, the material will have a cooling effect. This effect can be calculated from the measured temperature change [4].

Other phenomenon, such as permanent deformation and steric hardening may also rise in fatigue tests. Permanent deformation appears in cyclic bending test and the diametral tests, which changes the viscoelastic properties of the material [22]. Steric hardening is the hardening of bitumen over time, which is associated with a sol-gel transformation and asphaltenes in bitumen [26].

2.2.4 Asphalt Fatigue Models and Failure Criteria

For laboratory fatigue tests, there is no universal standard to define failure or damage in asphalt mixtures, and there is no model that identifies the contribution of each bias effect. Different failure criteria are associated with different models, some of which are summarized in this section.

2.2.4.1 Classical Approach

This approach is widely used and valid for the fatigue tests. Wöhler curve, also called fatigue curve (Figure 2-6) [27], correlates the level of loading to the corresponding life duration of the material. The fatigue life duration of each applied load level is defined as a 50% decrease of the initial modulus of the specimen by Van Dijk [28]. A particular strain, called ϵ_6 that corresponds to the fatigue life of 1,000,000 cycles, can be determined from the curve. This approach largely depends on the type of test and mode of loading used [23].

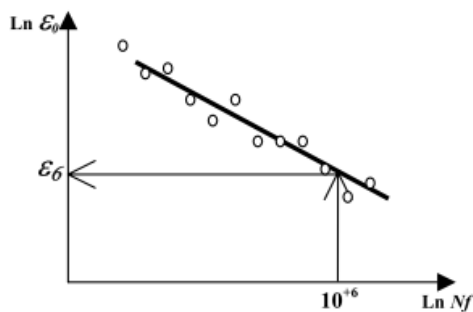


Figure 2-6. Wöhler curve determination of ϵ_6 [27]

2.2.4.2 Hysteresis Loop Approach

For a material that is not pure elastic, loading and unloading path does not overlap. For asphalt, the hysteresis loop may change differently due to different type of distresses. Al-Khateeb and Shenoy [29] pointed out the existence of the microcracks induced from fatigue loading introduces discontinuities in the stress path so that distortion of hysteresis loop occurs. They propose to use the distortion of hysteresis loop as a failure criterion. In addition, they used bending tests to validate their assumptions. As mentioned earlier, bending test are non-homogeneous test, and the distortion of hysteresis loop might be due to the test configuration.

2.2.4.3 Dissipated Energy Approach

Dissipated energy per cycle w_i is computed as the area within the stress-strain hysteresis loop, which represents the energy dissipated during the loading. For a fatigue test, if controlled with stress, due to creep of asphalt, the dissipated energy increases. Whereas when the test is controlled with fixed strain amplitude, due to stress relaxation, the dissipated energy decreases.

$$w_i = \pi \sigma_i \varepsilon_i \sin \delta_i \quad \text{Equation 1}$$

Using dissipated energy approach to analyze asphalt fatigue has been studied for many years. Shen and Carpenter [30] summarised the development of this approach and they found the ratio of dissipated energy change (RDEC) is the most promising index to describe damage accumulation. RDEC approach studies the relative amount of energy dissipation created by each additional load cycle.

$$RDEC = \frac{w_{n+1} - w_n}{w_n} \quad \text{Equation 2}$$

Where w_n means the dissipated energy produced in load cycle n . The RDEC versus loading cycles curve can be divided into three stage. The plateau stage indicates there is a constant percentage of input energy dissipated during the loading process, which is sign of fatigue damage. Fatigue failure shows clearly in Phase III, where a dramatic increase take place. From Figure 2-7, it can be also seen the conventional failure criteria, 50% stiffness reduction N_{f50} , always ends up at the plateau stage [31]. This approach has been demonstrated valid for both bending tests and uniaxial tension tests [30].

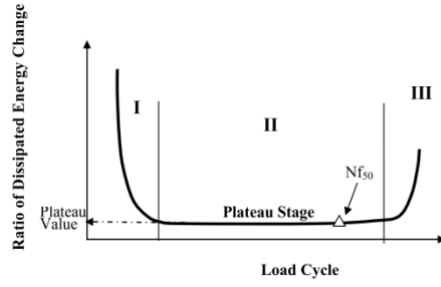


Figure 2-7. RDEC plot [32]

2.2.4.4 Département Génie Civil et Bâtiment (DGCB) Approach

This approach developed at the laboratory “Département Génie Civil et Bâtiment” (Department of building and Civil Engineering) of ENTPE by Di Benedetto [33]. This approach aims to separate fatigue damage from the bias effects during loading processes. It assumes a linear evolution of the modulus with number of applied load cycles within quasi linear intervals in Phase II of the fatigue process.

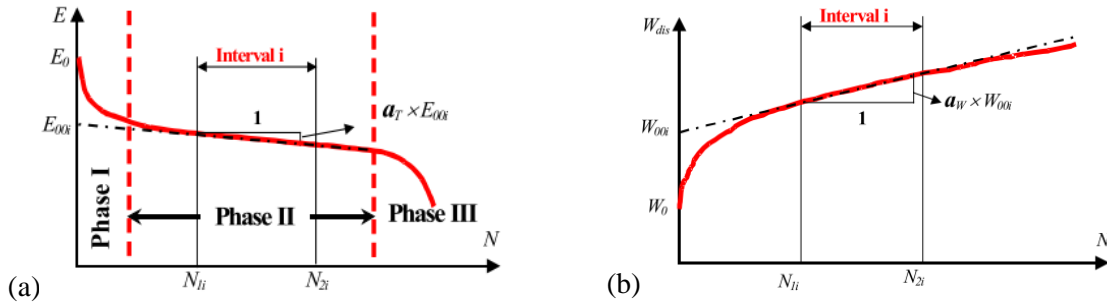


Figure 2-8. Interval in "DGCB" model (a) stiffness evolution, (b) dissipated energy evolution [34]

The slope of straight regression line for each interval can be seen as a combination of fatigue and bias effects. It was found the bias effects are directly related to the energy dissipation. E_{00i} is the initial stiffness of the interval i and a_T is the slope for the regression line. E_0 is the modulus at the beginning of the test.

$$\mathbf{a}_F = \mathbf{a}_T - \mathbf{a}_B = \mathbf{a}_T + \mathbf{a}_W \frac{C_i(E_0 - E_{00i})}{E_{00i}} \quad \text{Equation 3}$$

where, a_B represents the bias effects contributing to the loss of stiffness, which might have a positive or negative effect; a_W represents the slope of the linear regression of dissipated energy in this interval and normalized by the dissipated energy in first cycle; and C_i in Equation 3 relates to the interval

selection as stated in Table 2-2 and follows the non-linear damage evolution. By comparing the “true” fatigue damage parameter a_F , the fatigue resistance property of the material can be evaluated. This model proves the intrinsic fatigue damage does not depend on the type of loading applied [23].

Table 2-2. Coefficient C_i in "DGCB" approach [23]

Interval	$i = -1$	$i = 0$	$i = 1$	$i = 2$
Cycles	40,000 to 60,000	40,000 to 80,000	50,000 to 150,000	15,000 to 300,000
C_i	5/6	4/5	3/4	2/3

2.2.4.5 Viscoelastic Continuum Damage (VECD) Approach

A constitutive model can be derived from the viscoelastic continuum damage model. This model aims to create a behavior law to express the behavior of bituminous material [35]. The model uses work potential theory and the damage evolution law [36] to describe the continuum damage equation in an elastic media. It also uses the elastic-viscoelastic correspondence principle [37] to correlate the viscoelastic behavior with the elastic behavior. The last part of this approach is to combine the aforementioned theory together to create a behavior law that describes damage growth for a viscoelastic material. The application of this approach on bituminous material was proposed by Kim and his colleges [38].

	Elastic	Viscoelastic
No Damage	$\sigma = E\varepsilon$	$\sigma = E_R\varepsilon^R$
With Continuum Damage	$\sigma = C(S)\varepsilon$	$\sigma = C(S)\varepsilon^R$

Figure 2-9. VECD explanation

$C(S)$ refers to a stiffness function with a damage parameter S (an internal state variable) and it is called pseudo stiffness. The corresponding number of load cycles with 50% reduction in pseudo stiffness can be defined as the failure point in this model. When viscoelastic material undergoes a given stress, strain

is a time dependent variable. For a linear, nonaging viscoelastic material, the stress-strain equation needs to capture the time dependent response.

$$\sigma = \int_0^t E(t - \tau) \frac{d\varepsilon}{d\tau} d\tau \quad \text{Equation 4}$$

$$\varepsilon^R = \frac{\sigma}{E_R} = \frac{1}{E_R} \int_0^t E(t - \tau) \frac{d\varepsilon}{d\tau} d\tau \quad \text{Equation 5}$$

To write it in a simpler way, a format similar to Hook's law is used. With introduction of a reference modulus, E_R , the strain can be expressed as pseudo strain ε^R . Using this approach, pseudo stiffness verses damage curve can be defined to describe the modulus loss in the material under both monotonic loading [35] and cyclic loading [39].

There are other existing models to simulate asphalt concrete behavior or estimate fatigue life of pavement structure. For example, an empirical model, which uses Miner's law and the strain at the bottom of HMA layer to estimate the fatigue life [40]. These models are used more in empirical pavement design and are not the focus of this research. There are other models developed from a fracture mechanical approach, which are beyond the author's knowledge at this stage. Those models need to be studied in the future.

2.3 Self-healing of Asphalt

2.3.1 Self-healing Mechanisms

Healing is an intrinsic property of asphalt cement. Asphalt cement are expected to heal themselves during hot summers and long rest periods. The mechanism of self-healing process is very complex. Phillips (1998) summarized the healing process of asphalt cement as a three-stage mechanism: (1) the closure of microcracks due to the consolidation of stresses and flow of asphalt cement, (2) the closure of microcracks due to wetting (adhesion of two crack surfaces driven together by surface energy) and (3) the complete or partial recovery of mechanical properties as a result of the diffusion and randomization of asphaltene structures [10]. The first stage is considered to be the fastest stage, but it only results in stiffness recovery. The second and third stages occur much slower but improves the stiffness and strength of the material. Several models have been proposed to explain these steps in different scales.

A capillary flow-based model [13] has been assumed to explain the meso-crack healing. In a fresh opening crack, molecular diffusion may not happen due to the large width between the crack faces. However, healing still happens, to explain this, a capillary mechanism is proposed. Capillary flow theory describes asphalt cement flow in the mixture at certain conditions, such as a proper temperature. At such temperature, bitumen behaves as a Newtonian fluid. And can be considered as a liquid. Use the equilibrium of force, sum of weight of healing material (F_h) and the dissipation force (F_d) caused by bitumen movement should be equal to the hydrostatic force exerted by the weight of asphalt concrete (F_f) plus the surface tension force (F_t) (Figure 2-10).

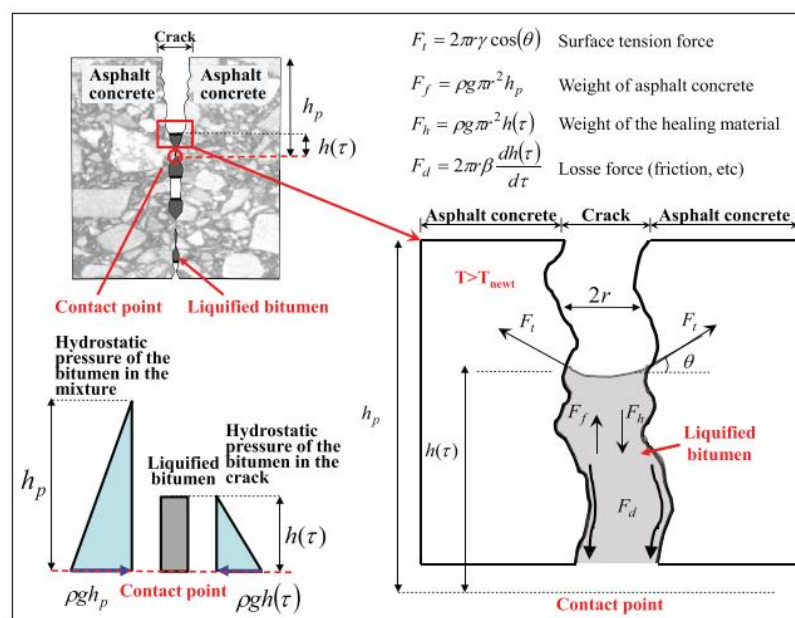


Figure 2-10. Scheme of capillary healing model [41]

On the microscale level, molecular diffusion process has been studied in various research. These mechanisms are largely inspired by studies developed in polymer healing system. Many factors have been studied, such as temperature, surface free energy, chemical constitution, etc. Based on these theories, longer rest periods and higher temperature conditions can speed up the healing process [42]. However, due to the complexity of asphalt compositions, the mechanism still remains unclear, and very little progress has been made in explaining asphalt healing in macroscale.

2.3.2 Common Healing Tests

Many tests have been developed to study the self-healing capability of asphalt materials. In nano/microscale, the research is mainly done with asphalt cement. The methods include, but are not limited to, scanning electron microscopy (SEM) and atomic force microscope (AFM) [43]. With the help of these methods, healing processes can be observed and modeled in many ways. In mesoscale, similar to microscale, visualisation tools are used. Typical methods include fluorescence microscopy (FM) (Figure 2-11) and X-ray computed tomography (X-ray CT) [13]. However, to analyze the results adequately, a comprehensive knowledge of mathematics, statistics and image processing is needed.

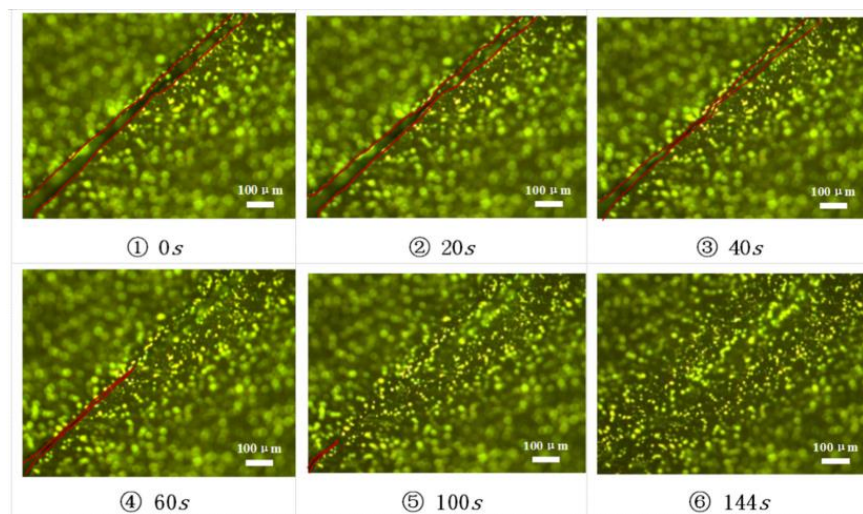


Figure 2-11. FM images of the crack healing process of SBS modified asphalt [43]

The most commonly used macroscale asphalt healing tests are fatigue-based test, fracture-based test, and field-based test. García et al. conducted fracture-based test to evaluate the healing response by applying rest periods between two fractured surfaces in the asphalt body. However, there are some concerns about this type of tests, including uneven contact surface and plastic deformation [42]. This type of tests is usually conducted on asphalt cements, which is beyond the scope of this research.

There are two categories of fatigue related healing tests. The categories based on the way that rest period is introduced into the regular fatigue test. A rest period means a time period without load application to the system. The first category is an interrupted type, which applies rest periods after continuous loading periods. The second category is an intermittent type, which has a rest period

following each load cycle. The second type of loading sequence is considered to be more realistic as it seems like real situation in field.

Sun et al. [43] studied healing stages of bituminous material, and they found that the shortest healing time of a microcrack in asphalt at room temperature needs around 2 minutes (Figure 2-11). In order to have fatigue damage in a mixture sample, tests in the second category may take months to conduct. Therefore, the second type of test usually is conducted in binders and mastics [8]. To study healing in an asphalt mixture level, the test in the first category should be used.

The other challenge is to evaluate material strength during the rest period without damaging the specimen or applying cyclic loadings. To solve this problem, non-destructive testing approach might be the most suitable approach as it can provide engineering measures of the materials without the need of mechanical loading application. Further details about the non-destructive testing for asphalt mixtures are discussed in the following section.

2.4 Non-destructive Testing for Asphalt Mixtures

2.4.1 Current NDT Methods on Bituminous Material

There are many NDT methods that has been used on bituminous material. For pavement structural, the Ground Penetrating Rader (GPR), Impact Echo (IE), Falling Weight Deflectometer (FWD), Infrared Thermography (IRT), and Spectral Analysis of Surface Waves (SASW) can be used [44]–[47]. In field, the environment factors, such as temperature, humidity, and the present of other materials, can greatly affect the accuracy of the results. Surface waves based techniques are promising for the field application. In laboratory, various type of tests has been adapted to estimate bituminous material properties. Most commonly used tests on the cylindrical specimens are Ultrasonic Pulse Velocity (UPV) Test and Impact Resonant (IR) Test [48].

2.4.1.1 UPV test

UPV is one of the most popular test that has been used in many research [15] [47] [48]. The test setup is quite simple, as shown in Figure 2-12. A sample is sandwiched with a transmitter and a receiver. The transmitter and receiver are made of piezoelectric crystals that can transform electric currents into ultrasonic waves. Both of these piezoelectric sensors are attached to the sample using a coupling agent such as vacuum grease and connected to an oscilloscope. As this test was conducted at a very high

frequency, the asphalt mixtures can be seen as elastic material. The travel time (t) the wave passes through the specimen can be recorded. The signals can be stored for future signal processing. By measuring the distance (L) between two sensors, the wave velocity can be calculated using L/t . The wave velocity depends on the material density, Poisson's ratio, and the elasticity of the material. This test is easy to conduct, and the analysis is very simple. However, the correlation between velocity and strength for composite materials needs to be studied. This test may not be sensitive to flaw detection. There is a standard for concrete specimens, not for bituminous material.

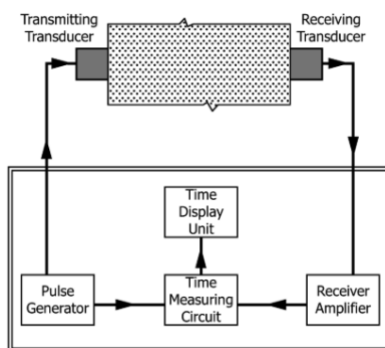


Figure 2-12. Schematic test setup for UPV test (ASTM C597)

2.4.1.2 IR Test

The Impact Resonant Test uses the resonant frequency of the specimen to calculate Young's modulus of elasticity. ASTM C215 presented this method for testing a concrete specimen. Based on the location of the impact point and the accelerometer, the transverse, longitudinal, and torsional resonant frequencies can be recorded. Based on the previous research, the standard listed some coefficients that can be used to estimate the stiffness of the specimen. Research has been conducted using this method on asphalt specimens at various of temperatures to estimate the stiffness of asphalt concrete at those temperatures and to construct the master curve of asphalt at higher frequencies [50]. The results show that this test is efficient and reliable, and can be coupled with the dynamic modulus test to estimate the low temperature properties of the asphalt concrete.

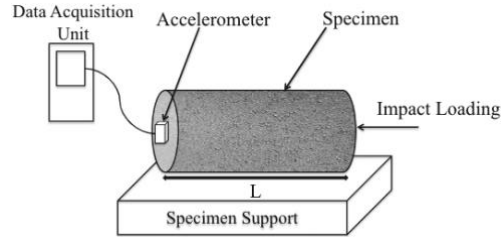


Figure 2-13. Schematic of Impact Resonant Test [51]

This research combines the NDT method with conventional asphalt cracking and fatigue tests. The IR Test uses an external impact to generate the input signal, which is hard to control. While the UPV test controls the input signal with the setting of the device and is thus more suitable for this research. However, these tests are conducted to evaluate the bulk property of the material. For a heterogeneous, high-damping material, such as asphalt concrete, the current wave velocity analysis method may not be sufficient to capture the microstructural changes in the material. Wave attenuation analysis is more sensitive than wave velocity in the detection of system flaws [15]. Instead of calling the NDT method used in this research the Ultrasonic Pulse Velocity Test, Ultrasonic Pulse Propagation Test (UPPT) is more suitable to distinguish from the conventional analysis method. However, limited research on using this analysis approach on bituminous material has been done so far.

2.4.2 Device Setting in This Research

Chapters 4 and 5 of this study use A1560 SONIC to customize ultrasonic measurements and data acquisition. This device is connected to a computer, which allows manual triggering and recording of the ultrasonic signals. The device allows either a single-crystal transducer as both pulser and receiver or dual-crystal transducers. In this research, a dual-crystal transducer setting is used. The device generates a group of 2^X pulses each time, and the received signal is the result of an average of the output signals, which cancels out the noise and increases the resolution of the data. This setup is selected to ensure a good resolution of the output signal. Here is a brief explanation of the setup:

- Sampling Frequency (MHz):
Number of sampling points per second. 5 MHz
- Analog (High-pass):
Signals frequency Higher than this number can pass 10 kHz
- Analog Gain (dB):

- An amplifier that boosts up the amplitude of the input signal 20 dB
- Number of Periods:
 The number of half-squares in the input pulse 2
- Period of Signal (ns):
 The Time difference when sending out the input pulses 6666 ns
- Transducer Frequency (kHz)
 The resonant frequency of the transducer 150 kHz
- Transducer Type:
 Testing mode for this device. Dual Crystal
- Transducer Half-Peak Voltage (V):
 Transmitter output voltage 20 V
- Vector Length:
 Length of the data acquisition vector 4096
- Averaging Factor (2^X):
 Number of the readings for one received signal ($2^6 = 64$) 6

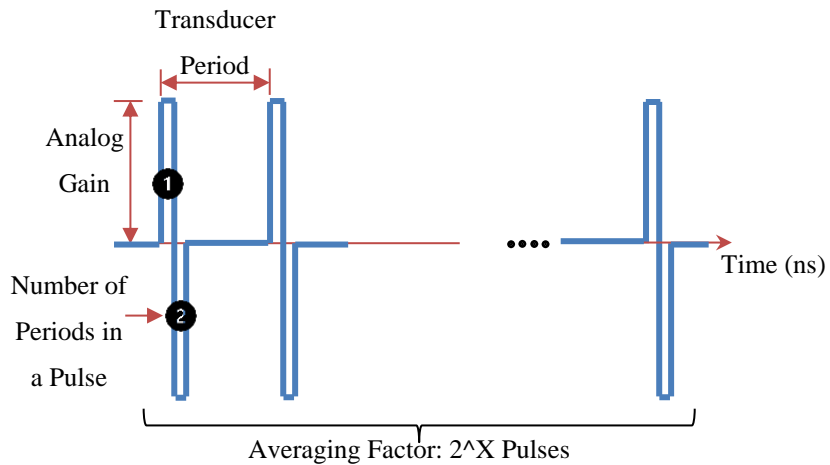


Figure 2-14. Schematic of Input Signal

Chapter 3

Validation of Polymer Modified Binder Characterization through Ultrasonic Pulse Propagation and Indirect Tensile Testing of Asphalt Concrete Specimens

Summary

Linear Amplitude Sweep (LAS) test and the Multiple Stress Creep Recovery (MSCR) test were used to estimate the Superpave asphalt fatigue and rutting performance. Several laboratory mixture tests have been developed to predict the performance of asphalt concrete mixtures. Elastomers have been used extensively in the industry to prolong the service life of pavements. However, many existing standardized test methods are mainly focused on the linear viscoelastic range of conventional asphalt concrete mixes. Therefore, it is crucial to evaluate the suitability of these tests for elastomer-modified asphalt concrete materials as they have a significantly extended elastic range. This research aims to evaluate the feasibility of using the Ultrasonic Pulse Propagation Test (UPPT) and Indirect Tensile Asphalt Cracking Test (IDEAL-CT) to characterize the elastomer-modified asphalt concretes through a comparison with the previous asphalt binder tests, LAS and MSCR, that was conducted with the same binder.

UPPT is a non-destructive method that has been studied in various research on asphalt mixtures. Although, the traditionally used analysis of UPPT provides materials modulus based on the wave propagation velocity and the specimen's density, current time-domain analysis methods may not be adequate to properly characterize bituminous materials properties. This study utilizes a new wave attenuation analysis approach to complement wave velocity data. After the non-destructive test, the IDEAL-CT was conducted on the same specimens. IDEAL-CT has demonstrated excellent potential to evaluate asphalt concrete cracking performance. The development of the IDEAL-CT index (CT_{index}) uses the stress intensity factor initially developed for materials with brittle fractures. This research uses two pieces of equipment to assess the reproducibility of the test results when using different setups, and the results were analyzed with several existing indices. The test results from those two tests were compared with the previous asphalt cement test results.

The elastic behaviour can contradict the observed changes in the current cracking index. Furthermore, the results show that the fracture mechanics-based indices cannot effectively characterize the elastic response for elastomer-modified asphalt concrete specimens. In contrast, the load-displacement curve area until the fracture point has excellent potential to evaluate asphalt concrete cracking performance. The UPPT results show that more energy is absorbed as the base binder becomes more viscous, and more energy is transmitted as the dosage of the polymer increases. This suggests that the wave attenuation analysis has good potential as a non-destructive technique for characterizing polymer-modified bituminous materials. The results from these two asphalt mixture tests were in good agreement with the previous LAS and MSCR binder test results.

3.1 Introduction

Recent advances in transportation systems have highlighted the need for more resilient construction materials to extend the service life of pavements. Various asphalt modifiers have been proposed to improve the crack resistance of asphalt binders through altering their stiffness or visco-elastic behaviour. Examples of such modifiers are elastomers, such as Styrene-Butadiene Rubber copolymers (SBR), Styrene-Butadiene-Styrene (SBS) block copolymers, and natural rubbers, which are able to recover to their pre-loaded state [1, 2]. In 1992, Valkering et al. [53] noted the benefit of SBS-modified asphalt binders, including their efficient dispersion at high temperatures, ability to form a continuous polymer network on cooling, and improved elasticity and temperature susceptibility. Furthermore, SBS-modified asphalt binders have demonstrated superior ageing resistance, blend stability, higher softening points, relatively better cohesive strength, and recyclability [54]. Despite the added cost due to polymer modification, SBS-modified asphalt binder have been successfully used to enhance the performance of flexible pavements [55].

Asphalt is a complex material, from both chemical composition and physical properties perspectives. To better characterize asphalt materials, several test methods and protocols have been developed with the aim of quantifying its engineering properties and ultimately estimating its in-service performance. However, it would be challenging to accurately characterize the performance of Polymer-Modified Binders (PMB) using most of the existing tests that measure the materials properties within their Linear ViscoElastic (LVE) region, such as the Ring-and-Ball Softening Point (SPt) test (AASHTO T53) and the inverse of the loss compliance ($G^*/\sin \delta$) test (AASHTO T315) [6]. To better characterize asphalt, more recently developed tests can be used to evaluate the materials over a wider range of temperatures,

strain, stress levels. Linear Amplitude Sweep (LAS) test (AASHTO T391) and the Multiple Stress Creep Recovery (MSCR) test (AASHTO T350) [6-8] are examples of such test methods. These binder tests are intended to provide an estimation of the fatigue and rutting performance of the asphalt concrete mixtures prepared with the same binder.

Cracking of flexible pavements is considered as one of the major failure mechanisms and distress modes, especially in recent years and after the introduction of Superpave mixes. To meet this challenge, various cracking tests for asphalt mixtures have been developed during the past two decades. The National Cooperative Highway Research Program (NCHRP) 9-57 published a comprehensive literature review of these tests in 2016, including the review of test standards, cracking parameters, configuration, variability, simplicity, sensitivity to mix design parameters, and equipment cost and availability [59]. In 2017, Zhou et al. [5] proposed the IDEAL-CT (Indirect Tensile Asphalt Cracking Test) as a new testing protocol. Results from this research suggested that the cracking index from IDEAL-CT (CT_{index}) can provide a good correlation with the field performance of asphalt mixtures. The CT_{index} has become a popular tool for quality control of asphalt mixtures due to its efficiency and simplicity [11–13]. Studies have revealed that the CT_{index} works particularly well for unmodified or reclaimed asphalt, which can become brittle under certain loading conditions [10–12]. In order to broaden its applicability, ASTM International (ASTM) has adapted the test protocol under ASTM D8225 [62]. However, the original development of the CT_{index} was not designed to consider elastomer-modified asphalts, which exhibit a significantly more extended elastic range. The IDEAL-CT procedure was followed in this research, and the load-displacement curves were generated. In addition to CT_{index} , several indices from the Indirect Tensile (IDT) test were calculated for comparison, including the Flexibility Index (FI), the Cracking Resistance Index (CRI), and the Fracture Strain Tolerance (FST). This chapter investigates the performance of these indices in comparison with the IDEAL-CT results.

The use of ultrasonic wave propagation methods in asphalt concrete testing has been explored in recent years, with varying levels of success [15], [63], [64]. Ultrasonic wave characteristics, such as its velocity and attenuation, depending on the material properties, such as mass density, microstructure, and elastic modulus [65]. Therefore, wave characteristics can be used to measure changes in the medium [66]. The most commonly used non-destructive testing (NDT) method for concrete quality assessment is the ultrasonic pulse velocity (UPV) test, which uses wave velocity to estimate the modulus of specimens. However, for heterogeneous, high-damping materials, like asphalt concrete, the current wave velocity

analysis method may not be sufficient to capture the microstructural changes in the material. Popovics & Popovics, (1992) proved that the wave velocity alone is inadequate to estimate the material strength reliably [66]. Wave attenuation analysis is more sensitive than wave velocity in detecting system characteristics. However, limited research on using this analysis approach on bituminous material has been done so far. Amplitudes related to wave characteristics to assess the quality of Marshall hot mix asphalt specimens with various compaction levels has been studied, and it showed that wave attenuation could be used in assessing the in-situ asphalt concrete [15]. The review of the existing literature indicates that using the wave attenuation method has the potential to evaluate the quality of asphalt concrete mixtures.

It should be noted that this study builds on a comprehensive experimental study conducted in the past by Aurilio et al. (2018), where they compared the performance of SBS modified asphalt binders by using the MSCR test [67] and the LAS test [8]. Therefore, utilizing the same materials in this study has provided a unique opportunity to evaluate the capability of the UPPT wave attenuation technique and IDEAL-CT in better understanding the behaviour of polymer-modified asphalt mixes with different SBS contents. This chapter aims to explore the potential of ultrasonic pulse propagation test (UPPT) and IDEAL-CT in characterizing the performance of elastomer-modified asphalt concrete mixtures by comparing their results with the corresponding results from the MSCR and LAS tests on the same asphalt binder. Additionally, pulse propagation in asphalt mixtures is analyzed with several wave attenuation methods. The wave characteristics from UPPT measurements are compared with those of the IDEAL-CT conducted on the same specimens.

3.1.1 Theoretical Background of Cracking Test Indices

Some of the indices used in this research were originally developed for the indirect tensile test whereas some were adapted from the semi-circular bending (SCB) test and modified by Seitllari et al.[61]. The following sections will discuss these indices in detail.

3.1.1.1 Cracking Test Index (CT_{index})

Zhou et al. introduced the CT_{index} to measure the cracking resistance of asphalt mixtures [5]. The index is based on Pairs' law and the cracking propagation equation developed by Bazant and Prat [68], as well as the modulus estimation for disk geometry specimens developed by Liu [69]. The CT_{index} is

calculated using Equation 6, and the higher the value, the greater the performance of the asphalt mixtures.

$$CT_{index} = \frac{G_f}{|m_{75}|} \times \left(\frac{l_{75}}{D} \right) \quad \text{Equation 6}$$

where G_f is the fracture energy, $|m_{75}|$ is the slope at 75% of peak load, l_{75} is the displacement at 75% of peak load, and D is the diameter of the specimen.

3.1.1.2 Flexibility Index (FI)

The Flexible Index (FI) is used to measure the cracking performance of an asphalt mixture. The index is defined by Equation 7 in AASHTO TP124-16 and is calculated as the ratio of the fracture energy to the slope of the inflection point of the post-peak load-displacement curve, taking 75 percent of the peak load point. A higher index value indicates a better cracking resistance of the asphalt mixture.

$$FI = \frac{G_f}{|m|} \times 0.01 \quad \text{Equation 7}$$

where $|m|$ is the slope at the post-peak inflection point.

3.1.1.3 Cracking Resistance Index (CRI)

The SCB test is used to evaluate the cracking potential of asphalt mixtures [70]. The cracking resistance is determined by normalizing G_f using the peak load value (P_{max}), as shown in Equation 8. Higher CRI values indicate that the material is more brittle.

$$CRI = \frac{G_f}{|P_{max}|} \quad \text{Equation 8}$$

3.1.1.4 Fracture Strain Tolerance (FST)

The FST index was developed by Apeageyi et al. for the low-temperature fracture test utilizing the DCT test [18]. The index is the ratio of the fracture energy to the fracture strength and is expressed in Equation 9.

$$FST = \frac{G_f}{S_f} \quad \text{Equation 9}$$

where S_f is the fracture strength, $S_f = \frac{2P_{max}}{t \times D}$, t is the thickness of the specimen, and D is the diameter of the specimen.

3.2 Thoracal Background of Signal Processing

3.2.1 Wave Velocity Equations

An ultrasonic wave can propagate through a material by oscillating particles. The longitudinal waves, also known as compression or primary waves (P-wave), travel in the longitudinal wave propagating direction. The particles oscillate in parallel with the wave propagating direction. P-waves are the fastest among all modes and can be used to study the material's elastic properties. For elastic material, the velocity of the P-wave can be estimated using Equation 10. Likewise, the velocity of shear waves (aka secondary wave or S-wave), which make the particles oscillate perpendicular to the wave propagating direction, can be calculated using Equation 11 as expressed by V_s . Therefore, the S-wave velocity can be calculated from the P-wave velocity based on their interrelationship, as presented by Equation 12. Given that the mechanical properties of asphalt concrete materials change with testing temperature and loading frequency, the value of Poisson's ratio of the specimens was adopted from the literature [64]. In this study, for all specimens, 0.285 was used for the Poisson's ratio at the selected test temperature.

$$V_P = \sqrt{\frac{E(1-\nu)}{\rho(1+\nu)(1-2\nu)}} \quad \text{Equation 10}$$

$$V_S = \sqrt{\frac{E}{2\rho(1+\nu)}} \quad \text{Equation 11}$$

$$V_S = V_P \sqrt{\frac{(1-2\nu)}{2(1-\nu)}} \quad \text{Equation 12}$$

where ρ is density, ν is Poisson's ratio, and E is Young's modulus for an elastic material. When a viscoelastic material undergoes high-frequency loading, it can be treated as an elastic material, and its elastic property can be quantified using the velocity from the above equations. However, this application inherently includes some approximations.

3.2.2 Fourier Transformation

Fourier Transformation can transfer the signal from the time domain to its frequency domain counterpart. The signals in the frequency domain generated from the source and received in the receiver with the measured data have been successfully imitated by changing material properties in the past [72].

The mathematical explanation of these transforms is widely available [73]. A Fast Fourier Transform (FFT) computes the discrete Fourier Transformation with a resolution in the frequency domain depending on the sampling frequency of the test. By applying the FFT algorithm a series of dot products between the signal and complex sine waves is calculated. Each sine wave has a unique frequency, and the magnitude of the dot product describes the relationship between the signal and the sine wave at this frequency. A frequency spectrum of the time signal can be generated by plotting the magnitude of the dot production versus the corresponding sine wave frequency. Both the time and frequency domains contain crucial information about the characteristics of the signals.

3.2.3 Wave Attenuation

Ultrasonic waves can travel long distance, however, they will eventually experience attenuation due to absorption and scattering by objects in their surrounding environment. This attenuation is an exponential decrease in the amplitude of the wave and is caused by the fact that the high-frequency sound waves interact with the particles in their surroundings.

The SBS polymer is dispersed throughout the asphalt cement creating an elastic crosslinked network. This phenomenon generally improves the asphalt concrete performance by increasing the stiffness and changing the materials response to loading. These changes to the asphalt concrete physico-chemical properties may contribute to wave absorption loss in the viscoelastic matrix or enhance the contacts between the particles and promote wave propagation. Therefore, by comparing the output signal attenuation, the characteristics of asphalt concrete specimens can be evaluated.

3.3 Materials and Methods

3.3.1 Materials Selection and Volumetric Design

For this study, two groups of asphalt concrete mixes were prepared using PG 58-28 and PG 64-28 as the base binder. The mixes incorporated 0, 2, 3, and 4% dosages of Styrene-Butadiene-Styrene (SBS) polymer by weight of the binder. Additionally, two different sources of SBS, namely SBS-A and SBS-B, were used in the research. It has been previously established that the addition of SBS polymers to asphalt cement affects the microstructure of the asphalt concrete and can improve its mechanical performance [74]. The recommended practice for laboratory-scale modification of the asphalt binders was followed carefully. Details of the blending process can be found in a previous publication by the

authors [58]. Asphalt concrete specimens were prepared according to the Superpave mix design for SP12.5-FC2, as noted in Table 3-1. A minimum of three replicates were prepared for each mixture type. The bulk specific gravity and air void levels of each specimen were calculated in accordance with AASHTO T166 and AASHTO T209, respectively. The specimens were compacted using a Superpave Gyratory Compactor to a height of 62 mm and a diameter of 150 mm. The specimens were short-term aged prior to compaction. A target air void level of 6.5 ± 0.5 percent was successfully achieved.

Table 3-1. Superpave 12.5 FC2 Asphalt Mix Design

Property		SP 12.5 FC2 Mix
Gradation	Sieve Size (mm)	Percent Passing (%)
	12.5	96.0
	9.5	84.0
	4.75	56.4
	2.36	40.4
	0.075	5.5
Air Voids (%) at N_{design}		3.8
Design Mineral Aggregate, VMA (%)		16.1
Voids Filled with Asphalt, VFA (%)		76.2
Asphalt Cement Content (%)		5.2
Dust Proportion		1.1

3.3.2 Methodology

The presented study employs two major methodologies, namely experimental and analytical methods. The first part of the experimental work examines the ability of the IDEAL-CT to characterize SBS modified asphalt concrete mixes. In an effort to assess the reproducibility of the results, two pieces of equipment were employed. The acquired data was then analyzed and translated to different existing indices (i.e., FI, CRI, and FS as introduced before), with the objective of finding a reliable index that can characterize the elastomer-modified asphalt concretes under the IDT mode.

The second part of the study focuses on the analysis methods of the UPPT measurements. To this end, the traditional time-of-flight (TOF) and the elastic modulus estimation analysis techniques were employed, as well as two wave attenuation quantification approaches. With respect to the wave attenuation analysis, the first method compared Fast Fourier Transform (FFT) areas and used wave energy loss to characterize the mixture. Whereas, the second approach estimated the arrival of the compression, shear, and reflected waves, which were then windowed into two waveforms and converted into the frequency domain using the FFT. The magnitude of the frequency spectra is used to evaluate the absorption loss in the viscoelastic matrix, which is evidenced by the decrease in wave amplitude.

Finally, the cracking resistance and viscosity behavior of both asphalt binder and mixture was compared. The LAS and IDEAL-CT test results were used to compare the cracking resistance of the elastomer-modified asphalt. Additionally, the UPPT results were compared to the MSCR results to establish a correlation between the ultrasonic wave attenuation characteristics in asphalt mixtures with the creep characteristics of SBS-modified asphalt binders. Figure 3-1 presents the methodology employed in this research. It offers a concise summary of the steps taken to complete the study.

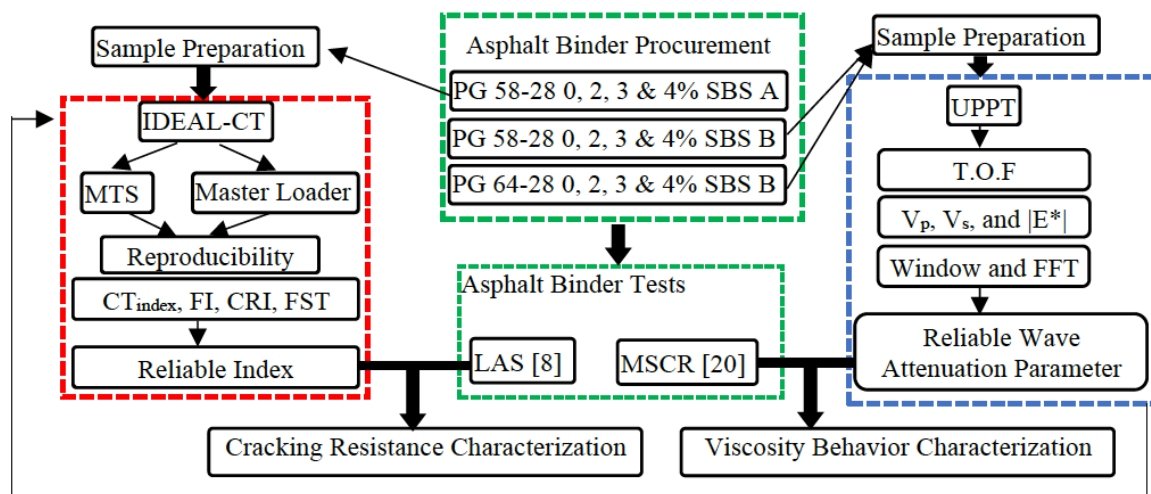


Figure 3-1. Flow chat of the methodology

3.3.3 Indirect Tensile Asphalt Cracking Test (IDEAL-CT) Procedure

For this study, the IDEAL-CT was conducted according to ASTM D8225 at room temperature with a constant loading rate of 50mm/min. Two loading devices were used, an MTS 810 test system and a

Humboldt Master Loader device of model HM-3000. The MTS system is equipped with a servo-hydraulic loading mechanism, and a 100kN load cell for measuring load magnitude, and a conditioning chamber. Data was collected from the actuator LVDT and the load cell at a rate of 10 Hz/channel. The Master Loader device uses a electromechanical stepper motor to drive the plate at a constant loading rate, and the loading strips were a part of the test fixture. Data acquisition rate in this device was 6 Hz. The ASTM D8225 requires a data acquisition rate of 40 data points per second, however, neither of the two devices met this requirement [14]. Since the Master Loader did not have an environmental chamber, all the specimens were tested within two hours of the required temperature conditioning, and it was verified that the temperature variation remained within the recommended range of $\pm 1^\circ\text{C}$.

3.3.4 Ultrasonic Pulse Propagation Test (UPPT) Procedure

The UPPT setup is shown in Figure 3-2. A pulse was generated with the function generator, and then sent to the oscilloscope and amplified with the piezo driver. The amplified pulse is then sent to the transmitter. A sample is sandwiched between a transmitter and a receiver. The transmitter and the receiver are piezoelectric crystals that can transform electric currents into ultrasonic waves. These piezoelectric sensors are attached to the sample using a coupling agent such as vacuum grease. The output signal received from the receiver is transferred to the low-pass filter to eliminate the ambient frequency and then sent to the oscilloscope. The low-pass filter can remove the electronic noise. Both input and output signals can be recorded and stored for postprocessing. The TOF of the first arriving wave that passes through the specimen can be estimated by comparing the signals recorded from the transmitter and the receiver. By measuring the distance (L) between two sensors, the group compression wave (V_p) can be calculated using L/t . The schematic test setup is shown in Figure 3-3, and an example of the recorded signals and group P-wave travel time is presented in Figure 3-4.

As discussed earlier, the group P-wave velocity for the materials investigated in this study was about 3450 m/s. To receive a clean signal, the thickness of the sample should be large enough to cover at least two wavelengths of the emitted signal [75]. Therefore, the 150 kHz transducers were used, as the wavelength of the signal would be approximately 2.3 cm, which is smaller than half of the thickness of the specimen.

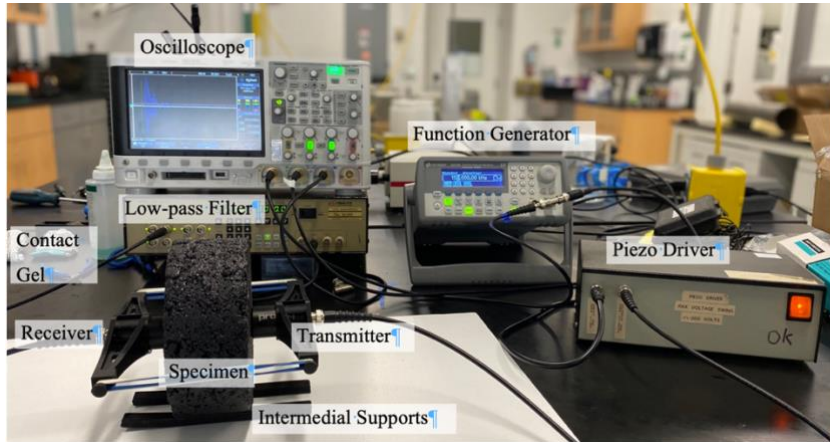


Figure 3-2. Photo of UPPT setup

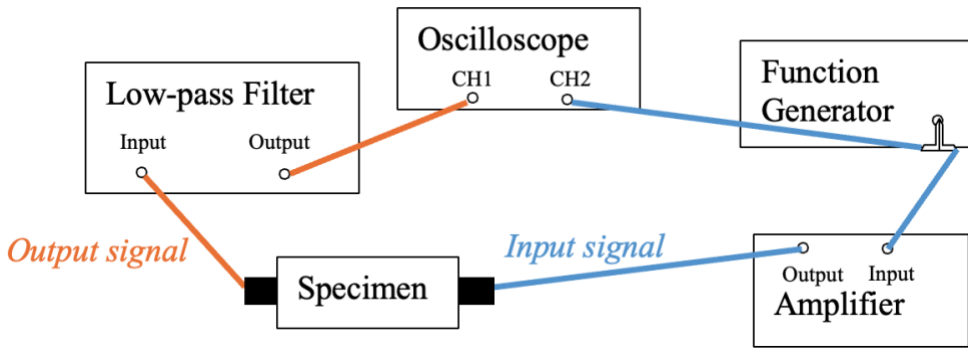


Figure 3-3. Schematic UPPT test setup

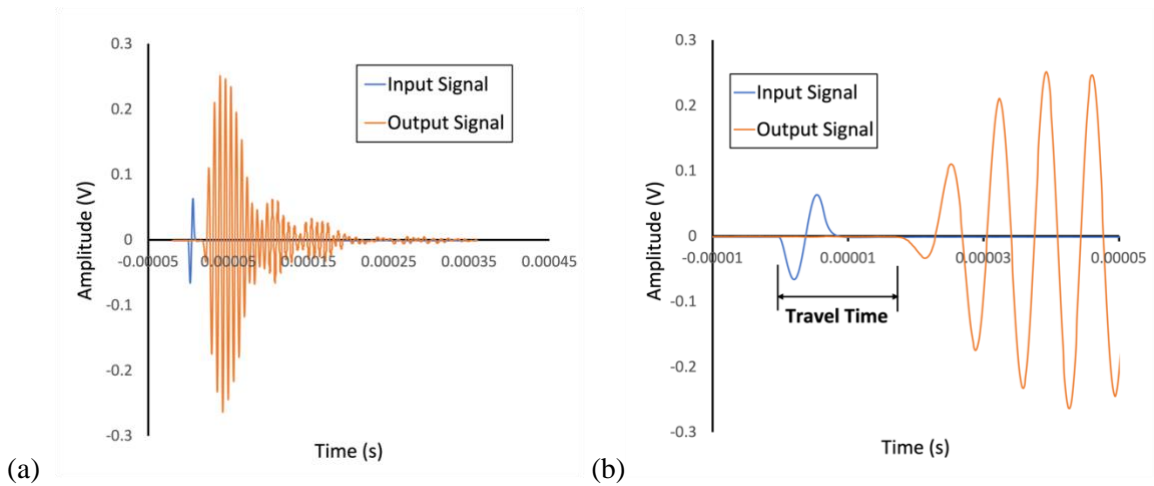


Figure 3-4. Example of (a)input and output signals (b) travel time

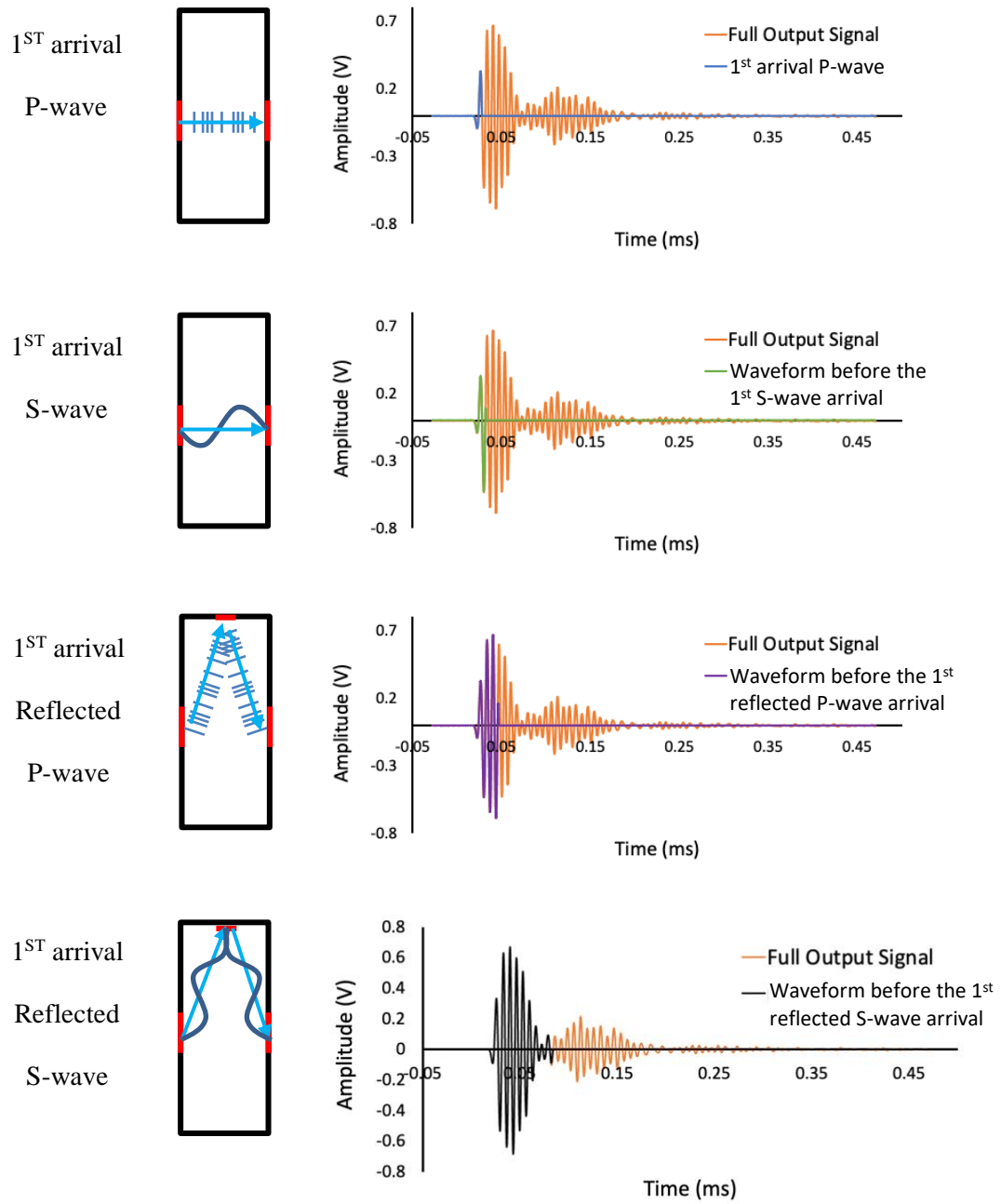


Figure 3-5. Schematic of wave propagation and windowed signal

The signal amplitude is highly sensitive to the contact between the specimen and the ultrasonic transducer [76]. As the asphalt concrete surface typically has a non-uniform and rough macrotecture, maintaining full contact with the platen of the transducer requires filling the gap using an appropriate

coupling agent. Therefore, adequate amounts of the coupling gel were applied to the interfaces until the magnitude of the output signal was stabilized. Consequently, the amount of the applied gel was not constant among the specimens, however, the goal was to keep it to the minimum amount that was needed to establish an acceptable wave transmission.

Based on the specimen's geometry, the fastest wave pathway (without scattering and maximum one-time reflection) can be estimated, as shown in Figure 3-5. Since the P-wave and S-wave velocity can be calculated using the test setup and equations mentioned earlier, the arrival time of the first S-wave, the reflected P-wave, and the reflected S-wave can be estimated. The signal can be windowed into two waveforms based on the arriving time of the group waves to ensure the consistency of the analysis approach. By comparing the changes in the amplitude of frequency spectra, the absorption of the energy can be estimated. The windowed signal is schematically presented in Figure 3-5.

3.4 Results and Discussion

3.4.1 IDEAL-CT Verification

Monotonic load was applied in IDT mode to the polymer-modified asphalt concrete specimens using two different devices at a relatively fast rate of 50 mm/min. Visual inspection of the specimens after breaking revealed that all the specimens experienced cohesive failure and no aggregate cracking was observed. By comparing the four indices calculated based on the test results, it can be concluded that the CT_{index} and the FI yielded similar results. Both of these indices employ fracture energy and the post-peak inflection point to assess the cracking resistance of asphalt mixtures. Similarly, the CRI and FST, which quantify the brittleness of the specimens, provided the same trends with and were only different in terms of their magnitudes. Figure 3-6 illustrates the comparison of the different indices used in this study. The error bar in the plot represents first standard deviation from three replicates. The results of testing the SBS-B samples using the MTS equipment showed an increase in elasticity with higher SBS concentrations; however, cracking resistance decreased. The corresponding results obtained using the Master Loader indicated a more brittle behaviour than expected, but with a clearer trend when considering the SBS-B concentrations. When testing the SBS-A specimens with the Master Loader, a clear difference could not be recognized in terms of different SBS concentrations. Additionally, the CT_{index} displayed a more scattered trend compared to the other indices. This could be attributed to the fact that CT_{index} calculation relies on post-peak response of the specimens, which is known to be subject

to more variability due to the randomness of damage evolution in the specimens. It should be also noted that presence of polymer modified asphalt binders can also affect the post-peak behaviour of asphalt mixtures as compared to the conventional unmodified mixes. It is anticipated that the polymer modified specimens exhibit a more ductile behaviour, which can deviate from the linear elastic assumptions where the index calculation is originally rooted in.

When the same material tested on different equipment, the results of the indices revealed unexpected behavior as the concentration of SBS increased. Table 3-2 shows that there was no significant differences between each SBS B group when analyzing using CT_{index} for specimens tested on MTS. CRI cannot identify the difference for the specimens tested by the Master Loader.

Table 3-2. ANOVA Table for CT_{index} and CRI

		Source Variation	of	SS	df	MS	F	P-value	F _{crit}
CT _{index}	SBS on MTS	Between Groups		29590	3	9863	9.54	0.01	4.07
		Within Groups		8274	8	1034			
		Total		37864	11				
	SBS on MTS	Between Groups		2210	3	737	0.41	0.75	4.07
		Within Groups		14487	8	1811			
		Total		16696	11				
	SBS on Master Loader	Between Groups		40861	3	13620	7.60	0.01	4.07
		Within Groups		14335	8	1792			
		Total		55197	11				
	SBS on Master Loader	Between Groups		44497	3	14832	4.28	0.04	4.07
		Within Groups		27751	8	3469			
		Total		72248	11				
CRI	SBS on MTS	Between Groups		50554	3	16851	6.71	0.01	4.07
		Within Groups		20105	8	2513			
		Total		70659	11				
	SBS on MTS	Between Groups		89421	3	29807	7.58	0.01	4.07
		Within Groups		31450	8	3931			
		Total		120871	11				
	SBS on Master Loader	Between Groups		4255	3	1418	0.49	0.70	4.07
		Within Groups		22940	8	2868			
		Total		27196	11				
	SBS on Master Loader	Between Groups		23011	3	7670	1.99	0.19	4.07
		Within Groups		30883	8	3860			
		Total		53894	11				

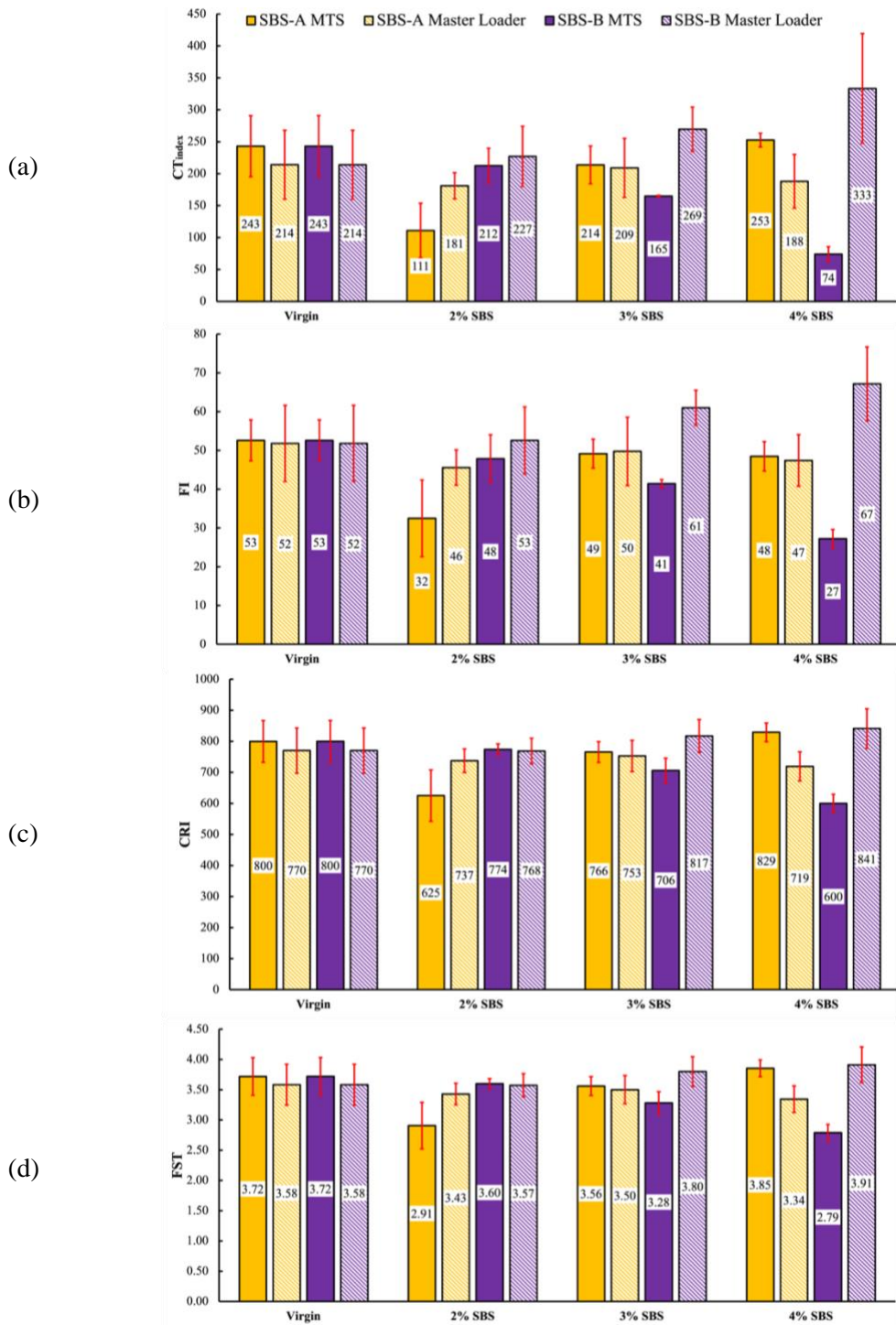


Figure 3-6. (a) CT_{index} , (b) FI, (c) CRI, and (d) FST comparison plots

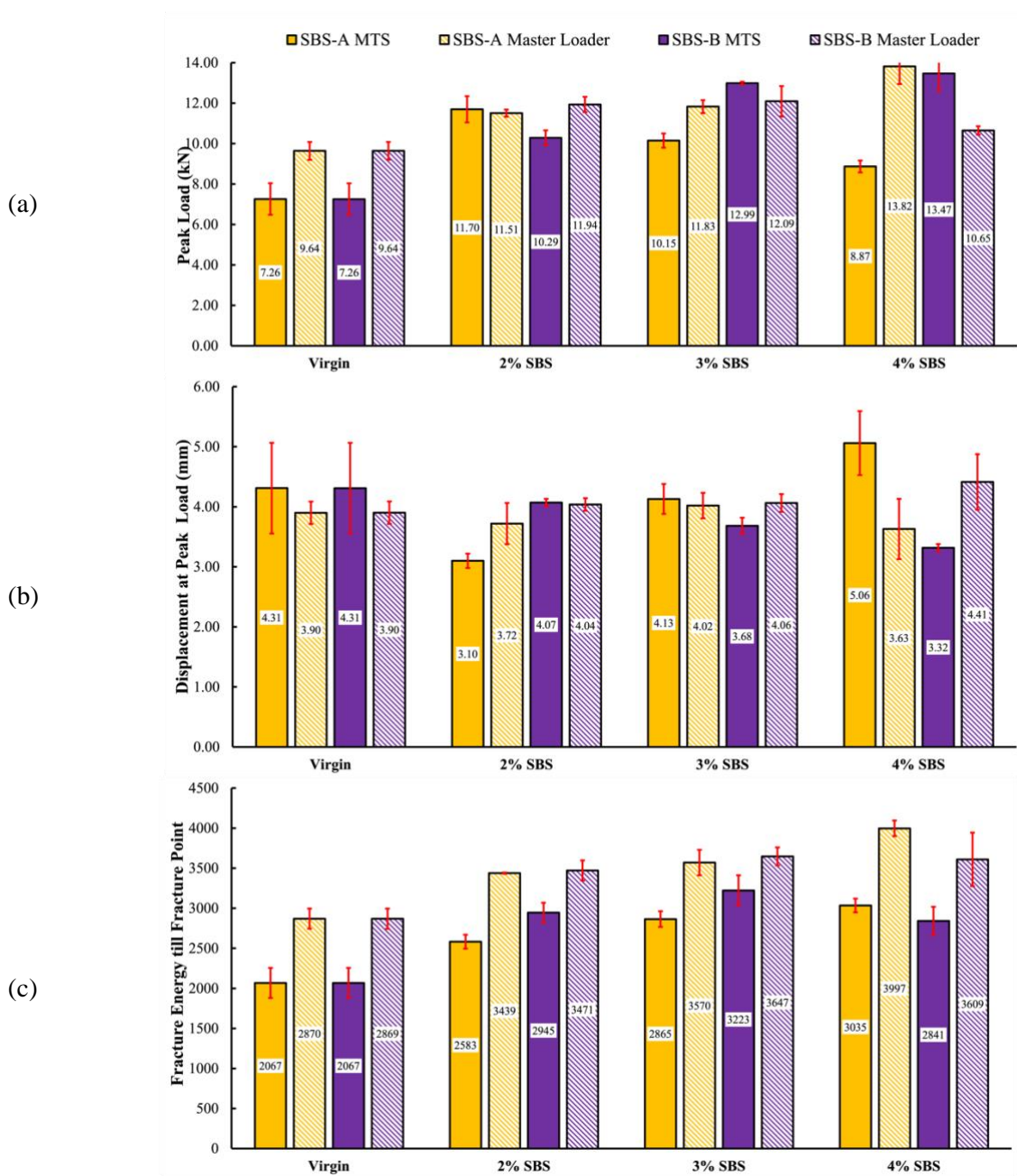


Figure 3-7. (a) Peak Load, (b) Displacement at Peak Load, and (c) Fracture Energy till Fracture Point comparison plots

To further investigate this phenomenon, it was deemed necessary to review the raw data to determine the source of this discrepancy in the results. To this end, Figure 3-7 presents the peak loads, displacement corresponding to the peak load, and the fracture energy till the fracture point to rank and

compare the different mixes. From Figure 3-7, it can be recognized that using the two loading equipment resulted in different trends of changes depending on the SBS concentration. Similar observations can be made when looking at the results for the SBS-A and SBS-B specimens. For the SBS-A group, the peak load increased with an increase in polymer concentration when Master Loader was used while the MTS equipment showed an inverse trend. For the SBS-B group, the peak load increased in relation to the MTS equipment, and the trend was not clear when Master Loader was used. The variation in SBS composition may explain the reversal of trends observed in this research. The overall trend in Figure 3-7(a) appears to be an increase in the peak load with an increase in the SBS concentration. However, the peak load magnitudes from different devices differ from each other to some extent. The discrepancy in magnitudes may be attributed to several factors such as: i) the inherent differences in the loading mechanism between a servo-hydraulic and an electrostatic loading device, ii) the potential variability of the prepared specimens, and iii) the test temperature variation, yet it is difficult to ascertain the exact cause of the variation. Studying the displacement values corresponding to the peak loads, it can be recognized from Figure 3-7(b) that the observed trends of changes are not generally sensitive to the changes in SBS content and/or testing equipment. On the other hand, when comparing the fracture energy values computed unto the specimens fracture point, a consistent trend can be observed when loaded with different devices.

It can be concluded that the peak load magnitude and its corresponding displacement value cannot be used alone to evaluate the fracture behaviour of polymer-modified asphalt mixtures. Although trends of changes for these values could be identified as a function of the SBS content of the specimens, the results were not necessarily consistent. Despite the differences in fracture behaviour between elastomer-modified asphalt mixtures and conventional asphalt mixtures, the current indices used to characterize the performance of asphalt mixtures may not be adequate to accurately assess the performance of SBS-modified specimens. As an alternative, the fracture energy till the fracture point can be used to measure the cracking resistance of elastomer-modified asphalt concrete mixtures.

3.4.2 Wave Attenuation Analysis

Non-destructive ultrasonic testing was conducted on the specimens with the same input signals, and the output signals were collected for analysis. Table 3-3 presents the signal travel time for each specimen. Table 3-3 indicates that the modulus values measured for different replicates of each mix type yield very similar results, which can indicate the high repeatability of the test. However, when comparing

different mix types, the results indicate that the wave velocity approach cannot distinguish the differences in the modulus of the specimen with similar volumetric properties. This is somehow expected as the wave velocity mainly reflects the bulk properties of the specimens at the very high frequency ranges that can be associated with the upper asymptote of the modulus master curve for a viscoelastic material.

Theoretically, ultrasonic waves lose energy as they propagate through the specimen. The energy in the time signal positively correlates with the area under its corresponding frequency spectra. Therefore, the area under the FFT can be used to estimate the energy in the received signals. Two analysis approaches were used in this research. The first approach applied the FFT on the full signal. Whereas, the other approach windowed the signal into two waveforms and then transferred it into its frequency domain with FFT.

Figure 3-8 shows the area under the full signal FFT. Unlike the high-frequency modulus values (in Table 3-3), the output wave energy can be an excellent indicator to characterize the asphalt concrete mixes as it shows a clear trend of changes with the increase in the SBS content of mixes. To avoid any discrepancies due to the testing configuration, the characteristics of the input signal were kept the same among all the specimens. Therefore, it can be expected that the asphalt mixtures with a more viscous asphalt binder would absorb more wave energy so that the energy of the corresponding output signal would diminish as compared to the other softer groups of specimens. In addition, the SBS polymers might have improved the binder adhesion to the aggregates or even the stiffness of the specimens, which can explain why the FFT areas of the modified specimens are larger than the unmodified ones.

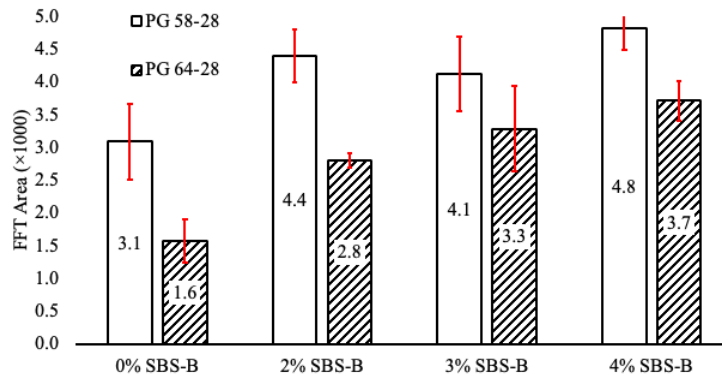


Figure 3-8. FFT Area for full output signals

Table 3-3. Summary of Specimen Properties

Specimen		Number of Gyration	Bulk Specific Gravity	Air Voids (%)	Time of Flight (T.O.F) (ms)	Elastic Modulus (MPa)
PG 58-28	0% SBS -B1	33	2.490	6.52	0.0182	22.3
	0% SBS -B2	35	2.486	6.69	0.0172	25.0
	0% SBS -B3	43	2.495	6.34	0.0167	26.6
	2% SBS -B1	61	2.488	6.66	0.0180	22.8
	2% SBS -B2	53	2.473	7.21	0.0185	21.5
	2% SBS -B3	61	2.487	6.71	0.0180	22.8
	3% SBS -B1	77	2.495	6.64	0.0175	24.2
	3% SBS -B2	66	2.485	7.01	0.0175	24.1
	3% SBS -B3	61	2.495	6.62	0.0187	21.2
	4% SBS -B1	109	2.500	6.65	0.0175	24.3
	4% SBS -B2	68	2.491	7.00	0.0185	21.6
	4% SBS -B3	60	2.487	7.15	0.0187	21.1
PG 64-28	0% SBS -B1	64	2.502	5.95	0.0177	23.7
	0% SBS -B2	50	2.497	6.15	0.0172	25.1
	0% SBS -B3	54	2.492	6.34	0.0170	25.6
	2% SBS -B1	31	2.499	6.10	0.0172	25.1
	2% SBS -B2	50	2.482	6.76	0.0177	23.5
	2% SBS -B3	41	2.490	6.45	0.0170	25.6
	3% SBS -B1	38	2.490	6.86	0.0177	23.6
	3% SBS -B2	49	2.480	7.21	0.0177	23.5
	3% SBS -B3	37	2.488	6.92	0.0175	24.1
	4% SBS -B1	38	2.505	6.36	0.0167	26.7
	4% SBS -B2	32	2.508	6.26	0.0172	25.2
	4% SBS -B3	38	2.508	6.26	0.0167	26.7

Four windows have been applied and separated the output signal into two waveforms. The two waveforms were then transformed into the frequency domain using FFT. Figure 3-9 shows the results of the frequency spectra. The windowed waveform in Figure 3-9(a) is much cleaner than 3-9 (b). However, the window distorts the signal range to match the flat ends after zero padding. The window length for the first arrival waves is shorter than the window length for the other part of the signal, and thus the plots in Figure 3-9(b) have a similar shape to the FFT of the unwindowed signal. The dominant frequency in the spectra shifts from 100kHz to 150 kHz due to the dominant wave propagation mode. In this chapter, only the amplitude of the dominant frequency was used. The other feature in Figure 3-9 is that there is a clear drop around 150 kHz due to the low resolution in the frequency spectra using the discrete Fourier transform. As a potential remedy, a wavelet transformation would be able to address this issue. However, exploring wavelet transform was out of the scope of this study.

Figure 3-9 also presents the amplitude at the dominant frequency of the windowed waveform. A statistically significant difference was not found between the specimens. Moreover, the data is more scattered when the windows are narrower. However, based on the average value of the amplitude ratio of the first arrival P-wave spectra, the modified binders absorbed more energy when the P-wave was transmitted through the specimen. A more apparent trend can be seen when the window gets wider and covers more waveforms (See Figure 3-10). In most cases, the amplitude ratio for the PG 64-28 asphalt concrete specimens is larger than that of the PG 58-28 specimens, that might be associated with the improved adhesion and consequently more efficient wave transmission when SBS network is present in the mixtures.

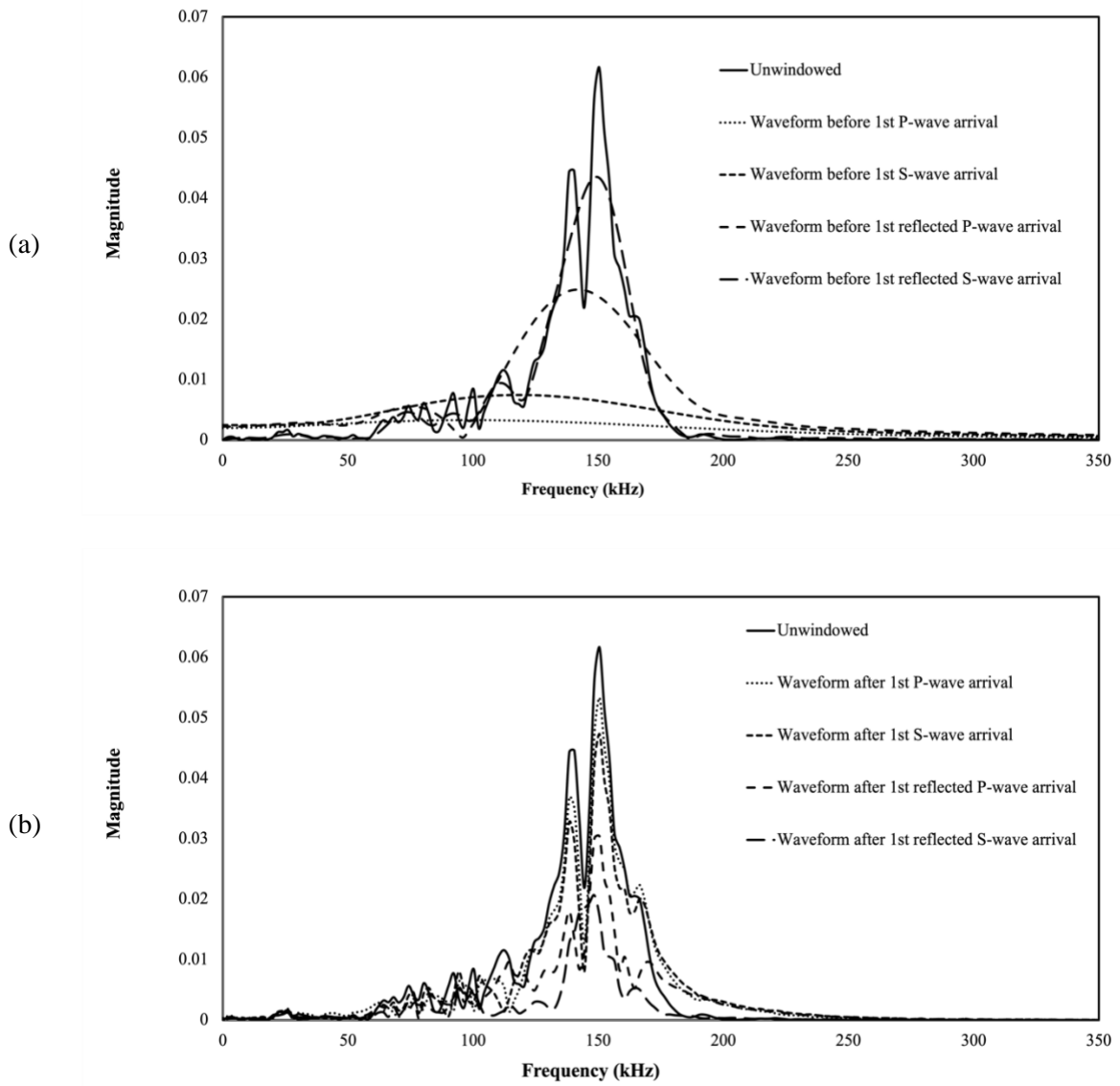


Figure 3-9. Frequency spectra of the windowed waveforms (a) first arrivals, (b) the tail parts

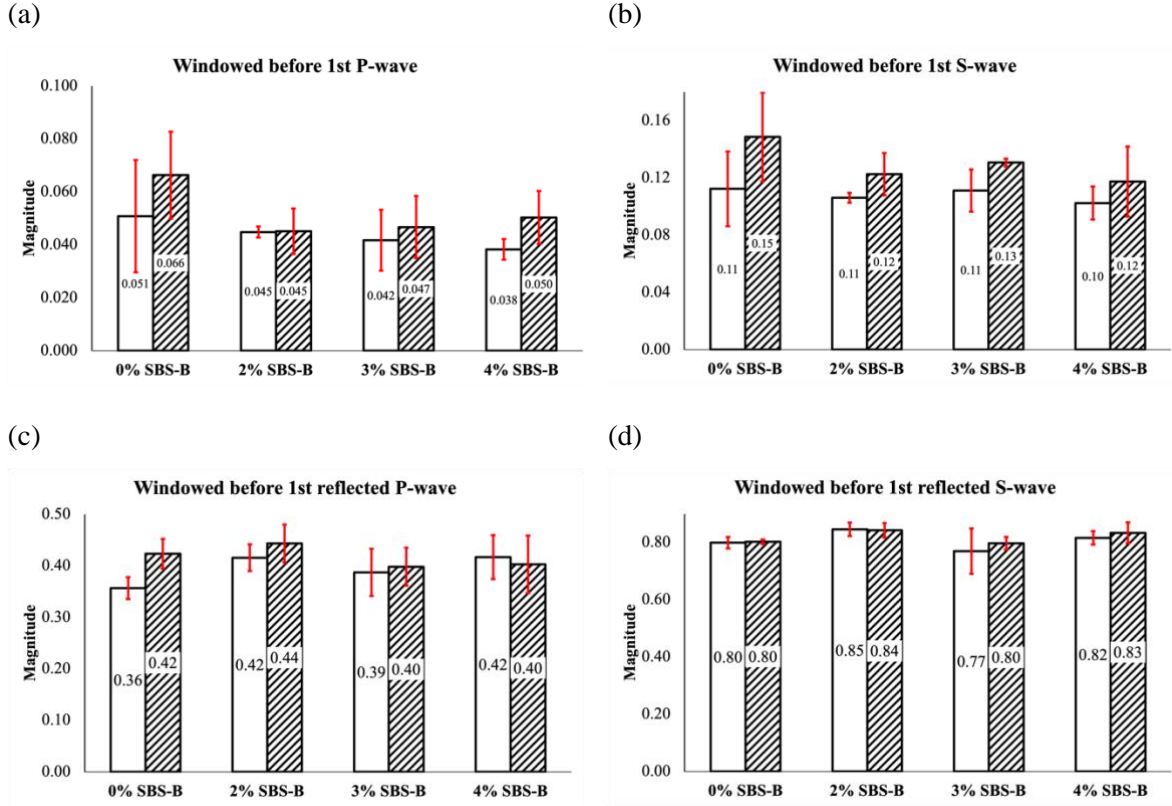


Figure 3-10. Amplitude ratio of windowed and unwindowed dominant frequency

3.4.3 IDEAL-CT and LAS Test Results

A separate group of IDEAL-CT test was conducted after performing the NDT measurements. Figure 3-11 provides a summary of the calculated fracture energy unto the fracture point for the different mixes. The fracture energy was then compared to the wave attenuation results.

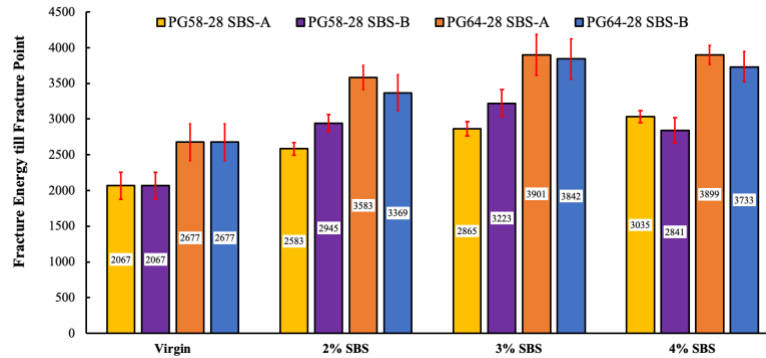


Figure 3-11. Fracture Energy values

Aurilio et al. had previously conducted LAS tests on the very same neat and SBS-modified asphalt binders that were used in this study the [8]. The damage level was set to 50 percent, and the test temperature was 19°C, which corresponds to the intermediate temperature of a PG 58-28 as determined using AASHTO M320. Aurilio et al. reported that the LAS results proved a strong correlation (i.e., $R^2=0.98$) between the number of cycles to failure and the SBS concentration. The binder studies showed that increasing the polymer concentration improved both the SBS-A and SBS-B cracking resistance. Figure 3-12 compares the consistency of fracture energy parameter from the IDT of the mixtures with number of cycles to failure from the LAS test results from the binder study. The plot reveals a strong correlation between the results from the two tests, with SBS-A showing a very good agreement and SBS-B exhibiting a weaker relationship. This difference in a relationship is consistent with both loading devices and may be attributed to variability in sample preparation. The overall trend, however, is in agreement with what is expected.

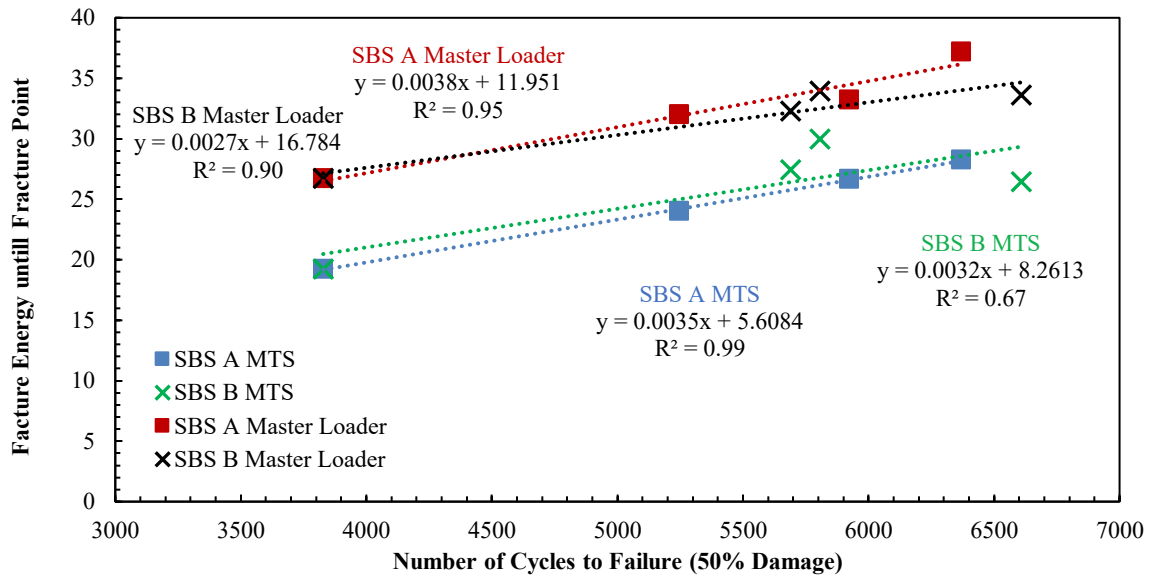


Figure 3-12. Comparison between Indirect Tensile Test and the Linear Amplitude Sweep (LAS) test results

3.4.4 Mix UPPT and Binder MSCR Test Results

In addition to the relationship between the asphalt binder cracking from the LAS test results and the mixture cracking evaluation from the IDEAL-CT, the creep characteristic of the asphalt binder used in this study can also be correlated with the ultrasonic wave attenuation characteristics. The Multiple

Stress Creep Recovery (MSCR) test results for the binders used in this study have been published in a previous publication [67], and their creep compliance (J_{nr}) is shown in Figure 3-13. The compliance generally decreases with the increase in polymer concentration indicating an increase the materials elastic response. This research used the SBS-B modified asphalt binders for asphalt concrete sample preparation.

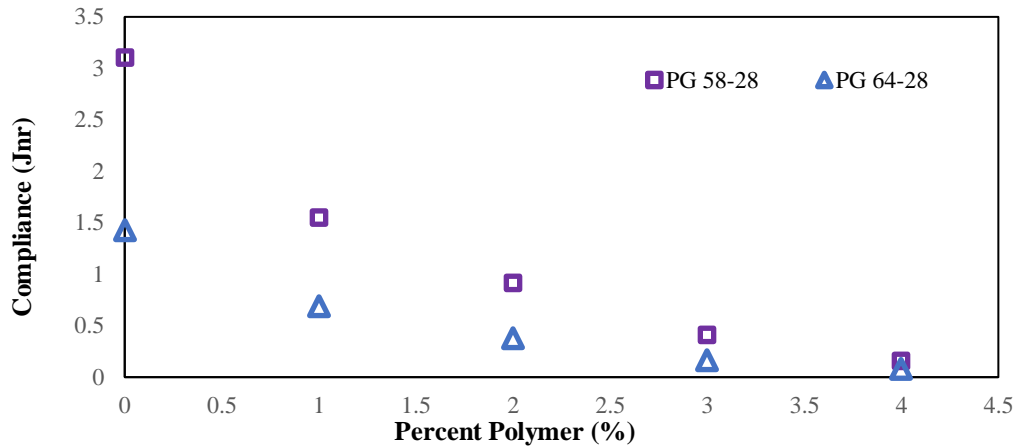


Figure 3-13. J_{nr} vs. Percent polymer [67]

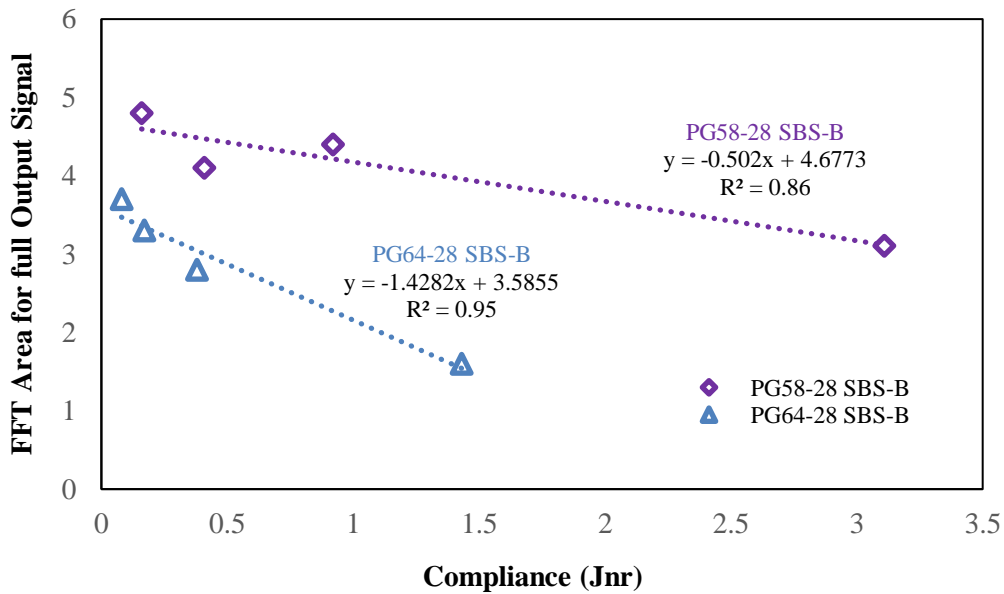


Figure 3-14. Wave attenuation vs. J_{nr}

Figure 3-14 illustrates the relationship between the output signal energy changes and the creep compliance of the binders. The PG64-28 group, which are stiffer, exhibits a significantly lower output signal energy than the other group, indicating that more energy is absorbed during wave propagation. As the polymer concentration increases, the compliance value decreases (see Figure 3-13), whereas the FFT area for the full output signal increases (see Figure 3-8). Thus, the relationship is negatively correlated in Figure 3-14. However, the slope difference between the two groups reveals the amount of wave energy being absorbed during propagation process is not solely dependent on the polymer dosage in the asphalt concrete mixtures. It can be concluded that the wave energy change is more significant when transmitting through a more viscous matrix.

3.5 Conclusions and Recommendations

This chapter investigates the possibility of using IDEAL-CT and wave attenuation methods to assess the quality of asphalt concrete specimens with similar bulk properties. Twelve types of SBS-modified laboratory mixtures (SP 12.5 FC2) were used. Based on the results of this study, it can be concluded that the existing cracking indices, including the Cracking Test index (CT_{index}), the Flexibility Index (FI), the Cracking Resistance Index (CRI), and the Fracture Strain Tolerance (FST) cannot effectively characterize the SBS-modified asphalt concrete behaviour. The fracture energy up to the fracture point was found to be highly correlated with the results of the LAS test, which indicates that this parameter may be a more reliable indicator for assessing the cracking performance of elastomer-modified asphalt concrete. From the results of the UPPT, it can be concluded that a traditional wave velocity analysis is not capable of capturing the differences between the asphalt specimens of the same volumetric properties but containing different polymer contents. However, the repeatability of the test both within replicates and among different mixes was found to be very high. To mitigate this drawback, two wave attenuation approaches were also utilized to study the changes in the asphalt concrete specimens due to different modification methods. The results show that using the energy in the frequency spectra can efficiently distinguish the asphalt concrete with different binder grades in terms of comparing the wave energy absorption. The UPPT results also recognized the trend of stiffness change in the mixtures. The second wave attenuation approach compares the decay in amplitude after windowing the signal based on the group wave arrival time. However, it is very challenging to select the proper window length. A more apparent trend can be seen when a wider window is used for the analysis. However, the effects of adding SBS to the mixture were not clearly capture using this approach. The results of the wave

attenuation analysis show a strong correlation between the received output signal energy with the binder creep compliance values from the MSCR test results. This indicates that the absorption energy is closely related to the viscosity of the medium through which the wave propagates. In addition, the SBS network can improve wave transmission through asphalt concrete.

Further research is necessary to confirm the findings observed in this study and to provide recommendations on the use of IDEAL-CT for evaluating elastomer-modified asphalt concrete. Additionally, potential provisions should be considered with analyzing the test results. For the. The effect of using different aging levels, moisture contents, modifier types, and different binder grades on the UPPT wave characteristics needs to be further studied in the future.

Chapter 4

Dynamic High-Frequency Healing with Rest Period (D2HRP) as a New Test Protocol for Determination of Intrinsic Healing Rates of Bituminous Mixtures

Summary

Asphalt cement has an inherent self-healing ability allowing for the repair of microcracks caused by loading. To assess this capacity, an essential first step is to induce well-controlled micro-damage in the test specimen. Ease of conducting and predictability of crack initiation region in an indirect tensile (IDT) test make it a promising candidate for evaluating asphalt healing. However, the current IDT protocol and analysis method only provide a rudimentary understanding of the material behaviour. Therefore, coupling IDT, as a destructive test to induce damage, with non-destructive testing methods can offer significant benefits, especially for studying the recovery of material properties with and without mechanical loading application. This chapter uses an innovative test setup that combines an interrupted IDT with an ultrasonic pulser/receiver front-end unit to monitor the specimen property changes with higher sensitivity during healing. Several signal processing techniques, such as Fast Fourier Transformation (FFT), Continuous Wavelet Transform (CWT), and Wavelet Synchro Squeezed Transformation (WSST), have been employed to analyze the features of the signal transmitted through the specimen. Windowing the time signal and its frequency spectra at the selected time and frequency, respectively, can be used to eliminate unwanted features of the signals. Comparing the reconstructed signal in the time and frequency domain, it has been determined that applying a window to the frequency spectra is the most effective method for removing unwanted features of the signal. To this end, compacted asphalt concrete specimens prepared with different mix designs, performance graded binders, ageing levels, and modifiers are used. The initial results indicate that this setup can effectively evaluate the asphalt's intrinsic self-healing properties. Moreover, the proposed test can successfully distinguish changes in healing between stiffer and more aged binders.

4.1 Introduction

Self-healing is an intrinsic response of asphalt that can contribute to closing and repairing the microcracks, thus restoring the mechanical properties of the asphalt mixture and ultimately delaying

the occurrence of severe failures in the future. Research into the healing properties of asphalt mixtures began in the 1960s [77]. Many studies have been conducted to understand and quantify the intrinsic self-healing capabilities of bituminous materials [42], [78]. However, the mechanism of the self-healing phenomenon remains unclear due to the complexity of asphalt composition and the complicated mechanical behaviour of the asphalt binder and mixture.

Healing in bituminous material can be seen as the reversal of the fatigue process that involves: (1) crack closing (or wetting) and (2) regaining strength at the wetted crack surface [8], [57]. The first step is the results of the adhesion of two crack surfaces driven together by surface free energy, the material's creep compliance, and the consolidation due to the applied stresses. In contrast, the second step is dominated by molecular diffusion and randomization of asphaltene structures. Wool and O'Connor used a reptation model to estimate the polymer's intrinsic healing rate, which was later adopted to describe the healing process of bituminous material [79], [80]. Lytton correlated the surface free energy of asphalt binders with the rate of the wetting process. The total surface energy was estimated as a combination of nonpolar and polar acid-base components representing physical and chemical bonds, respectively [81]. At the molecular level, the asphalt binder containing more molecules with longer chains and fewer branches would have greater self-diffusivity, so their healing rate should be faster. With the help of the Fourier transform infrared spectroscopy (FTIR), two parameters: the methylene-to-methyl-group (CH_2/CH_3) ratio and the methylene-to-methyl-hydrocarbon (MMHC) ratio, which indicates the length of molecule chains and the amount of branching in chains, were proven to be correlated to the healing capability of asphalt binders [82], [83]. However, self-healing does not rely solely on wetting or diffusion processes. It is impossible to separate them in practice. Moreover, these parameters may not capture the healing capability of asphalt mixtures under external factors, such as damage level, loading methodology, aging condition, temperature, duration of the rest period, etc.

A standard method to quantify intrinsic healing is to compare the material's mechanical properties, such as shear modulus, complex modulus, and strength, before and after the healing process [8], [57], [78]. The asphalt healing test is usually conducted by starting to apply several high-level load cycles to the test specimen, then allowing it to rest or heal at the same or elevated test temperatures. The process can be repeated for several trials till the failure of the specimen. To monitor the properties of the material, a lower level of cyclic loading can be applied to the specimen during the rest period, which theoretically should not induce any damages in the material. However, there are some concerns about this type of test, including the control of damage level, uneven contact surfaces, plastic deformation, and the bias

effects caused by the cyclic loading, such as thixotropy and heating [84]. There is a need to have a test that can control the damage to the material and monitor the healing process without causing any bias effects or disturbing the rest periods.

Non-destructive testing (NDT) is a type of testing that can assess the properties of a material, component or system without causing damage. NDT is beneficial for detecting potential safety hazards, ensuring that materials meet quality standards, and non-intrusively detecting defects in materials. Recent equipment improvements and a better understanding of materials have contributed to the development of this technology. With the rapid advancement of personal computer systems for digital data acquisition and processing in the early 1980s, significant improvements were made in seismic techniques that were previously believed to be impractical [5]. Various NDT methods have been developed and applied in engineering with varying degrees of success by numerous engineering and related research organizations [6], [7], [8]. Several wave-based methods, such as ultrasonic pulse velocity (UPV), impact echo (IE), and spectral analysis of surface waves (SASW), have gained increased use for material property evaluation for decades. NDT methods are faster, more practical, and more economical than traditional destructive methods; they are essential for assessing infrastructure conditions. The use of wave propagation-based methods can be instrumental in studying the characteristics of the induced damage during the mechanical loading process [15]. Such techniques are also unique as they can provide engineering measures of the materials without needing mechanical loading, which is highly important during the rest periods in asphalt crack-healing tests.

This chapter investigates the Dynamic High-frequency Healing with Rest Period (D2HRP) as a novel test protocol to quantify the asphalt intrinsic healing rate based on an ultrasonic wave propagation approach. Combining the ultrasonic pulse velocity test with an indirect tensile (IDT) test, this innovative test protocol allows for direct measurement of the material properties during the rest period without disrupting the healing process. The devices used in the D2HRP test protocol are introduced first. Then the results of eight groups of asphalt mixtures are analyzed and discussed. Several signal-processing methods were used to remove unwanted features from the signals before using them to estimate the healing rate of the asphalt mixtures. Details of the signal-processing methods were provided in the technical background section. Healing rate estimation from direct measurement is proposed using this test protocol. The test was conducted at two intermediate temperatures to study its sensitivity. A comparison among the asphalt mixtures is discussed, and the healing capability of the asphalt mixtures is ranked.

4.2 Theoretical Background

4.2.1 Indirect Tensile Test

IDT test is performed by applying a mechanical loading to a cylindrical specimen with a constant vertical displacement rate until a fracture failure happens. The test provides an indirect measurement of the tensile strength of specimens. The IDT test is simpler and more practical as compared to direct tension test, so it is commonly used for construction materials evaluation. However, a viscoelastic material may experience significant levels of permanent deformation under this type of testing; thus, the failure mechanism would be a combination of rutting and cracking. Therefore, some variations of the test use either lower temperature or a faster loading rate so that the asphalt mixture would exhibit a more elastic behaviour [5], [85], [86]. A load-displacement curve can be generated from these tests. Numerous performance indicators have been developed using the peak load, post-peak inflection point, work of fracture, fracture energy, fracture strength, toughness, etc. [61]. Most of the analyses assumed that the test specimen is elastic and has a brittle failure mode, which is not always the case for asphalt concrete specimens and may need to be revisited.

4.2.2 Fast Fourier Transformation (FFT)

A signal can be considered the sum of a set of sine waves with different frequencies. Fast Fourier transformation computes dot production between a time signal and the set of complex sine waves. The magnitude of a dot product describes the relationship between the signal and the sine wave at a specific frequency. A larger magnitude refers to the sine wave frequency being similar to the signal frequency. By plotting the magnitude of the dot production versus the corresponding sine wave frequency, a frequency spectrum of the time signal can be generated. The frequency set was selected based on the sampling rate. Since the selected frequencies are discrete, the computation rate would be fast, and the resolution of the frequency spectra would be dependent on it. This transform is ideal for stationary signals, which have constant frequency. Equation 13 can be used to apply FFT on a time signal $x[n]$:

$$X[k] = \sum_{n=0}^{N-1} x[n] e^{-j \frac{2\pi n k}{N}} \quad \text{Equation 13}$$

where N is the size of the domain; k and $n \in 0, 1, \dots, N - 1$; $e^{-j\frac{2\pi nk}{N}}$ represents a complex sine wave based on Euler's formula and the sine wave formula, with the angle $\frac{2\pi k}{N}$ uniformly distributed along the unit circle in the complex plane with a total of N points.

4.2.3 Continuous Wavelet Transform (CWT)

The Continuous Wavelet Transform can provide frequency information for a given time period of a signal. It uses convolution of the signal and a wavelet. The convolution uses dot production of the wavelet that slides through a time signal and returns the corresponding magnitudes along with the time series. By changing the wavelet frequency and plotting the convolution results versus the time, a scalogram can be generated, which represents the frequency of a signal over time. The magnitude relates to the similarity between the signal and the wavelet. The summation of all dot product magnitude at the same frequency on the scalogram returns a frequency spectrum of the time signal. For a continuous signal, the frequency spectra created using FFT and CWT are very similar. A typical Continuous Wavelet Transform formula can be expressed by Equation 14:

$$X_{\psi}(a, b) = \frac{1}{\sqrt{a}} \int_{-\infty}^{+\infty} \psi\left(\frac{t-b}{a}\right) dt \quad \text{Equation 14}$$

where $\psi(t)$ is the mother wavelet, which can be used as a basis for constructing other wavelets. It will be scaled by a factor of a and be translated by a factor of b . An example plot of the scalogram and the frequency spectra created using FFT and CWT can be found in Figure 4-1.

4.2.4 Wavelet Synchro Squeezed Transform (WSST)

Wavelet Synchro Squeezed Transformation provides a way to further concentrate the representation from the Continuous Wavelet Transformation. It uses the CWT results and extracts the instantaneous frequencies from it, followed by squeezing the wavelet transforms coefficients that have the same phase velocities into one coefficient. Thus, the WSST eliminates the smearing observed in the scalogram from wavelet transformation, but the coefficients of Wavelet Synchro Squeezed Transform do not match the other methods. A detailed explanation can be found in the literature [87][75]. This time-frequency analysis was used in this research to identify the dominant mode of the signal.

The resonant frequency of the transducers used in this study is 150kHz to ensure that the distance between the transducers is large enough to cover at least three wavelengths of the emitted signal [75]. The P-wave velocity for the materials investigated in this study was approximately 3450 m/s, so the

wavelength was roughly 2.3 cm. The distance between the transducers was approximately 15.2 cm, which was over six times larger than the wavelength. Figure 4-1 shows the frequency and the time-frequency plots (scalograms) when analyzing the same signal with FFT, CWT and WSST. All the plots show that the dominant frequency range is between 100 and 250kHz and centred around the transducer's dominant frequency. The amplitudes of the FFT and CWT in frequency spectra are in good agreement, while the WSST amplitude is significantly smaller than the other amplitudes. The WSST sharpens the time-frequency plot of CWT. It is clearer in the WSST scalogram that three concentrated frequencies are around 30, 60, and 140 kHz.

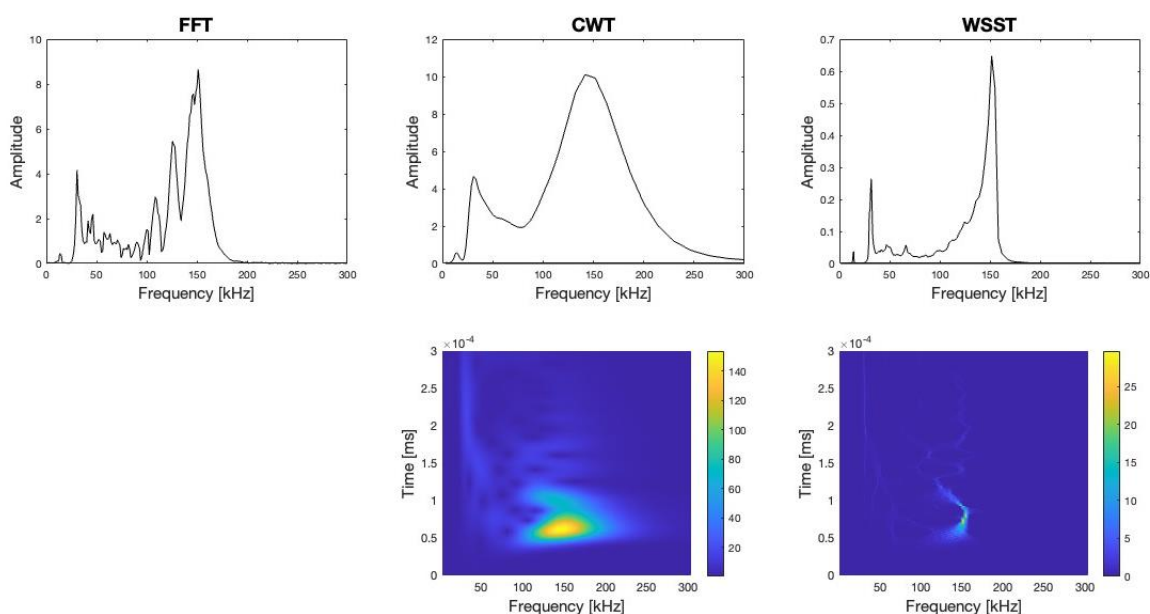


Figure 4-1. Comparison of FFT, CWT, WSST

4.3 Experimental Program

4.3.1 Materials Used

The mixtures used in this study were prepared in accordance with the material specifications for Superpave mixtures SP12.5 and SP12.5FC2 in Ontario, Canada. The detailed properties of the mixes are listed in Table 4-1. The main aggregates used in the SP12.5 FC2 mix design are Ontario Trap Rock (OTR), also known as diabase, from a quarry site on the shores of Lake Huron, while the aggregates used in the SP12.5 mixtures are local limestone aggregates. The hardness, strength and durability of

diabase are better than those of limestone. A total of eight groups of asphalt mixtures were prepared using two mix designs. Three types of mixes were prepared using PG 58-28 and PG 64-28 asphalt, including 1) the control mixes, 2) the experimental mix modified with Styrene-Butadiene-Styrene (SBS), and 3) the experimental mix that was conditioned through storing the specimens in an oven at 85°C for five days to simulate long-term aging conditions.

Table 4-1. Volumetric properties of tested asphalt mixtures

Property		SP 12.5 Mix (M1)	SP 12.5 FC2 Mix (M2)
Gradation (% Passing)	Sieve Size (mm)		
	12.5	95.0	96.0
	9.5	83.0	84.0
	4.75	58.0	56.4
	2.36	40.0	40.4
	0.075	3.0	5.5
Air Voids (%) at N_{design}		4.0	3.8
Design Mineral Aggregate, VMA (%)		14.6	16.1
Voids Filled with Asphalt, VFA (%)		72.6	76.2
Asphalt Cement Content (%)		5.3	5.2
Dust Proportion		0.66	1.1

Four groups of the mixtures followed the SP12.5 mix design, including PG58-28 control, PG58-28 oven-aged, PG58-28 modified with 3% SBS, and PG64-28 control. Similarly, the other four groups of mixtures followed the SP12.5FC mix design. However, the dosage of SBS is changed to 4% by weight for this group of mixtures. Details of the SBS modification process can be found in previous research [58]. M1 and M2 are used hereafter to refer to the SP12.5 and SP12.5 FC2 mixes, respectively. A minimum of two replicates were used for each group. All specimens were initially conditioned for four hours at 135°C before compaction with an AFG2 SUPERPAVE™ Gyratory Compactor to a height of 63 mm and a diameter of 150 mm. The specimen dimensions are the same as the Hamburg Wheel Tracking (HWT) test and the Indirect Tensile Asphalt Cracking Test (IDEAL-CT). Therefore, the results of this test can be directly compared with the other test results. For the long-term aged groups, the loose asphalt mixtures were short-term aged according to AASHTO R30-02 first, then continued with the 5-day long-term aging at 85°C. Afterwards, the specimens were compacted at their designated compaction temperatures. The binder contents were controlled to be $\pm 0.5\%$ with the target binder

content, and the target air void level of $7\pm 1\%$ was successfully achieved for all the specimens. The SP12.5 group specimens were tested at 20°C , while the SP12.5FC2 group specimens were tested at 10°C to compare the temperature sensitivity of the proposed test setup.

4.3.2 Proposed Hybrid Test Setup

Figure 4-2 shows the proposed test setup that was developed in the Center for Pavement and Transportation Technology (CPATT) at the University of Waterloo. A cylindrical specimen is positioned in the IDT test fixture enclosed by an environmental chamber. The test consists of three loading phases, denoted as First Loading Phase (L1), Rest Period (RP), and Second Loading Phase (L2). Figure 4-3 shows a schematic of the test protocol. During both loading phases, an MTS 810 frame with a 100 kN load cell was used to load the specimen in its diametral plain using a constant vertical displacement rate of 1mm/min. The first loading phase (i.e., L1) was stopped right after the peak load was reached. After the first loading phase, a 1-hour rest period was applied. During the rest period, no loading was applied to the specimen. A pair of biaxial displacement extensometers with a gauge length of 75mm and capacity of $\pm 0.55\text{mm}$ were used to measure the geometry changes in vertical and horizontal directions during the first loading phase and the rest period. Extensometers were manually removed from the sample before reloading the specimen in L2 to avoid potentially damaging the instrumentation. The data acquisition rate was set to be 10Hz/channel in the loading phase and 1Hz/channel during the rest period.

An ACS A1560 SONIC-LF, which is a portable pulser-receiver unit that can customize a wide range of ultrasonic measurements and data acquisition, was used simultaneously during the test. Two 150 kHz ultrasonic transducers were affixed radially, aligned with the horizontal extensometer, and confined by the holders and a rubber band, as shown in Figure 4-2. Two "L-shaped" metal pieces were glued on both sides of the specimen to ensure a flat contact surface with the transducers, as well as to prevent the movement of the transducers during the test process. A group of square pulses were sent to the system every 10-second during the loading phases and at least every one minute during the rest period. The received signal is therefore based on an average of a group of output signals, which cancels out the noise and increases the resolution of the data. The received signals were recorded and then analyzed in the postprocessing stage. Details about data analysis are discussed in the next session.

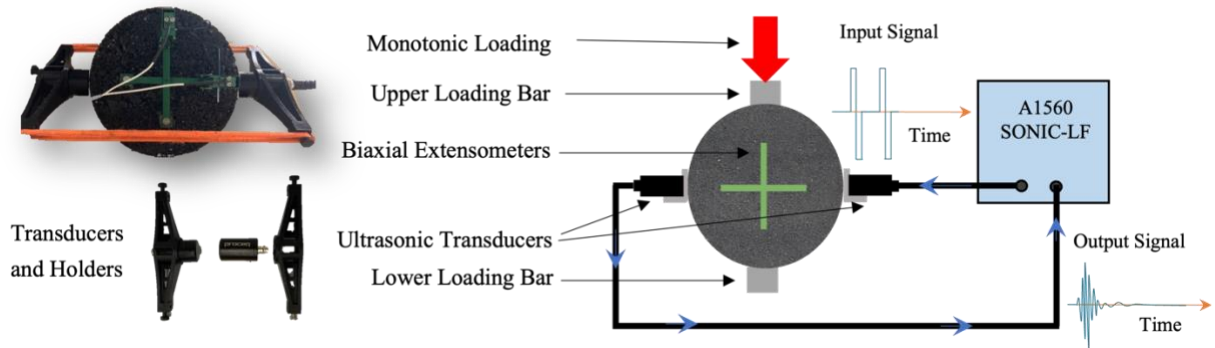


Figure 4-2. Photograph and schematic of test setup

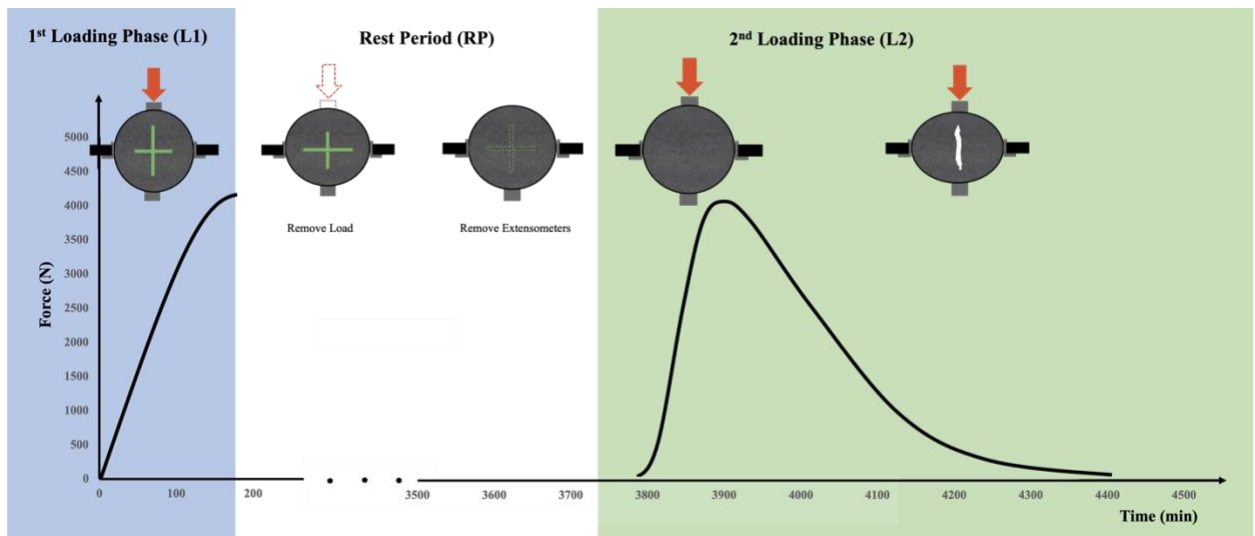


Figure 4-3. D2HRP Test Protocol

With regard to healing, some potential external factors can influence the intrinsic healing rate of asphalt concrete specimens, such as temperature, moisture, healing time, load level, and damage level. The proposed test protocol in this study minimizes the influence of external factors by conditioning the specimen in a thermal chamber with a constant temperature and moisture level and allowing the specimens to have an uninterrupted rest period. The healing process can be very slow at low temperatures, and plastic deformation can be severe at high temperatures. Therefore, the proposed test temperature is within the intermediate temperature range for the tested materials. To induce micro-damage in the test specimen, the peak load was selected as the stopping point for the following reasons and hypotheses:

- (1) Macro damage will be induced in the post-peak stage, beyond the damage that asphalt can intrinsically heal.
- (2) At intermediate temperatures, plastic deformation cannot be completely eliminated. Most of the plastic deformation occurs before the specimen reaches its peak load. Stopping at the peak load point ensures damage build-up in the specimen.
- (3) Previous research has shown that the fracture energy up to the fracture point can be used to characterize asphalt mixtures.
- (4) Stopping at the peak load is easy to program in most of the loading devices.

Each specimen was loaded up to its corresponding peak load point at the end of the first loading phase. To this end, separate groups of specimens were prepared and loaded until complete failure, and their corresponding displacement to the peak load was recorded. The displacement was later used to set up the D2HRP test procedure in the mechanical loading and ultrasonic equipment setup. An alternative way to set up the end of the first loading phase is to use a 'failure detect' function to make the system stop at 98% of its peak load. However, the sensitivity of this function needs to be verified.

Table 4-2. Ending Point of First Loading Phase

Specimen		Displacement (mm)	Load (kN)	
M1	PG 58-28	Control	3.00	4.38
		Loose Mix Aged	3.00	6.43
		3%SBS	3.30	5.54
	PG 64-28	Control	3.00	5.47
M2	PG 58-28	Control	3.30	8.37
		Loose Mix Aged	2.50	11.36
		4%SBS	3.40	10.54
	PG 64-28	Control	2.90	11.19

The average peak load and the corresponding displacement are summarized in Table 4-2. As expected, the ductility of the mixtures is significantly enhanced by modifying SBS in the mix, so the SBS groups have a relatively extended displacement corresponding to their peak load. The aged specimens are stiffer and more brittle than the unaged ones, so they reach their peak load more quickly. As mentioned before, the mixture group 1 (M1) was tested at 20°C, and the other group (M2) was tested at 10°C.

4.4 Analysis

Two data sets were collected from the tests: one from the large-strain mechanical testing and the other from small-strain ultrasonic measurements. Changes in both the transmitted signals' time and frequency domain were studied, synchronized with the loading data from the extensometers and plotted for each phase. Before assembling the data from both data sets, some treatments need to be applied first. The healing rate of the asphalt mixtures is finally quantified.

4.4.1 Mechanical Test Data Analysis

4.4.1.1 Load-Displacement Curve Analysis

Permanent deformation accumulation in the specimens would be inevitable when testing asphalt concrete specimens during the IDT testing. This results in densification of some portions of the specimen along the loading path in the very early stage of loading. The tensile stress builds up in the same spot during loading, resulting in specimen fracture. One drawback of this setup in the proposed protocol is the shape change and the non-homogeneity of the specimen. It is assumed that the specimen is intact before loading, and after the first loading phase the specimen reaches its ultimate point. The initial and end points of the first loading phase indicates the total induced damage to each specimen. The ratio of the fracture energy up to the fracture point (W_f) before and after the rest period is compared as provided by Table 4-3. W_f is calculated using the area of the load-displacement curve till the peak load point. $W_f(L1)$ and $W_f(L2)$ denote the fracture energy calculated from the first and second loading phases, respectively. The ratio of the fracture energy can be used as a main criterion to assess the healing capability of asphalt mixtures [88]. However, due to the short healing time (i.e., one hour) and relatively low temperature in this research, the ratio may not be able to accurately describe the healing ability of the specimen.

The coefficient of variation (COV) values in Table 4-3 show that the variation of fracture energy in M1 specimens tested at 20°C is generally higher than those of the M2 group. The major reason for this could be attributed to the higher testing temperature for M1 group. From the literature, the efficiency of healing is reduced when the specimen ages or the healing temperature is lower [88], [89]. However, the results of this research do not indicate any significant effects of aging on the healing capacity of the mixes through studying the fracture energy ratios. This analysis did not give the same ranking for

different types of asphalt mixtures, which indicates that this comparison may not be sufficient to quantify the healing capability of the asphalt mixtures.

Table 4-3. Work of Fracture Comparison

Specimen			$W_f (L1)$ [Nmm]	$W_f (L2)$ [Nmm]	$\frac{W_f (L2)}{W_f (L1)}\%$	COV %
M1 (20°C)	PG 58-28	Control	8030.5	3804.7	47.4	2.2
		Loose Mix Aged	12527.5	6575.4	52.6	9.3
		3%SBS	10553.4	5902.2	56.8	15.4
	PG 64-28	Control	10115.1	6828.6	67.1	30.4
M2 (10°C)	PG 58-28	Control	17257	13372	77.6	7.1
		Loose Mix Aged	17063	12663	74.5	9.1
		4%SBS	23926	14704	61.8	8.8
	PG 64-28	Control	21237	15266	71.9	3.5

4.4.1.2 Extensometer Data Analysis

The shape change of the specimen can be estimated using the readings from the extensometers. Only Loading Phase 1 and part of the Rest Period data were recorded, as the extensometers were removed before starting Loading Phase 2. Figure 4-4 shows a typical plot of vertical and horizontal displacements measured during L1 and part of the rest period via the extensometers. It can be recognized that the displacement magnitude in the vertical direction (loading direction) is considerably larger than the change in the horizontal direction (transverse direction) due to permanent deformation. The gauge length was 75mm and was set up at a relatively large offset before starting the test to maximize its working range during the loading process. For the particular specimen presented in Figure 4-4, the vertical displacement at the end of L1 was found to be -0.91mm, whereas the horizontal displacement was 0.44 mm. The specimen shape shrank to 99.4% after loading when using the measured displacement and the gauge length to estimate the area of the elliptical specimen. As the specimen shrank, its bulk density increased. As discussed before, the extensometers were removed before the L2 stage and therefore the trend of changes in the vertical and horizontal displacement could not be fully captured. Using non-contact extensometers could be a potential solution to overcome this issue.

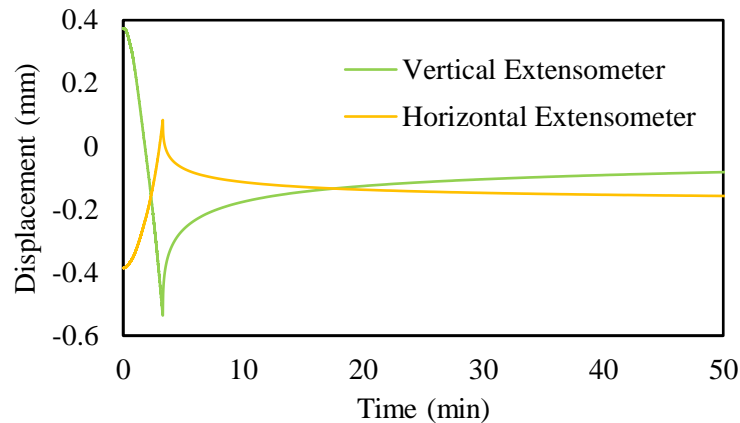


Figure 4-4. Extensometer Readings for M2 PG 58-28 Control Specimen

4.4.2 NDT Data Analysis

4.4.2.1 Time Domain Analysis

The receiver transforms the ultrasonic wave back into an electric current. The current or voltage magnitude and corresponding time can be recorded as the output signal in the time domain. The velocity of the first arrival wave, often called primary wave or P-wave, is correlated with the elastic modulus and density of the material, and the magnitude of the wave amplitude depends on the attenuation mechanisms of the material. P-wave travels faster for materials with larger elastic modulus and smaller densities. Figure 4-5 shows some examples of the output signals in this method. It should be noted that the magnitude of the signal at the end of loading phase 2 (L2 End) is amplified ten times.

Despite the fact that the distance between the transducers changes during the testing, the P-wave arrival time was found to be similar for all the loading stages before the macrocrack formation. The P-wave magnitude after the rest period is almost the same as the starting point of the first loading phase. The specimen homogeneity, Poisson's Ratio, and density collectively affect the wave propagation process, which is very hard to quantify. For some specimens, the P-wave magnitude after the Rest Period is even larger than the magnitude before the application of Loading Phase 1, which can be attributed to the changes in the pore structure of the specimen and the air voids due to the plastic deformation. Therefore, the traditional UPV-based methods that solely use P-wave velocity to estimate the bulk elastic modulus and P-wave magnitude to assess the materials property may not be good indicators for understanding the damage and healing process of asphalt concrete mixes.

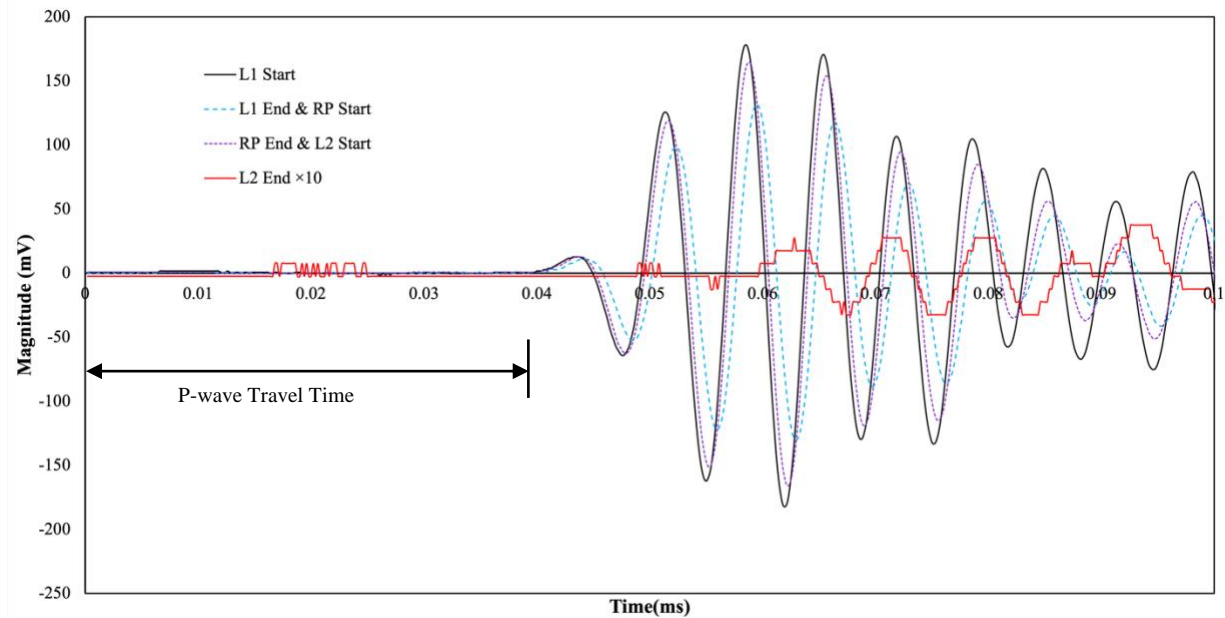


Figure 4-5. Time Signal for M2 PG 58-28 Control Specimen

4.4.2.2 Frequency Domain Analysis

Both FFT and CWT were used for the frequency domain analysis. Figure 4-6 shows a typical plot in the frequency domain for this test protocol. The frequency spectra of the signal collected at the end of Load Phase 2 has been magnified five times to clearly show the trend. The area under the frequency spectra relates to the energy of the signal. The input signal power was kept the same for all the specimens and throughout the whole testing process. Therefore, the area under the output signal frequency spectra is proportional with the energy transmitted through the specimen, which can be used to quantify the condition of the specimen.

Several vibration modes can be excited at simultaneously in this method, for which their corresponding resonant frequencies can be identified. The frequency spectra plot shows frequency peaks around 20, 50, and 150 kHz. Analyzing the results throughout the whole testing process indicates that when the specimen completely fails, toward the end of loading phase 2 (L2 End), peak values below 100 kHz can still be identified. From the WSST scalogram (Figure 4-7), the frequency below 100 kHz represents a different vibration mode that would exist from the beginning of the test. Frequencies less than 100kHz would not be of interest in the proposed testing protocol because only the dominant vibration mode will be considered, for which the frequency ranges from 100 to 250 kHz in the test setup used in this study.

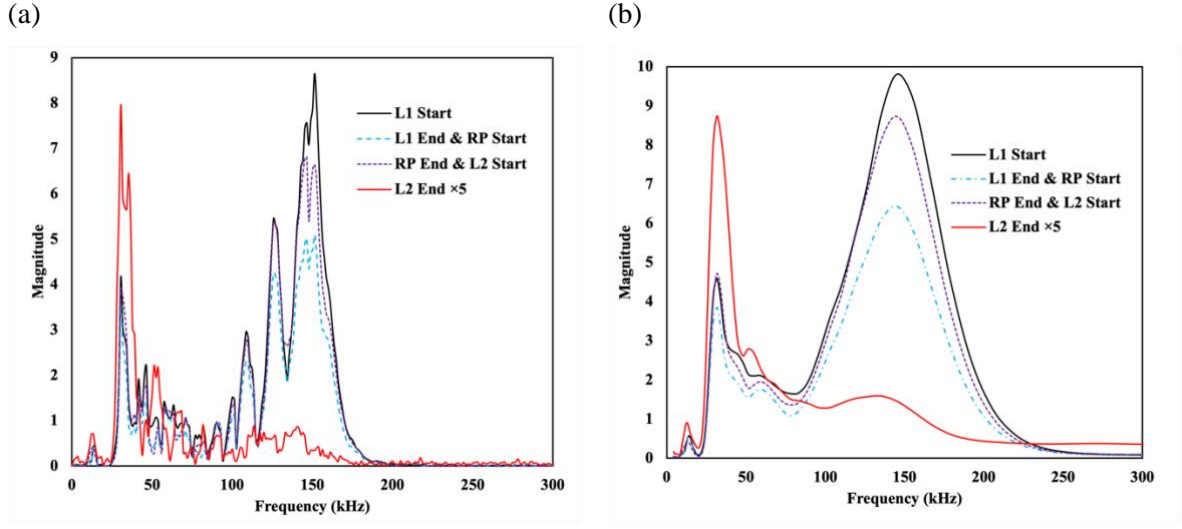


Figure 4-6. (a) FFT and (b) CWT for signals collected from M2 PG58-28 Control specimen

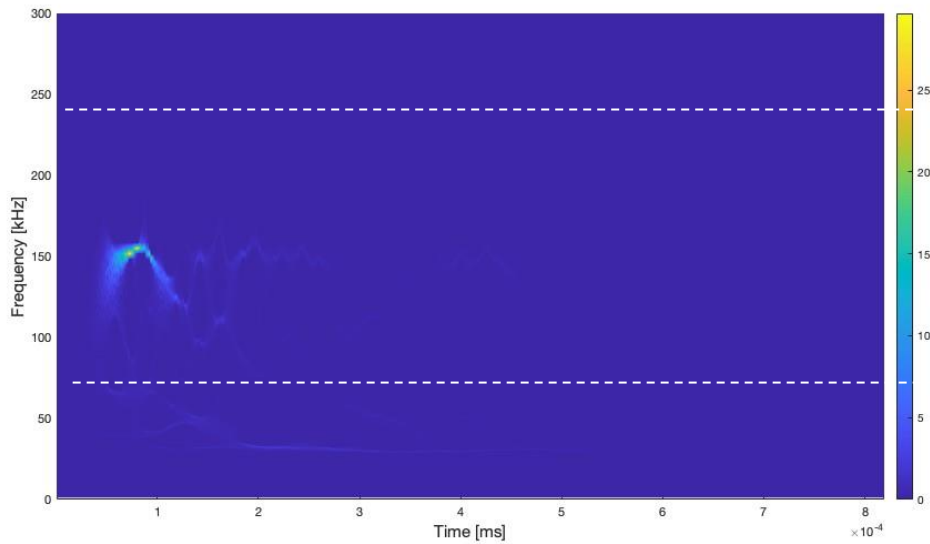


Figure 4-7. WSST for M2 PG58-28 Control specimen

4.4.2.3 Signal Processing through Unwanted Feature Removal

Three signal processing methods are compared in this study. The first method involved applying a window to the time signal to filter out the waveforms after receiving the reflected signal. The second method involved designing a narrow-band filter for the frequency spectra that could filter out the

dominant signal in the frequency range of 100 to 250 kHz directly. The convolution method was then used to combine the filter with the original output signal to get the filtered output signal. The third method used the WSST data information in the 100-250 kHz frequency range to reconstruct the time signal. The data before and after the filter in the time- and frequency-domain were plotted in Figure 4-8 and Figure 4-9, respectively.

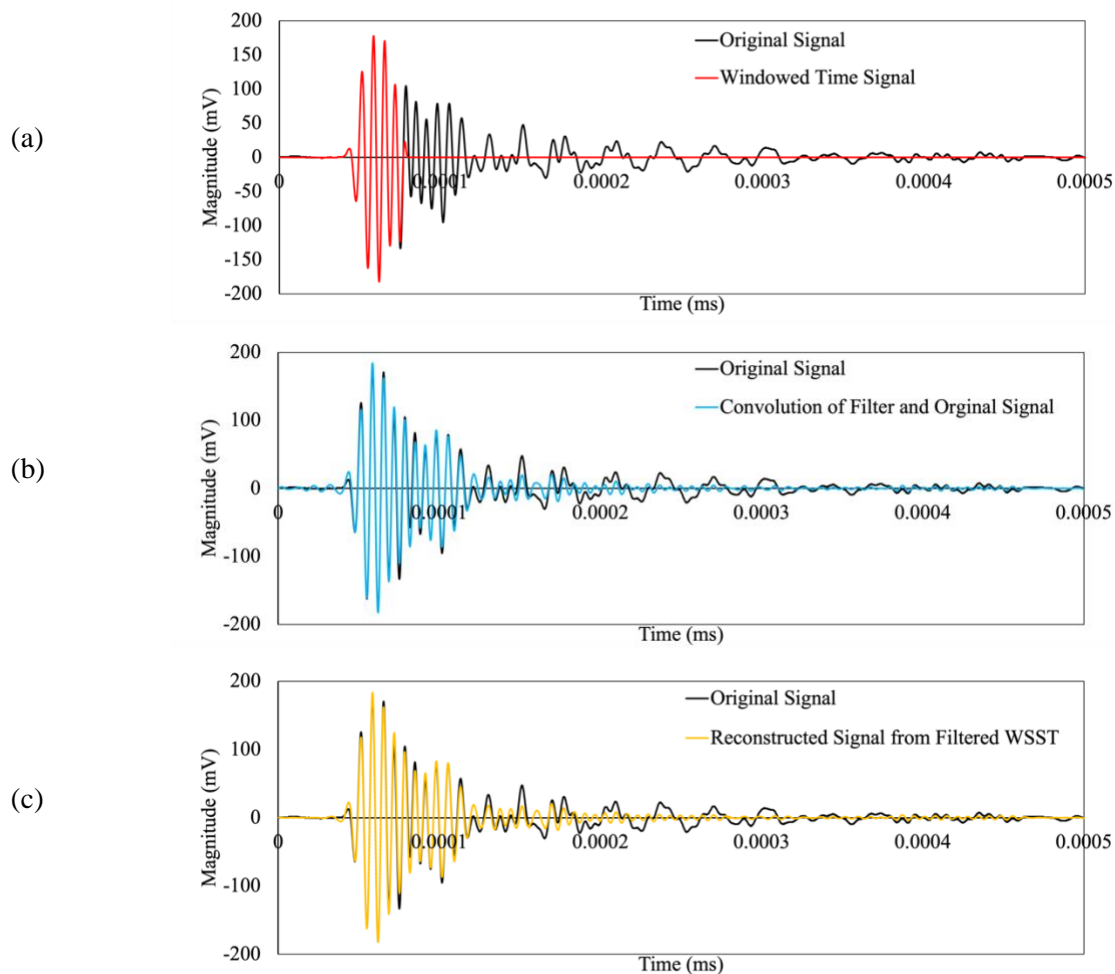


Figure 4-8. Time signal plot of original signal and (a) windowed time signal, (b) convolution of filter and original signal, and (c) reconstructed signal from filtered WSST

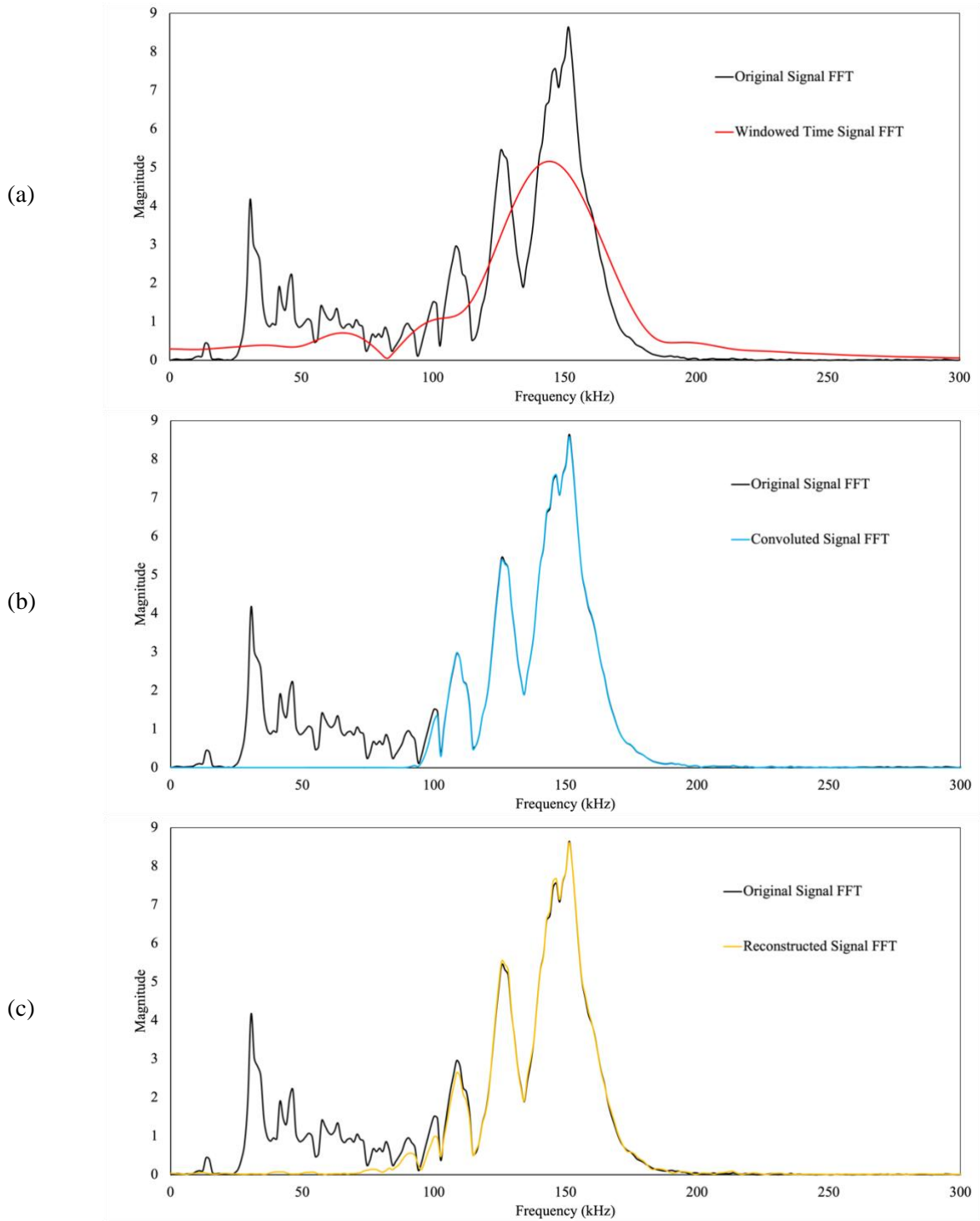


Figure 4-9. Frequency Spectra of original signal and (a) windowed time signal, (b) convolution signal, and (c) reconstructed signal.

The comparison of time plots in Figure 4-8 shows the noise of the tails can be effectively removed for all three filtering methods. From Figure 4-9, it is clear that filtering in the frequency domain preserves the features of the dominant frequency more effectively, as Figure 4-9(a) changed the peak value and the corresponding frequency of the Fourier Transformation of the original signal. Furthermore, clear reflective waves could not be detected when looking at the time domain in all the signals, making it hard to pick a consistent time window among the groups. Therefore, it was decided to directly apply a narrow band filter to the frequency spectra in this research. Figure 4-10 shows the filtered FFT and CWT data for a specimen in the M2 PG58-28 Control group, with the magnitude of the end-point of Phase 2 amplified by five times.

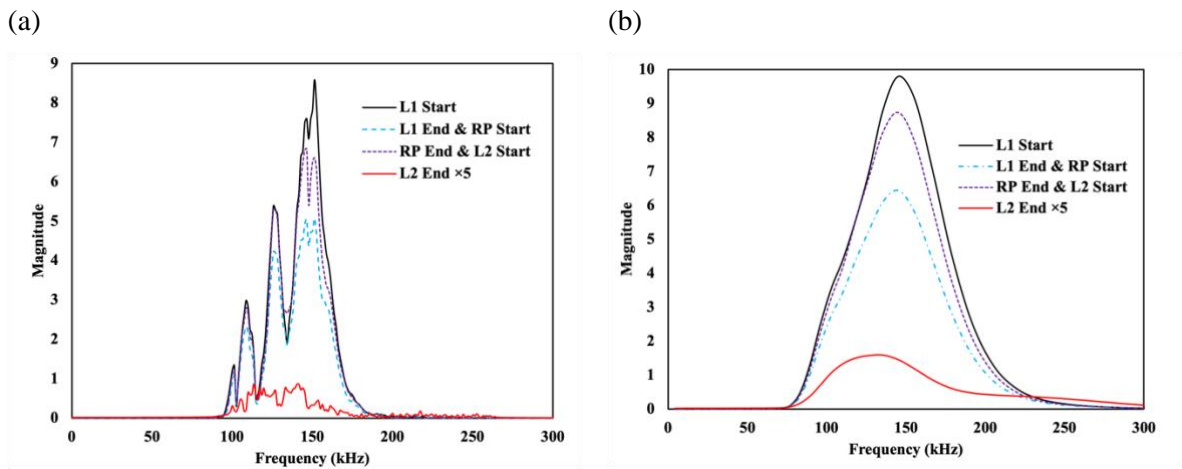


Figure 4-10. Filtered Fourier Transformation for M2 PG 58-28 Control Specimen

4.4.3 D2HRP Data Analysis

The observed changes in the signals during the test can be attributed to both the geometry changes and the change in the damage condition of the specimens. However, there is a considerable magnitude difference between the mechanical testing and the ultrasonic measurement data sets. Therefore, both sets of data were normalized for the sake of comparison. The data was normalized with respect to the first loading phase since the specimen was still undamaged at the beginning of L1 phase and assumed to reach its ultimate limit by the end of L1. Due to the adverse effects of the specimen geometry changes in the horizontal direction on the transmitted signals, the reciprocal of the normalized horizontal deformation from the biaxial extensometers was used. Figure 4-11 shows an example of the results for

one specimen after the normalization. More ultrasonic data points were taken at the beginning and end of the rest period to avoid missing essential data points when changing the data acquisition frequency.

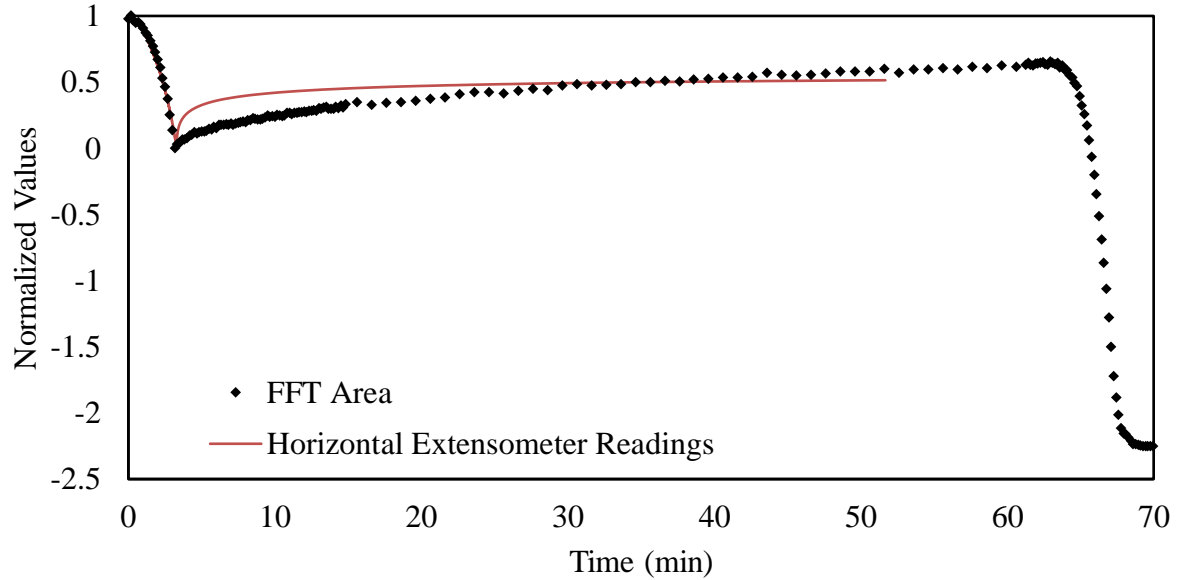


Figure 4-11. D2HRP Data Analysis for M2 PG 58-28 Control Specimen

This research focuses on the RP interval from 18 to 50 minutes to characterize the healing rate of the asphalt concrete, as the initial magnitude recovery may be biased by the elastic recovery response of the specimen, which will be evaluated in future tests from the loading and unloading sequences at low strain levels. When plotted on a logarithmic scale scatter plot, the normalized values observed during the selected interval follow a linear trend ($R^2 > 95\%$). A healing rate equation is proposed in this study which is inspired by the concept that the restoration of mechanical properties include the recovery and healing. Conducting logarithmic regression on each data set, an intrinsic healing rate can be calculated using the difference of the slopes from two trendlines. Although the data could also be presented on a linear scale, a logarithmic scale was used to better visualize the trend of changes. For example, the healing rate for the specimen presented in Figure 4-12 would be 0.18 per log minute.

$$\text{Healing Rate} = m_{\text{FFT Area or CWT area}} - m_{\text{horizontal extensometer reading}} \quad \text{Equation 15}$$

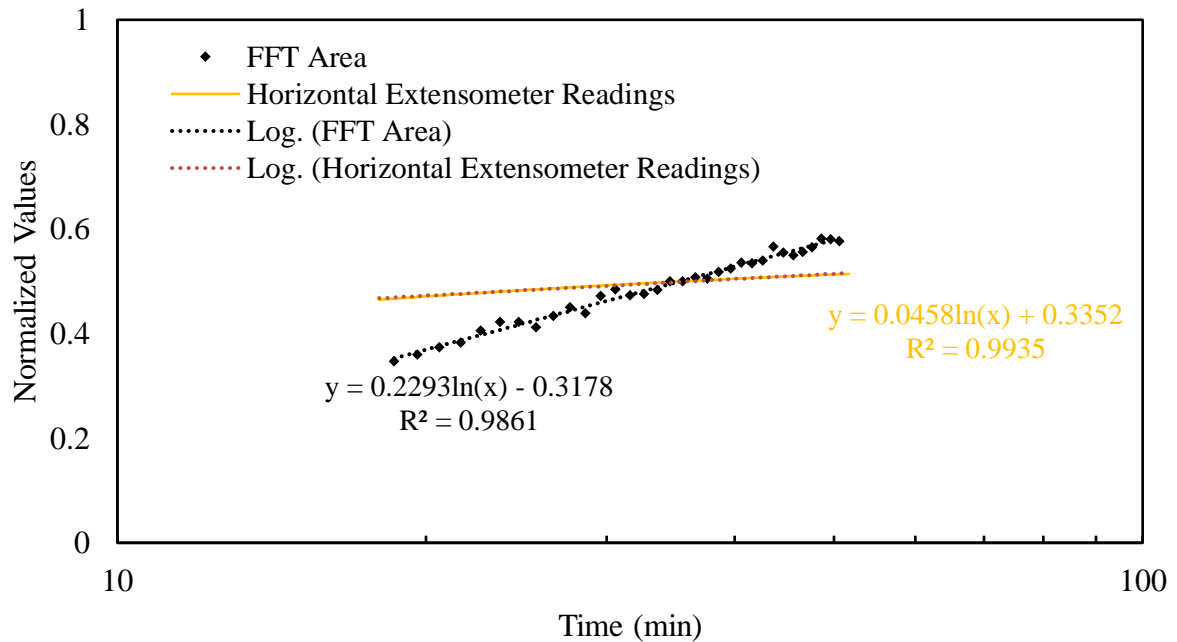


Figure 4-12. Healing Rate Calculation for M2 PG 58-28 Control Specimen

4.5 Results and Discussion

In order to study the sensitivity of the proposed test protocol to experimental factors, different Mix designs, Performance Graded binders, ageing levels, modifiers, and test temperatures were considered in this study. A minimum of two replicates were used for each mixture type. Table 4-4 summarizes the healing rates of each group of specimens. The specimen shape rate of change (R.O.C.) was calculated from the readings of the normalized horizontal extensometer. The rate of frequency spectra area change, calculated from the signal frequency domain analysis, used either the Fast Fourier Transformation or the Continuous Wavelet Transformation. Two sets of the intrinsic healing rate of asphalt specimens were generated based on the frequency domain analysis. For both the mix designs, PG 64-28 control specimens showed the fastest healing rate followed by the PG 58-28 control mix and PG 58-28 aged specimens, respectively. However, the ranking of the SBS-modified mixtures healing rate is not consistent in the two groups. This could be attributed to two main reasons: 1) the SBS dosage is different between M1 and M2 groups, resulting in a different crosslinked network in the specimen and 2) the specimen fracture behavior might be affected by the test temperature.

Table 4-4. Summary of D2HRP Analysis

Specimen		Shape R.O.C	FFT Area R.O.C.	CWT Area R.O.C.	Healing Rate (FFT Area)	Healing Rate (CWT Area)	Ranking within group
M1 (20°C)	PG58-28 control	0.0288	0.162	0.173	0.134	0.144	3
	PG58-28 aged	0.0310	0.097	0.100	0.066	0.069	4
	PG58-28 3%SBS	0.0585	0.301	0.342	0.243	0.283	2
	PG64-28 control	0.0468	0.422	0.381	0.375	0.334	1
M2 (10°C)	PG58-28 control	0.0493	0.252	0.262	0.203	0.213	2
	PG58-28 aged	0.0359	0.187	0.174	0.151	0.138	4
	PG58-28 4%SBS	0.0476	0.225	0.236	0.177	0.188	3
	PG64-28 control	0.0356	0.381	0.392	0.346	0.356	1

For the Mix design comparison, even though the M1 group has a higher binder content, the healing rate of the control and aged asphalt mixture in the M2 group is more extensive. It might be due to better adhesion between the asphalt binder and the aggregates. However, it needs to be verified with more experiments.

For the ultrasonic frequency spectra analysis, the Fast Fourier Transformation and the Continuous Wavelet Transformation provide consistent rankings of the different mixes. For most specimens, the CWT values are slightly larger than the FFT values, as the resolution of the discrete transformation might affect the results.

4.6 Conclusions and Future Work

A new test protocol, called Dynamic High-Frequency Healing with Rest Period (D2HRP), was proposed in this study. It couples a non-destructive test with a complementary destructive test to quantify the healing capacity of asphalt concrete mixes. Several signal processing methods were applied in the analysis. Synchro Squeezed Wavelet Transform (SSWT) was applied to the signal, where the dominant resonant mode frequency of the signal was selected from 100 to 250 kHz. A narrow band filter was designed and applied to all the received signals. Then, both Fast Fourier Transformation (FFT) and the Continuous Wavelet Transformation (CWT) were applied to the filtered signals. The rate of change in the geometry of the specimen and the energy change of the output signals were then

calculated, and a healing rate was directly extrapolated from the test results. Based on the work presented in this chapter, the following conclusions and recommendations are made:

- The D2HRP test is easy to conduct and is sensitive to the varying aging conditions. For the range of temperatures investigated in this study, the test temperature did not affect the results significantly.
- The healing capability for the binders with a higher high temperature performance graded (H-PG) was found to be greater than that of a binder with lower H-PG. It can also be concluded that the healing ability decreases with aging. The SBS-modified mixtures need to be further studied to fully understand their healing capacity changes at different conditions.
- Both FFT and CWT can be used to evaluate the healing rate of the specimen; however, the P-wave velocity or amplitude may not be good indicators for this purpose.
- The ratio of the fracture energy relies on the plastic deformation and elasticity of the specimen and does not provide a clear trend for asphalt mixtures when tested at different temperatures.

The new test setup presented in this chapter can help to study the intrinsic self-healing properties of asphalt mixes. However, the proposed methodology is still in an early stage and needs verification with more data. In terms of improving the proposed testing protocol, using non-contact displacement sensors could be investigated in future research. This can allow fully capturing the specimen behaviour throughout the whole test procedure, which is not possible due to the potential damage to the traditional extensometers mounted on the specimens in IDT test.

Chapter 5

Indirect Measurement of Fatigue and Healing of Asphalt Mixtures Using Ultrasonic Wave Propagation Approach

Summary

Asphalt fatigue and healing tests are used to evaluate the performance of asphalt mixtures under repeated loading and unloading cycles. However, several loading-dependent bias effects would alter the test result and lead to a misleading interpretation of the test results. Much research has been done with a degree of success to assess these effects quantitatively. However, these measurements are usually combined with a separate test, such as using a strain amplitude sweep test to study the nonlinearity of the material, which requires much effort and complex analysis. For asphalt healing tests, mechanical loadings are used in most of the tests to record the specimen's mechanical response, which may disturb the healing processes.

Ultrasonic tests are applied at a very small strain level, at which nonlinearity is assumed to be negligible, and the test is sensitive to temperature and practical to conduct. Therefore, this research study proposed a novel test protocol that combined the use of ultrasonic measurements with the asphalt fatigue healing test to quantify the bias effects. Three signal processing methods were used: signal energy comparison, time signal cross-correlation, and dynamic time warping. Comparing the signal energy changes during the fatigue process showed that this new protocol could separate true fatigue damage from other phenomena, such as local heating, nonlinearity, and thixotropy. Thixotropy was found to change the molecular arrangement of the specimen during loading and diminish quickly when loading was interrupted. Therefore, mechanical loadings should be avoided during rest periods, even at small strains. Although the use of signal similarity to evaluate fatigue damage rate is still preliminary, a clear difference was observed when testing the specimen at different strain levels.

5.1 Introduction

Fatigue cracking is a common type of distress that affects roadways, parking lots, walkways, and other paved surfaces. Repeated mechanical loadings cause this phenomenon and fatigue cracking can propagate and lead to significant pavement failure. Asphalt specimens are typically subjected to cycling mechanical loading until failure to simulate fatigue cracking in the laboratory. Various analysis

methods and models have been created to predict the fatigue life of asphalt concrete. The Rilem Technical Committee 182- PEB (Performance and Evaluation of Bituminous materials) conducted an interlaboratory investigation of different fatigue tests [23]. One of the main findings of that work was that fatigue tests are sensitive to loading conditions and testing setup. The Tension-Compression fatigue test on cylindrical specimens provided more consistent and reproducible results than the other investigated tests. During these cyclic tests on asphalt concrete, the stiffness, described by the norm of the complex modulus, decreases with the number of cycles (Figure 5-1). Several studies have been done to qualify and quantify the causes of this decrease [23][4][24][22][25]. Even though it is a fatigue test, fatigue damage is not the only reason that causes stiffness loss in the bituminous material during the test. The fatigue processes can be divided into three phases (Figure 5-1). Different effects that co-exist with damage during cyclic loading dominate the complex modulus degradation in each phase.

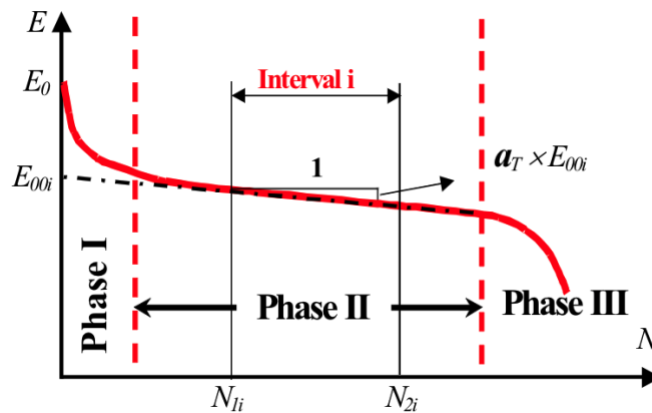


Figure 5-1. Stiffness evolution curve during a fatigue test [90]

Phase I is characterized by a rapid drop in the modulus. It is mainly due to the dominant asphalt cement viscosity decrease and other reversible phenomena. Phase II is typically a quasi-stationary stage where fatigue damage is dominant, and microcracks are formed. Bias effects also exist in this phase; however, they have a relatively lower impact than fatigue damage. Phase III is typically characterized by a rapid decrease of modulus caused by the rapid crack propagation, which leads to unpredictable behaviour. At this last stage, microcracks grow into macrocracks. Therefore, most studies focus on the first two phases, and laboratory-predicted fatigue life is usually located in Phase II to deduct the risk of

insufficient design. The non-fatigue effects in the fatigue test are called bias effects and have been studied intensively [3], [4].

Nonlinearity, thixotropy and local heating are the three main phenomena that dominate the first phase of the fatigue test [90]. During Phase I, at the first cycle, the sudden drop of the norm of complex modulus is partly due to nonlinearity. Nonlinearity can be estimated using complex modulus tests with a series of strain amplitude sweep tests [91]. The effect of nonlinearity is strain dependent and decreases when the strain amplitude moves toward zero. It is a reversible phenomenon at a relatively small strain level [4].

The increase in the specimen's temperature and the thixotropy also contribute to a significant part of the rapid drop in the modulus in Phase I. Thixotropy is initially described as the linear response of a structured viscoelastic liquid microstructure to imposed stresses and strains [92]. It was later adopted for the bituminous material study and considered a reversible phenomenon in asphalt cement [4], [93]. During the fatigue loading process, thixotropy causes dissociation and deformation of inter- and intra-molecular bonds in asphalt cement until it reaches a sol structure [22], which reduces the material's viscosity and modulus. The effect gradually vanishes when the material is at rest [92]. Heating is caused by viscous dissipated energy (molecular friction) during loading [4]. It reduces the modulus by separating the secondary intermolecular bonds due to thermal expansion, which is also a reversible phenomenon. During the fatigue process, the temperature within the specimen will increase in Phase I and relatively stabilize in Phase II. When loading disappears, the material will have a cooling effect. This effect can be calculated from the measured temperature change [4].

Other phenomena, such as permanent deformation and steric hardening, may also rise in fatigue tests [22]. Permanent deformation appears in the cyclic bending test and the diametral tests, which changes the viscoelastic properties of the material [22]. Steric hardening is the hardening of bitumen over time, which is associated with a sol-gel transformation and asphaltenes in bitumen [26]. Steric hardening is not significant at intermediate temperatures [94].

In 2005, Soltani et al. proposed a new fatigue test protocol using a three-loading stages Tension-Compression test [95]. In their research, the first and last stages are conducted at very low loading levels, which they believed to be below the endurance limit of the tested material. Fatigue damage occurs during the second loading stage when the applied stress or strain is sufficient to cause fatigue damage (Figure 5-2). However, since Stage I and Stage III are in the linear viscoelastic domain and

Stage II is in a nonlinear viscoelastic domain, the stiffness difference between the asymptotes may not only be caused by fatigue damage. On the other hand, at the third stage, the recovery of the modulus may not only be due to the reverse of the bias effects, but self-healing might also contribute to the modulus increase. Figure 5-2 shows that time in Stage III is significantly longer than in Stage II. In their research, Stage II was only 10 hours, and Stage III was almost four days.

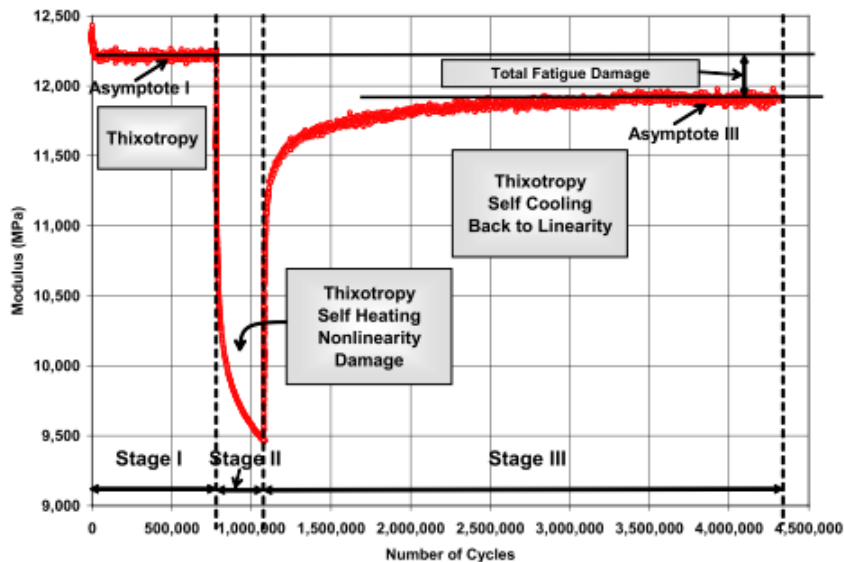


Figure 5-2. Soltani and Anderson’s research [49]

Di Benedetto et al. (2011) evaluated nonlinearity, heating thixotropy and fatigue effects with observations in the complex modulus tests. These effects during cyclic loading can be explained in the schematic representation in Figure 5-3 [4]. In their test, the loading phase was only 20 minutes, and it took approximately 24 hours to reach an asymptote in the rest period. With normalized data, the decrease in the modulus due to temperature was approximately 13%, 26% was attributed to the nonlinearly 55% to the thixotropy, and only 5% was due to true fatigue damage. From Figure 5-3, the modulus change caused by fatigue damage is minimal. Again, the healing effect should have been addressed.

Asphalt has an intrinsic self-healing property that can heal the microcracks by itself. It is generally agreed that the healing process involves crack closure driven by surface-free energy and a molecular diffusion process. The healing process can be considered a reversal process of fatigue [57]. Therefore, researchers have used modified fatigue tests to study the self-healing capability of bituminous material

on a macroscale [78][8][9][10]. The healing capability of the material is typically quantified by comparing the modulus change with and without rest periods [11]. However, the existence of reversible phenomena makes it even harder to quantify the healing effects.

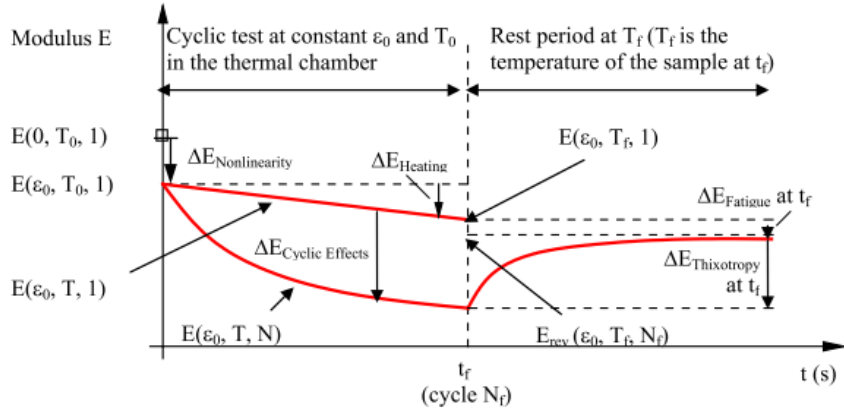


Figure 5-3. Schematic representation of different effects during cyclic loading [4].

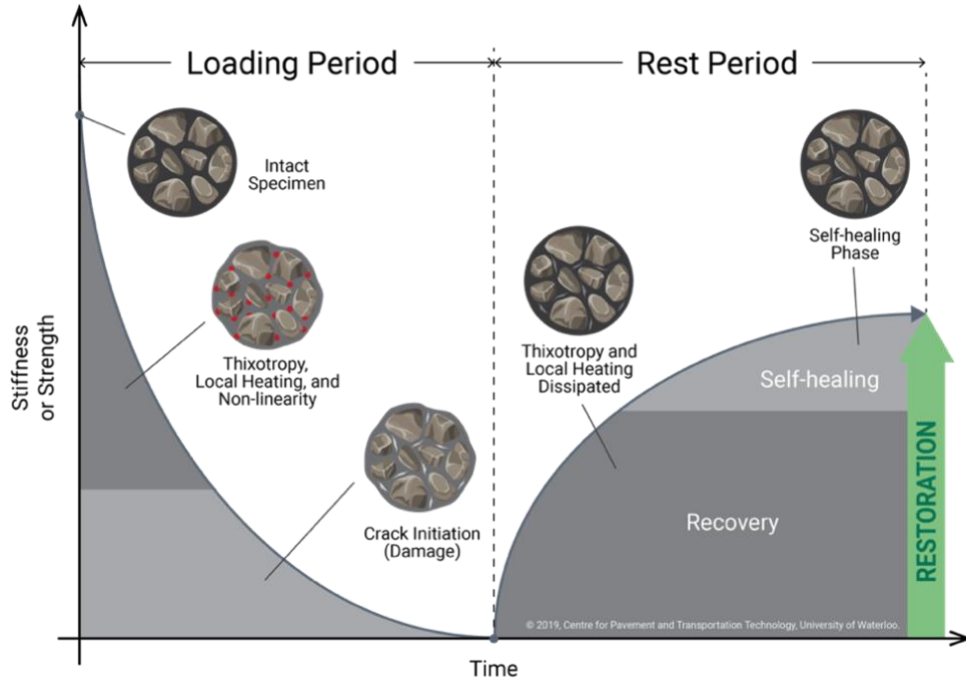


Figure 5-4. Schematic of asphalt mixture self-healing process [84]

Traditional healing quantification involves applying a strain or stress in the material's LVE during the rest period so that the mechanical response of the specimen can be recorded. However, due to thixotropy, cyclic loading may counteract the healing process and cannot eliminate the bias effect completely. Thus, a new method that does not introduce mechanical loading but can provide engineering measurements is ideal for monitoring the asphalt healing process. Wave propagation-based non-destructive testing (NDT) methods can be a good candidate as they meet this requirement. It applies a minimal strain so that nonlinearity can be ignored. Previous research has proved that wave propagation is sensitive to asphalt at various temperatures [64], [72]. However, using ultrasonic wave propagation methods to quantify a viscoelastic material's thixotropy or damage during a cyclic loading process is limited in the literature.

This research investigates the feasibility of using ultrasonic wave propagation measurements to quantify and separate the bias effects during the asphalt fatigue and healing test. The main hypothesis for this research is that the wave attenuation approach is sensitive enough to capture the microstructure change of the asphalt specimen during fatigue loading and resting processes.

The loading and unloading process also needs to be defined. In order to compare the healing capabilities of different specimens, the same level of damage needs to be applied. Thus, the fatigue test results need to be studied a priori, and the loading process must be applied until the predetermined fatigue damage level is induced. Another challenge is that the signal processing methods for analyzing the materials' viscoelastic behaviour must also be investigated. Most of the research that has been done on ultrasonic pulse propagation applications for asphalt mixtures has primarily been limited to testing static specimens. However, monitoring the signals' feature change during a cyclic loading process could provide insight into the specimen's microstructure change caused by the bias effects. Therefore, the second main hypothesis is that as a complementary tool, the new analysis of the ultrasonic wave propagation approach can improve the conventional asphalt fatigue and healing characterization techniques.

The Tension-Compression fatigue test was selected to induce fatigue damage to the specimen as the test is homogeneous so that the damage will be uniformly distributed. Moreover, the loading caps were parallel and glued to the asphalt specimen with epoxy, which could be used as flat surfaces to equip the ultrasonic transducers. However, the loading caps are connected to the frame's connection rods, and this loading transformation needs to be preserved. To this end, a test configuration was deemed

necessary to allow the ultrasonic transducers to properly send and receive pulses to the specimen during the loading and resting processes.

5.2 Theoretical Background

This research involves comparing the features or similarities of signals. Several features of the signals could be studied and compared, such as the peaks of the signal, the phase and velocity of the group waves, the dominant frequency and the corresponding amplitude in the frequency domain, and the overall energy in the signal. Many signal processing tools can help understand the aforementioned features, such as Fast Fourier Transformation (FFT), Continuous Wavelet Transformation (CWT), filters and windows, convolution, cross-correlation, and Dynamic Time Warping (DTW) [96].

When an ultrasonic signal propagates through an object, three possible outcomes can occur, including it passing through the object, being absorbed by transforming it into thermal energy or being reflected. According to Fermat's principle, the first arrival of a wave signature reflects the fastest wave pathway, and the arrival of the waves later in the coda results from the accumulation of differences in propagation velocity [97]. For an object with a different level of damage, when the same pulse is sent to transmit through it, it is expected to see the received signal with different energy and delays in the coda. Therefore, this research uses the following three methods to study the overall changes in the signals.

5.2.1 Signal Energy Comparison

Signal energy, E , can be used to characterize a signal, and it is calculated using the integral of the squared magnitude of the considered time signal, $x(t)$ (Equation 16). Based on Parseval's theorem, the signal energy calculated from the time domain equals the sum of all frequency components of the signal's frequency spectral energy density. When sending the same pulse into the specimen, if the specimen is damaged, it is expected that less energy being received as the wave cannot be transmitted through the cracks; instead, it will be reflected in other directions and propagate through the specimen at a longer distance, and more energy will be absorbed during this transmitting process.

$$E = \int_{-\infty}^{+\infty} |x(t)|^2 dt \quad \text{Equation 16}$$

5.2.2 Time Cross-Correlation

Cross-Correlation measures the similar or coherence between one signal $x_1(t)$ and the time-delayed version of another signal $x_2(t)$. The cross-correlation of two signals is defined as

$$R_{12}(\tau) = \int_{-\infty}^{+\infty} x_1(t)x_2^*(t - \tau) dt \quad \text{Equation 17}$$

The result of the Cross-Correlation exhibits a peak at a corresponding time τ that matches the delay between the two considered signals. In the literature, cross-correlation can be used to compare the full-length or windowed time signals [96]. This research compared full-length signals to evaluate the fatigue damage and healing process.

5.2.3 Dynamic Time Warping

Dynamic time warping (DTW) is a powerful tool that applies nonlinear mapping to match the two signals with phase differences. Figure 5-5 illustrates the difference between this method with the linear mapping method (Euclidean Matching) [98]. DTW was first introduced by Sakoe and Chiba in 1978 [99]. It has a variety of applications, including speech recognition, online signature recognition and data mining.

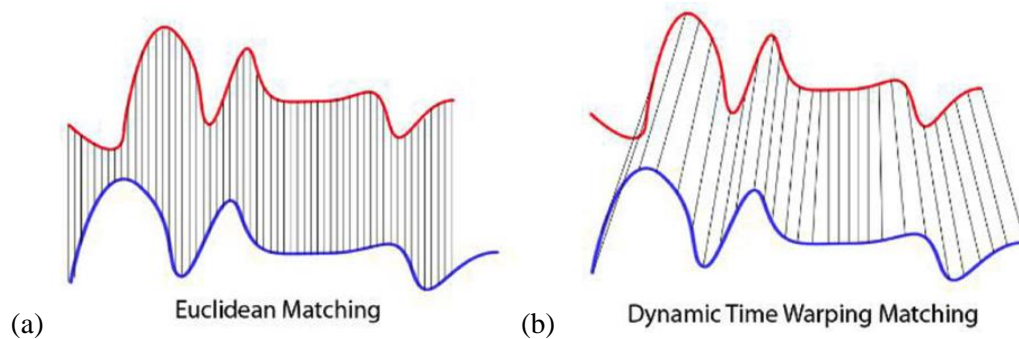


Figure 5-5. (a) Euclidean Matching (b) Dynamic Time Warping Matching [98]

The DTW algorithm first loop through all possible pairs of time points, one from each signal, to find their Euclidean distances. The minimum distance to the other signal is recorded for each time point in a signal. Then sum up all the minimum distances to represent a true similarity measurement between the two series. This research also implements this method to study the difference between received signals when the specimen is under different conditions.

5.3 Materials and Methods

5.3.1 Materials and Sample Preparation

Seven SP12.5FC2 laboratory asphalt mixtures were used in this study. The details of the mix design are summarized in Table 5-1. Four specimens were used for a traditional T/C fatigue test to get some necessary parameters for the setup of the proposed experimental protocol. Only three specimens were used to test the proposed protocol. Loose asphalt mixtures were compacted to a height of 115 mm and a diameter of 150 mm with a gyratory compactor. The binder contents were controlled to be $\pm 0.5\%$ with the target binder content, and the target air void level of $7\pm 0.5\%$ was successfully achieved for all the specimens. The compacted sample was then cored from its diametral direction to obtain a 75mm diameter by 120mm high cylindrical test specimens. After cored, the specimens were left on a cooling station for a week to dry fully. An air void of $5\pm 0.5\%$ was calculated by taking each specimen's bulk specific gravity and maximum theoretical gravity values, which were determined before gluing with the caps.

Table 5-1. Superpave 12.5 FC2 Asphalt Mix Design used in this study

Property		SP 12.5 FC2 Mix
Gradation (% Passing)	Sieve Size (mm)	
	12.5	96.0
	9.5	84.0
	4.75	56.4
	2.36	40.4
	0.075	5.5
Air Voids (%) at N_{design}		3.8
Design Mineral Aggregate, VMA (%)		16.1
Voids Filled with Asphalt, VFA (%)		76.2
Asphalt Cement Content (%)		5.2
Dust Proportion		1.1
Asphalt Binder Performance Grade		PG 58-28

After the specimens were completely dried, they were glued with epoxy to a pair of customized caps before putting into the testing frame. The alignment of the specimen is insured using a wood lathe modified for this purpose.

5.3.2 Test Equipment Setup

Two pieces of test equipment were used simultaneously in this test protocol. One can apply sinusoidal loading in tension and compression on the cylindrical asphalt specimen at a fixed frequency of 10 Hz. The other equipment generates ultrasonic signals, sends a group of pulses every five minutes to the tested specimen, and receives the output signals after the wave propagates through the specimen.

Figure 5-6 illustrates the setup of the equipment used in this study. This setup was developed in the Center of Pavement and Transportation Technology (CPATT) as part of the study on self-healing asphalt materials. A servo-hydraulic press (MTS810) is equipped with a 100kN load cell. An ACS A1560 SONIC-LF is a portable device customized to send and receive ultrasonic signals. A thermal chamber is used to condition the specimen at 10 °C. A dummy specimen, which has the same size as the tested specimen with a thermal probe embedded at its center (not shown in the figure), is also used to simulate the temperature of the tested specimen and ensure the specimen reaches temperature equilibrium. The extensions are hollowed in the center and secured with one bolt at its center to the loading frame and four bolts on the sides of the loading cap, which preserves load transformation and ensures the transducer contact with the flat surface of the plate directly. A 3D-printed holder was specifically designed to mount the transducers onto the top and bottom of the caps. A pair of hooked elastic was used to ensure consistent pressure on the transducers. The hooks are connected to the washers under the bolts that connect the extension with the cap. A coupling gel was applied to both sides of the caps to improve the transmission of the waves during the tests.

The axial strain is measured with three 75mm gauge length extensometers mounted around the specimen, spaced 120° apart. The extensometers measure the middle part of the specimen, and the strain is calculated from the average of the three displacements measured by the transducers. The surface temperature of the specimen is monitored with three surface temperature probes placed between the extensometers to obtain the heating and cooling evolution of the specimen during the test process. The ambient temperature is measured using the chamber's thermal probe. However, the temperature at the center of the specimen was not measured in this study. Two 150 kHz piezoelectric transducers are used to ensure the distance between the transducers is large enough to cover at least three wavelengths of the emitted signal [75].

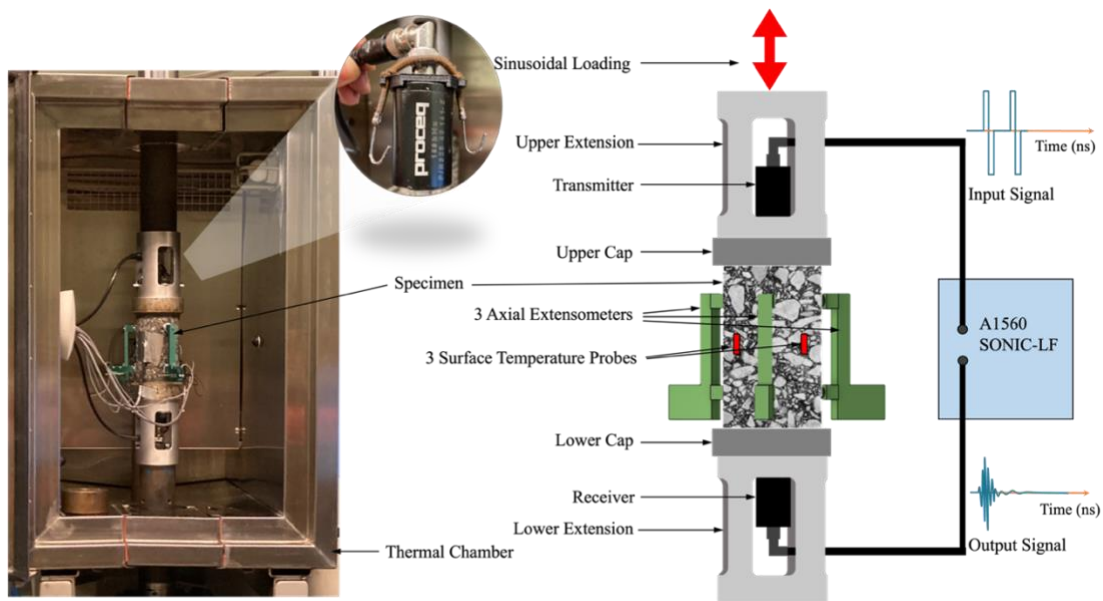


Figure 5-6. Experimental Setup

5.4 Proposed Test Protocol

The proposed test protocol consists of four stages: two conditioning stages and two loading stages. A schematic of the test procedure is shown in Figure 5-7. The test is conducted in strain-control mode during the loading stages and in force-control mode at zero in the conditioning stages. ‘Phases’ in the schematic refer to the fatigue phases. The proposed protocol differs significantly from classical asphalt fatigue or healing studies in that it uses ultrasonic parameters to evaluate the performance of the specimen and relies on the specimen’s temperature change during the loading process to separate various fatigue phases.

Two sets of data were collected: one is from the mechanical loading frame, with time, force, axial displacement, displacement measured by the extensometers, and temperature measured from the probe in the dummy specimen, the surface probes, and the chamber probes. Two consecutive cycles were recorded for each mechanical data acquisition in the loading stages, while only temperature data were recorded during the conditioning stages. This study uses two strain amplitudes (ϵ_A), ± 75 and ± 100 $\mu\text{m}/\text{m}$, to compare the sensitivity of the test protocol. The axial force and displacements in the consecutive cycles were used to obtain the axial stress amplitudes (σ_A) and strain amplitudes (ϵ_A), and

their lag phase (φ) between stress and strain. Then the complex modulus (E^*) and dissipated energy (W_{dis}) were determined:

$$E^* = \frac{\sigma_A}{\varepsilon_A} \quad \text{Equation 18}$$

$$W_{dis} = \pi \cdot \varepsilon_A \cdot \sigma_A \cdot \sin(\varphi) \quad \text{Equation 19}$$

The other set of data is the received ultrasonic signals. The strain level is in 10^{-6} to 10^{-7} in the NDT applications, which is much smaller than the mechanical loading applications. Sixty-four square input pulses were sent to the specimen every five minutes throughout all stages. The recorded output signal is the average of 64 output signals, which cancels out the noise and is statistically reliable. The sampling frequency of the received signal was 5 MHz so that both the front and the coda parts of the signal could be recorded with high resolution. Each group signal took approximately 0.5ms in total to be sent and received, which is almost instantaneous. The specimen's properties were considered constant, even at the loading stages. The received signal also filtered out the ambient frequencies below 100kHz so that the 10 Hz mechanical loading would not create changes in the output signals.

From the literature, the local heating within the tested specimen during cyclic loading is due to the viscous dissipated energy [23], [90]. In Phase I of the fatigue process, the drastic decrease of modulus and increase of phase angle was mainly caused by the thixotropy and nonlinearity. However, the change in the modulus and phase angle modifies the energy dissipation rate, which is associated with the heating effects during the loading process. When the effects of nonlinearity and thixotropy are stabilized, the temperature changes would be much more minor. Thus, it is used in this test protocol to identify the Phase I and Phase II of the fatigue process. However, the test protocol only measures the temperature at the specimen's surface, resulting from heat transfer from the inside and ambient temperatures. However, the changes at the surface of the specimen would be more minor than those in the center [4], and there will be a delay for this temperature to be stabilized.

There are several key points are indicated in Figure 5-7:

- Point “a”: In Stage I, at the stabilized specimen temperature during the fatigue process. This point can only be determined after the fatigue process is conducted.
- Point “b”: The starting point of Stage II. The specimen temperature is at 10°C. No load is applied.

- Point “c”: In Stage II, at the stabilized specimen temperature during the first cyclic loading process.
- Point “d”: The ending point of Stage II. The specimen temperature is at a stabilized temperature. The modulus is decreased by 10% from Point “c”.
- Point “e”: In Stage III is the ending point of the “cooling effect” during the rest period. The specimen temperature is at 10°C.
- Point “f”: The ending point of Stage III, Specimen temperature is at 10°C.
- Point “g”: In Stage IV, at the stabilized specimen temperature during the second cyclic loading process.

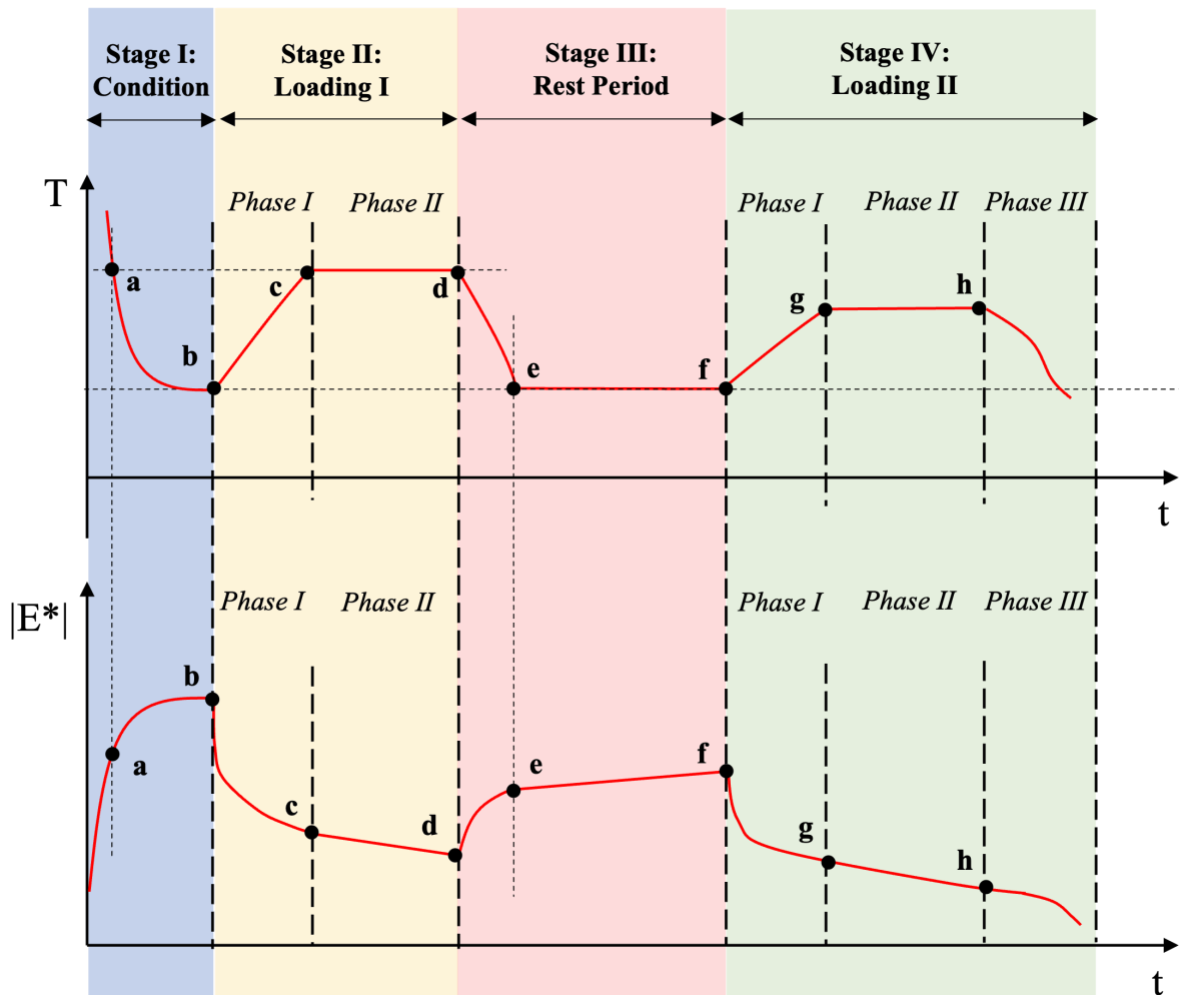


Figure 5-7. Schematic representation of proposed test procedure

Stage I: This is mainly the conditioning stage to ensure the temperature in the specimen is stabilized to 10°C before the loading. It lasts for at least 4 hours under force-control mode. The temperature probe in the dummy sample is used to simulate the temperature inside the specimen. The specimens were put at ambient temperature for at least 4 hours before conditioning. Ultrasonic measurements are done before the specimen is loaded, at ambient temperature, to understand how specimen properties change with the temperature as the only variable.

Stage II: The purpose of this stage is to produce fatigue damage in the specimen. The axial displacement and the displacements measured by the extensometers were offset before the loading started. The average displacement of the extensometers was used for the control, and a tapered sinusoidal loading was applied to the specimen. The loading was set to be stopped when there was a ten percent reduction in modulus from the ending point of fatigue Phase I. Four specimens underwent a fatigue test, with two being loaded at either ± 75 or ± 100 $\mu\text{m/m}$ strain level to estimate the number of cycles at which the loading should cease. The temperature and modulus were plotted versus the number of cycles. The stabilized temperature (T_{stabl}) and the corresponding point at the 10% modulus drop were determined before the test protocol was set up. Table 5-2 summarizes the data from the tested specimens that were used to determine the ending point of Stage II. From the table, the temperature change of the specimen when loaded at a higher strain level is more dramatic. Despite the difference in modulus, the number of cycles (N) at the reduced modulus of each group was reasonably consistent. The selection of the ending point of Stage II was rounded up to ensure enough damage was induced for the protocol setting.

Table 5-2. Ending Point of Stage II Determination

Specimen	ϵ_A ($\mu\text{m/m}$)	T_{stabl} ($^{\circ}\text{C}$)	E^* at T_{stabl} (MPa)	$E^*_{10\% \text{ reduce}}$ (MPa)	Cycle N at $E^*_{10\% \text{ reduce}}$	Cycle N at Ending Point
A1-1	± 75	10.2	3752	3378	198000	200000
A1-2		10.2	4116	3704	192000	
A2-1	± 100	10.5	3590	3231	96000	100000
A2-2		10.5	3071	2764	97000	

Stage III: This stage allows the specimen to heal and under force-control set at zero, with only temperature data being recorded. However, it would be beneficial if the axial displacement was also recorded, as it might give additional insight into changes in the specimen and the distance between the

transducers. This stage lasted 12 hours at a constant temperature of 10°C. Even though an elevated temperature might help the healing process, the test protocol used so far did not include a temperature change. If higher conditioning is used, the control mode should be changed to displacement control to minimize creep phenomena.

Stage IV: This stage was designed to reload the specimen to compare the mechanical response before and after the rest period. The setting is similar to Stage II's, except the loading period is 100,000 cycles longer than Stage II.

5.4.1 Bias Effects, Fatigue Damage, and Healing Estimation

Ultrasonic measurements were collected at the different stages of the test. The signal processing techniques described earlier were used to compare the data from the different stages. The bias effects, fatigue damage, and healing ability of the tested material can be estimated under different loading conditions.

The signal energy comparison can be used to study the overall trend of the energy change in the received signals and determine the proportion of each effect in terms of changing the features of the signal. Time Cross-Correlation (TCC) and Dynamic Time Warping (DTW) are the techniques used to compare the similarity between two signals. Selecting the reference point to quantify the different types of effects during the loading and unloading processes is crucial. Table 5-3 lists the types of effects and the points of interest that can be analyzed using the comparison methods. However, the comparison alone cannot separate the effect of nonlinearity and thixotropy as they happen simultaneously. The temperature effect can be studied using the data collected in Stage I when the specimen is not damaged, and the only changing variable is the temperature. The signal changes caused by the temperature change are much smaller than the changes due to the other effect, and it is considered that the temperature is stabilized during Phase II of the fatigue process. Besides, the nonlinearity and thixotropy effects are also stabilized in fatigue Phase II. Therefore, the fatigue damage can be directly obtained by comparing the similarities of the points during Phase II with the starting point of Phase II. A similar idea applies to quantify the healing potential of the asphalt mixtures. This way, all the effects can be quantified. Even though TCC and DTW are not traditional mechanical properties, like the modulus, phase angle, or dissipated energy, their magnitude can be used to quantify the material's microstructure or property changes due to these effects.

Table 5-3. Reference Points

Type of Effects	Reference Point	Point of Interest
Fatigue Damage	Point 'a'	Segment between Point 'c' & 'd'
Healing	Point 'e'	Segment between Point 'e' & 'f'
Temperature	Point 'b'	Points in Stage I
Thixotropy & Nonlinearity	Point 'a' & 'b'	Point 'c'

5.5 Results and Discussion

The test protocol that combines mechanical loading and non-destructive testing was applied to four specimens. However, the data for one specimen could not be used due to the movement of the transducer during the loading process. Therefore, only three sets of data were analyzed. Two specimens were tested at a strain amplitude of $\pm 75 \mu\text{m/m}$ and the third at $\pm 100 \mu\text{m/m}$. One example of the results used in the analysis of this protocol is presented in this section, focusing on a sample with a strain level of $75 \mu\text{m/m}$. Each data point for the modulus, phase angle, and dissipated energy was calculated using two consecutive cycles and plotted as a function of the time to compare the other data sets.

The temperature, modulus, phase angle, dissipated energy, and signal energy versus time for one full test following the proposed protocol are plotted in Figure 5-8. The temperature shown in Figure 5-8 (a) is the average temperature of the three surface thermal probes. The asymptote at Stages I and III is around 9.9°C , which can be seen as the actual ambient temperature in the chamber during the test. In Stages II and IV, the fatigue Phase I and II can be identified using the temperature plot. In Phase II of the fatigue process, the temperature stabilized in Stage I (first fatigue loading stage), while it showed an increasing slope in Stage II (second fatigue loading stage after the rest period). This indicates that more energy is dissipated during the second loading stage, indicating that the specimen was not healed to its original state. For a fatigue test, a nonlinear damage evolution exists [90]. It is difficult to quantify the restoration of the modulus before and after the rest period using the modulus data alone.

Although the temperature slope in Phase II of Stage II was not clear, the phase angle and dissipated energy slopes were quite obvious. The dissipated energy is highly correlated with the temperature change in the specimen [4], [95]. The difference between the measured temperature slope (Figure 5-8 (a)) and the other slopes (Figure 5-8 (b)&(c)) is due to the lack of measurement of the temperature inside the

specimen. Installing a thermal probe in the specimen may affect its integrity. Therefore, a non-destructive thermal measurement is needed for a more precise fatigue data analysis.

Figure 5-8 (e) presents the plot of signal energy evolution throughout the test protocol. The curve is similar to the modulus plot in Figure 5-7. A unique pattern can be seen in Stage II and IV due to the ultrasonic data acquisition rate. Data was collected every 5 and 10 minutes for the example specimen in Stage II and IV, respectively. The pattern has a frequency that matches the data collection frequency.

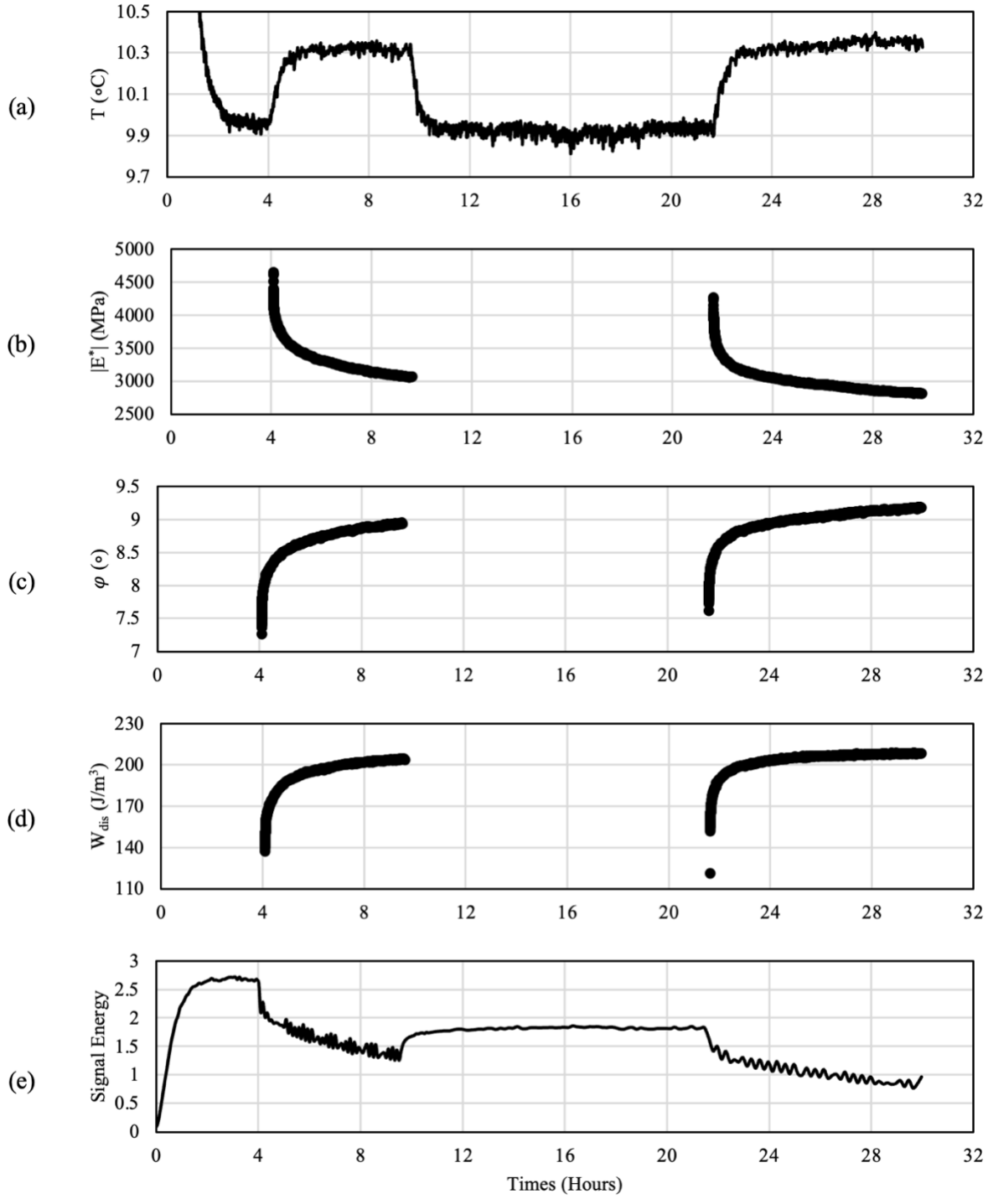


Figure 5-8. (a) Temperature, (b) Modulus, (c) Phase Angle, (d) Dissipated Energy, and (e) Signal Energy with respect to time during the entire test

5.5.1 Signal Energy Evolution

The signal energy is reproduced in Figure 5-9 with a higher resolution. The coordinates of the points in this plot must be determined first to quantify the proportion of each effect. The points were selected based on the Temperature data (Figure 5-8 (a)). The proportion of the bias effects and damage of the signal energy change in a fatigue process can be evaluated as follows:

- Heating effect: $\frac{b-a}{b-d} = \frac{2.63-2.55}{2.63-1.55} = 7.4\%$
- Thixotropy and nonlinearity effect: $\frac{(b-c)-(b-a)}{b-d} = \frac{(2.63-1.97)-(2.63-2.55)}{2.63-1.55} = 53.7\%$
- Fatigue damage: $\frac{d-c}{b-d} = \frac{1.97-1.55}{2.63-1.55} = 38.9\%$
- Healing: $\frac{f-e}{b-d} = \frac{1.82-1.75}{2.63-1.55} = 6.5\%$

The other two specimens share similar results. The specimen tested at a higher strain level has a more rapid energy decrease rate between Points ‘c’ and ‘d’, with a shorter duration. This analysis shows that the signal energy is very sensitive to damage in the specimen. However, it should be noted that the proportion of the bias effects contributing to the signal energy change cannot be directly correlated with the physical material properties, such as the modulus. An advanced modelling technique is needed to correlate the signal energy with the other material properties measured by mechanical loading.

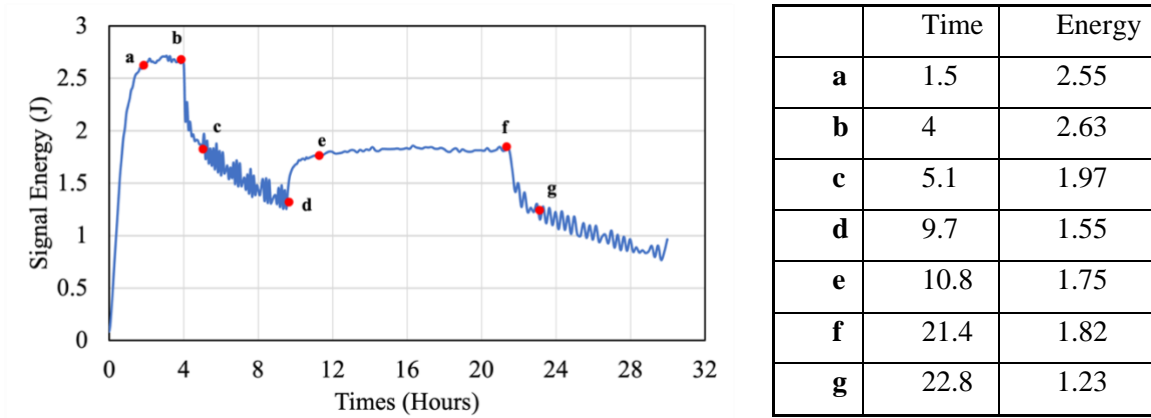


Figure 5-9. Signal Energy Plot

5.5.2 Time Signals Comparison

The signals received at the annotated points were extracted from the data set and plotted together in Figure 5-10 to better understand what features of the time signal have changed. Point pairs 'a' & 'c', 'c' & 'd', and 'e' & 'f' are plotted for both front and coda wave parts. The first pair compares the signals collected with and without loading at the same temperature, while the second pair compares the signals before and after being damaged. Finally, the third pair compares the signals before and after healing.

Signals collected at Points 'a' & 'c' have a larger amplitude than the other pairs. During the fatigue (Figure 5-10 (b)) and healing (Figure 5-10 (c)) processes, the front waveform has a slight magnitude change, and the coda waveform has some phase shifts, but the overall waveform shape remains the same. However, the first pair (Figure 5-10 (a)) has more dramatic changes, both in waveform shape and phase. This change is due to thixotropy that changed the molecular arrangements of the specimen. Point 'e' was selected roughly one hour after loading, and Point 'f' was recorded after 10 hours. This proves that no more thixotropy effect exists passing Point 'e', which disagrees with the previous findings that it takes a long time for thixotropy to vanish [4], [95]. This proves that relying on mechanical loading to evaluate the property of the specimen during the rest period may not be the most appropriate method to evaluate asphalt mixture healing capability.

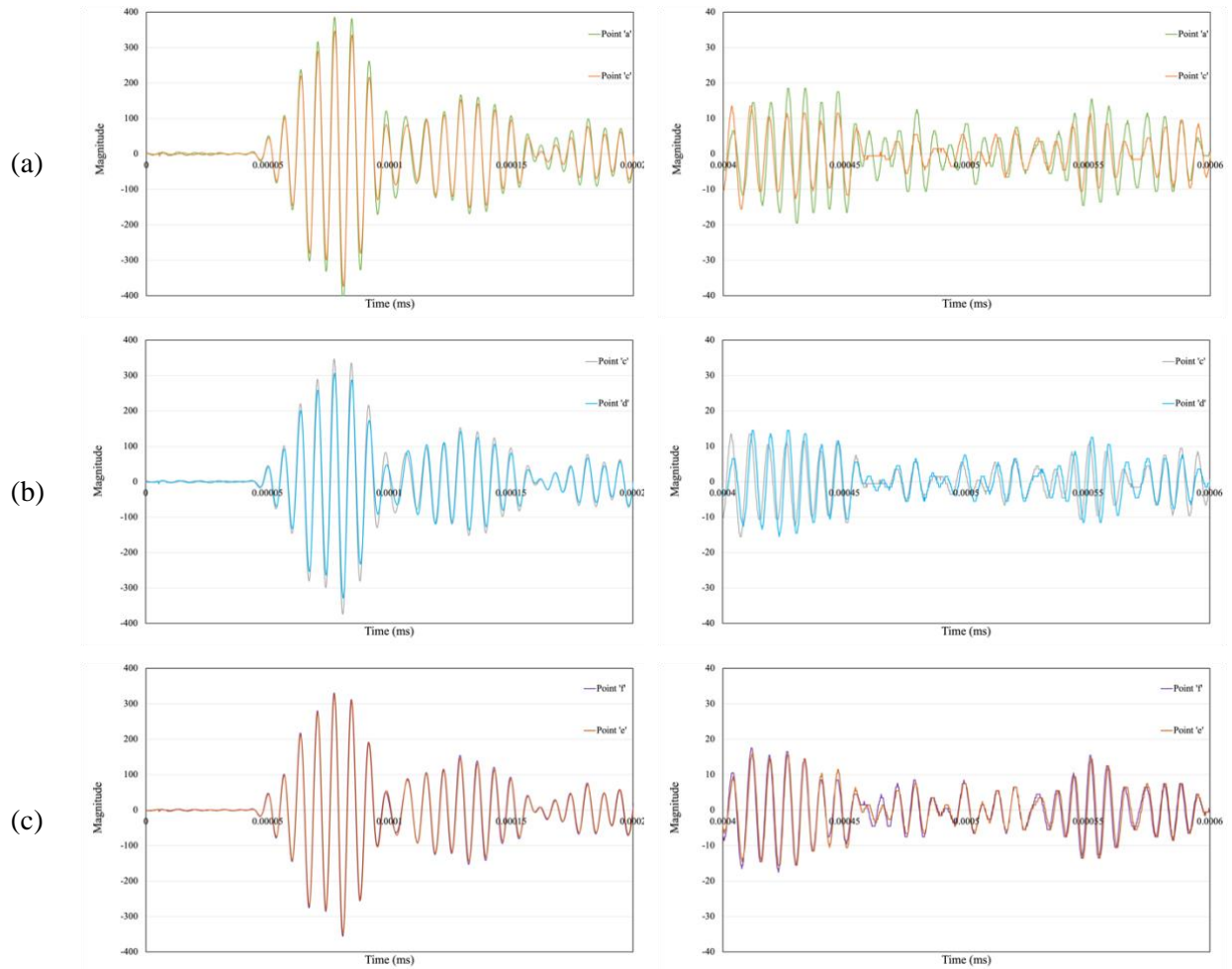


Figure 5-10. Time signal comparison between (a) 'a' & 'c', (b) 'c' & 'd', and (c) 'e' & 'f'

5.5.3 Using Signal Similarity to Evaluate Fatigue Damage of Asphalt Mixture

In this research, the assumption is made that the change in the signal caused by the temperature change in Phase II of the fatigue stages is neglected. A damage evolution curve can be generated by comparing the similarity of the signals collected in Phase II with the signals measured when the specimen was undamaged at the same temperature (Point 'a'). The two signal similarity comparison methods adopted in this research are Time Cross-Correlation and Dynamic Time Warping. First, Point 'a' and the fatigue phases were identified, then all the data points collected between Point 'c' and Point 'd' were compared with Point 'a' using TCC and DTW methods. The result of the example specimen is shown in Figure 5-11.

Figure 5-11(a) shows the results of using Dynamic Time Warping to compare the similarity of the signals. The lower the Distance is, the more similar the two signals are. Therefore, from the plot, Point 'a' has a distance of zero; when it compares itself, no warping distance is needed. When compared with Point 'a', the fatigue region (highlighted in red) has a linear change. The slopes during the fatigue region are associated with the damage level; a mild slope of the fatigue slopes is associated with less damage and visa versa. This method is sensitive to both magnitude and phase differences between two signals, which amplifies the signal difference in Stage I of the testing (before loading). The Cross-Correlation method mainly compares the phase shift in the signal, and the results are presented in Figure 5-11 (b). It minimized the signal changes before the loading started, and the fatigue portion had a better correlation than the other method.

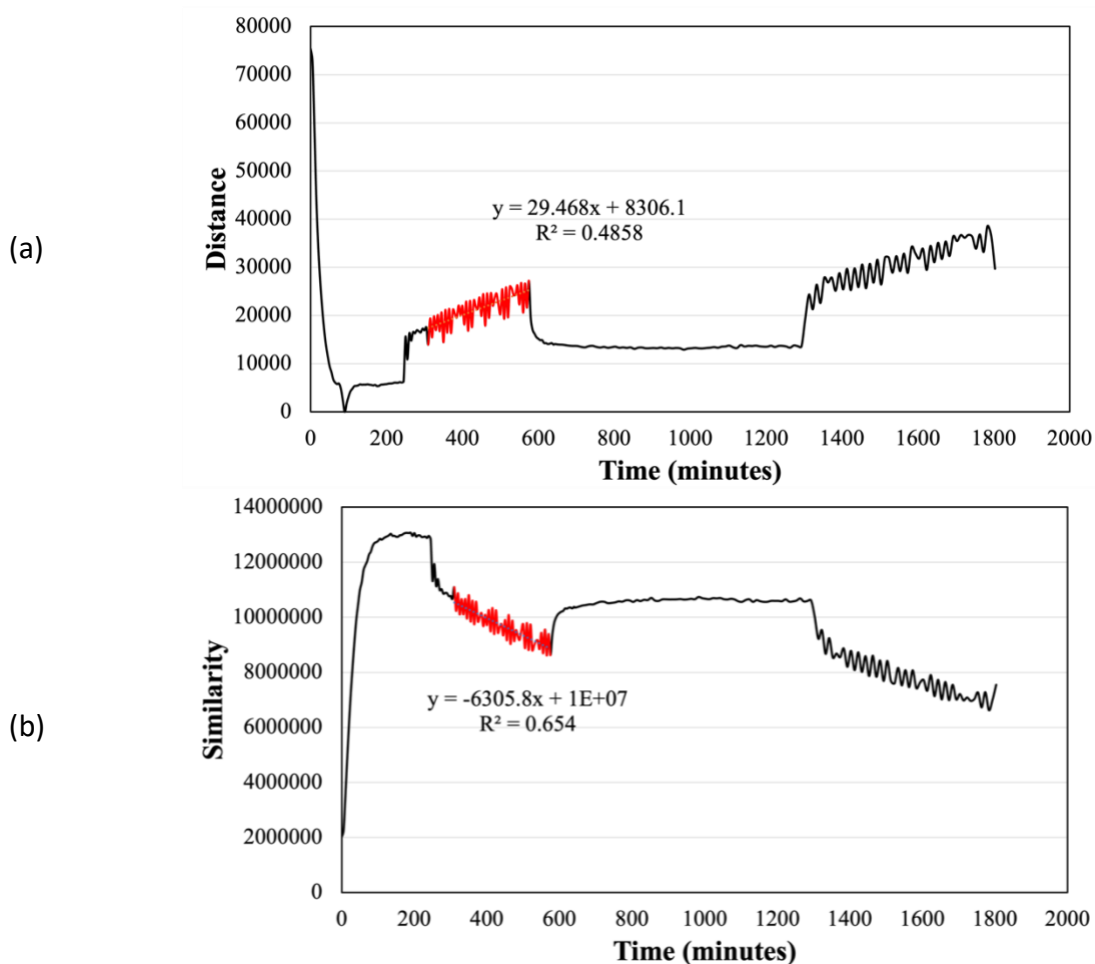


Figure 5-11. Data comparison using (a) Dynamic Time Warping and (b) Time Cross-Correlation

Table 5-4. Fatigue Damage Rate Comparison

Specimen	ϵ_A ($\mu\text{m/m}$)	$\Delta_{\text{Signal Energy}}$	$\Delta_{\text{Dynamic Time Warping}}$	$\Delta_{\text{Time Cross-Correlation}}$
1	± 75	-0.0018	29	-6306
2		-0.0009	14	-2979
3	± 100	-0.004	48	-12532

The rate of change for the fatigue damages is estimated using the slope of the fatigue portion. The changes in the signal energy plots (Figure 5-9, Point ‘c’ to ‘d’) are also being calculated. The results for all three specimens are summarized in Table 5-4. It shows that the ranking of the three specimens using all three methods is the same. Specimen 3 has a faster damage rate as it was tested at a higher strain level. However, the difference between Specimens 1 and 2 is significant and cannot be neglected. More data is needed to verify this type of analysis.

5.6 Summary and Conclusions

This research incorporated the Tension-Compression test combined with the Ultrasonic Wave Propagation (UWP) technique to study the feasibility of using UWP measurements to quantify and separate the bias effects during the asphalt fatigue and healing tests. This study adopted a new test configuration designed at CPATT from the University of Waterloo to allow continuous ultrasonic readings throughout the loading and unloading processes on an asphalt specimen. A new test protocol with four successive stages was proposed. In the protocol, an axial sinusoidal T/C fatigue test was conducted on cylindrical asphalt concrete specimens at 10 °C and 10 Hz. The test protocol used the surface temperature of the specimen to identify the fatigue phases and evaluate specimen properties change using three signal processing methods. The test results from the proposed protocol led to the following conclusions:

- Without the need for complicated modelling or analysis, this new protocol directly separates the ‘true’ fatigue damage from the other phenomena.
- The non-fatigue-related phenomena, such as self-heating, nonlinearity and thixotropy, could be quantified by comparing the signal energy change during the fatigue process.

- From the signal waveform comparison, thixotropy changed the molecular arrangement of the specimen during loading and vanished at a relatively fast rate when loading the specimen was stopped.
- Mechanical loadings should not be applied to the specimen during the rest period to preserve the elimination of the thixotropy effects.
- Using the similarity of the signals to evaluate fatigue damage rate is still in the preliminary stage. However, a clear difference is observed when testing the specimen at different strain levels.

Future studies are needed to validate this protocol on a large selection of mixtures and testing conditions. Using modelling, the test configuration can be used to draw a correlation between the signal features and the material properties. The healing of the specimen should be monitored under different conditions. A better way to measure the temperature profile of the specimen is needed to quantify the true fatigue or healing effects more precisely.

Chapter 6

Conclusions, Contributions, Recommendations and Future Work

6.1 General Summary

This research was conducted with the main purpose of improving the laboratory asphalt concrete fatigue and self-healing tests by combining NDT methods. The tasks to achieve the purpose can be broadly categorized into three major stages. This study was mainly conducted based on laboratory-collected data. Nine types of polymer modified binders and two batches of aggregates were used for this study. The asphalt binder was provided by Yellowline Asphalt Products Ltd., with 0 to 4% of SBS dosages. The aggregates were local diabase and limestone in Ontario.

Stage 1: UPPT on Undamaged Specimen

The main objective of this stage is to investigate the effectiveness of using IDEAL-CT and UPPT to assess the cracking susceptibility of elastomer-modified asphalt mixtures by comparing their results with a previous study on the same material. The UPPT was first applied to the specimen, and several wave attenuation analyses were applied to the test results. The specimens were then tested under monotonic loading, and the results show that the existing cracking index cannot effectively characterize the elastic response of the elastomer-modified asphalt mixtures. However, the fracture energy till the fracture point proved to have a good potential to characterize the asphalt mixtures. The UPPT results show that more energy is absorbed as the base binder becomes more viscous, and more energy is transmitted as the dosage of the polymer increases. This suggests that the wave attenuation analysis has a good potential to characterize polymer-modified bituminous materials.

Stage 2: UPPT Monitoring Specimen Property during Fracture Healing Test

An indirect tensile test has been selected as it predetermines the crack location. A loading, resting and reloading process was applied to the asphalt concrete specimen, and an ultrasonic pulse-receiver device was used to monitor the whole test process. The test setup is used to monitor the specimen property changes with higher sensitivity during healing, and several signal processing techniques are employed to analyze the features of the signal transmitted through the specimen. An intrinsic healing rate equation was proposed by studying changes in the ultrasonic signals and the measured physical properties of the specimen. The initial results indicate that this setup can effectively evaluate the asphalt's intrinsic self-healing properties and distinguish changes in healing between stiffer and more aged binders.

Stage 3: UPPT Monitoring Specimen Property during Fatigue Healing Test

The uniaxial tension-compression fatigue test was selected for this stage. Ultrasonic transmitters were mounted to the specimen to conduct UPPT. A novel test configuration that was designed by CPATT research group is used in this study. The specimen was conditioned in a chamber to meet the test condition. The temperature change process was also monitored with the UPPT, and the data were used to quantify the bias effects of the cyclic loading by comparing the property of the specimen with and without loading at the same temperature level. A modified tension-compression asphalt fatigue test was proposed by introducing a rest period during the fatigue test process. A test protocol was proposed to assess bituminous materials' fatigue damage and intrinsic healing ability. The results showed that this protocol is able to separate true fatigue damage from other phenomena, such as self-heating, nonlinearity, and thixotropy, by comparing the signal energy change during the fatigue process. It was also found that mechanical loadings should not be applied during the rest period, and that signal similarity can be used to evaluate fatigue damage rate.

6.2 Significant Contributions

This thesis focused on an important but less-addressed area. Using non-destructive tests to monitor a cracking process of a material is not common. Furthermore, most of the existing work on the application of ultrasonic wave-based methods in asphalt concrete materials solely rely on the time of flight and elastic modulus calculations, which would not be able to properly capture the micro-scale changes in the material. The followings are the major contributions of this study:

- This study focuses extensively on using the ultrasonic test to evaluate asphalt specimen properties. Several signal processing techniques, including Fourier Transformation, Wavelet Transformation, Wavelet Synchro Squeezed Transformation, Windowing, Filtering, Cross-Correlation, and Dynamic Time Warping, have been carried out for specimens at different conditions. Several wave features have been calculated and presented in this study. It provides a 'toolbox' that can be used when conducting ultrasonic testing on high damping, viscoelastic materials, like bituminous mixtures.
- This research proposed two test protocols that can evaluate intrinsic healing of asphalt materials using two configurations. The improved laboratory fatigue and fracture testing can promote sustainability in pavement materials and designs. Furthermore, this project also contributes to

better understanding of crack initiation and propagation processes in pavement materials, which can improve the existing state of pavement rehabilitation and maintenance techniques as well as pavement condition prediction models.

6.3 Recommendations and Future Works

Based on the outcome of this study, the followings recommendations are:

- Using an NDT technique such as the one proposed in this study is recommended in-lieu of the mechanical loading that has been typically used to monitor the specimen's mechanical response during the healing phase. This will minimize any undesirable disturbance to the specimen as well as any biases due to the small-amplitude mechanical loading.
- To effectively transmit the ultrasonic pulse waves through the specimens in a consistent manner, it was crucial to provide a flat surface for the piezoelectric transducers. Therefore, it would be highly recommended to glue a thin metal piece on the contact points of the specimen.
- For the DRHRP test protocol, extensometers were removed manually before the second loading phase to avoid damaging them. It would be better to utilize another type of extensometer, such as non-contact measuring devices, that can track the horizontal displacement with a larger capacity and throughout the whole testing process.
- For the fatigue healing test protocol in this study, only the surface temperature was recorded. However, with respect to the effect of temperature variation on the healing and mechanical properties of the asphalt materials, it would be better to have a thermal probe that can measure the temperature at different points withing the specimen.
- Both test protocols need to be verified with more asphalt mixtures at different conditions.

References

- [1] S. Tangella, J. Craus, J. A. Deacon, and C. L. Monismith, “Summary Report on Fatigue Response of Asphalt Mixtures,” in Transportation Research Board Conference, Feb. 1990.
- [2] P. Court, “Project 9-44 Developing a Plan for Validating an Endurance Limit for HMA Pavements HMA Endurance Limit Validation Study Research Plan,” Advanced Asphalt Technologies Engineering Services for the Asphalt Industry, Virginia, 2008.
- [3] S. Mangiafico, C. Sauzéat, H. Di Benedetto, S. Pouget, F. Olard, and L. Planque, “Quantification of Biasing Effects during Fatigue Tests on Asphalt Mixes: Non-Linearity, Self-Heating And Thixotropy,” *Road Materials and Pavement Design*, vol. 16, no. Supplement 2, pp. 143–180, 2015, doi: 10.1080/14680629.2015.1077000.
- [4] H. Di Benedetto, Q. T. Nguyen, and C. Sauzéat, “Nonlinearity, Heating, Fatigue And Thixotropy during Cyclic Loading of Asphalt Mixtures,” *Road Materials and Pavement Design*, vol. 12, no. 1, pp. 129-158, 2011, doi: 10.1080/14680629.2011.9690356.
- [5] T. S. F. Zhou, S. Im, L. Sun, “Development of an IDEAL Cracking Test for Asphalt Mix Design, Quality Control and Quality Assurance,” *Road Mater. Pavement Des.*, vol. 18, pp. 405–427, 2017, [Online]. Available: <https://doi.org/10.1080/14680629.2017.1389082>
- [6] H. Chen, Y. Zhang, and H. U. Bahia, “The Role of Binders in Mixture Cracking Resistance Measured by IDEAL-CT Test,” *International Journal of Fatigue*, vol. 142, Jan. 2021, doi: 10.1016/J.IJFATIGUE.2020.105947.
- [7] C. Yan, Y. Zhang, and H. U. Bahia, “Comparison Between SCB-IFIT, Un-notched SCB-IFIT And IDEAL-CT For Measuring Cracking Resistance of Asphalt Mixtures,” *Construction and Building Materials*, vol. 252, p. 119060, 2020, doi: 10.1016/j.conbuildmat.2020.119060.
- [8] J. Qiu, “Self Healing of Asphalt Mixtures Towards a Better Understanding of the Mechanism,” Section of Road and Railway Engineering, *Delft University of Technology*, Zutphen, the Netherlands, 2012.
- [9] D. Sun, G. Sun, X. Zhu, A. Guarin, B. Li, Z. Dai, J. Ling, “A comprehensive review on self-healing of asphalt materials: Mechanism, model, characterization and enhancement,” *Advances in Colloid and Interface Science*, vol. 256, pp. 65-93, 2018, doi: 10.1016/j.cis.2018.05.003.

- [10] J. Qiu, M. van de Ven, S. Wu, J. Yu, and A. Molenaar, "Evaluating Self-Healing Capability of Bituminous Mastics," *Experimental Mechanics*, vol. 52, no. 8, pp. 1163–1171, Oct. 2012, doi: 10.1007/s11340-011-9573-1.
- [11] B. Liang, F. Lan, K. Shi, G. Qian, Z. Liu, and J. Zheng, "Review on The Self-Healing of Asphalt Materials: Mechanism, Affecting Factors, Assessments and Improvements," *Construction and Building Materials*, vol. 266, p. 120453, 2021, doi: 10.1016/j.conbuildmat.2020.120453.
- [12] B. H. Leegwater G, Tabaković A, Baglieri O, Hammoum F, "Terms and Definitions on Crack-Healing and Restoration of Mechanical Properties in Bituminous Materials," in *RILEM International Symposium on Bituminous Materials*, Switzerland AG, 2022, pp. 47-53.
- [13] Á. García, "Self-healing of Open Cracks in Asphalt Mastic," *Fuel*, vol. 93, pp. 264–272, Mar. 2012, doi: 10.1016/j.fuel.2011.09.009.
- [14] Z. Jiang, "Innovative Nondestructive Testing (NDT) for Condition Assessment of Longitudinal Joints in Asphalt Pavements," Ph.D. dissertation, Department of Civil and Environmental Engineering, University of Waterloo, Ontario, 2007.
- [15] Z. Jiang, J. Ponniah, G. Cascante, and R. Haas, "Nondestructive Ultrasonic Testing Methodology for Condition Assessment of Hot Mix Asphalt Specimens," *Canadian Journal of Civil Engineering*, vol. 38, no. 7, pp. 751–761, 2011, doi: 10.1139/L11-046.
- [16] F. Olard, "Comportement Thermomécanique Des Enrobés Bitumineux A Basses Températures. Relations entre les propriétés du liant et de l'enrobé," Ph.D. dissertation, INSA Lyon, 2003.
- [17] H. Di Benedetto, M. N. Partl, L. Francken, and C. De La Roche Saint André, "Stiffness Testing for Bituminous Mixtures," *Materials and Structures/Materiaux et Constructions*, vol. 34, no. 236, pp. 66–70, 2001, doi: 10.1007/bf02481553.
- [18] N. I. Nur, E. Chailleux, and G. D. Airey, "A Comparative Study of The Influence of Shift Factor Equations on Master Curve Construction," *International Journal of Pavement Research and Technology*, vol. 4, no. 6, pp. 324–336, 2011, doi: 10.6135/ijprt.org.tw/2011.4(6).324.
- [19] F. Olard and H. Di Benedetto, "General '2S2P1D' Model and Relation Between the Linear Viscoelastic Behaviours of Bituminous Binders and Mixes," *Road Materials and Pavement Design*, vol. 4, no. 2, pp. 185–224, 2003, doi: 10.1080/14680629.2003.9689946.

- [20] Cater A, Donovan H, Macinnis K, Strynadka T, *Hot Mix Asphalt Textbook*, Canadian Technical Asphalt Association, Canada, 2018.
- [21] P. Tavassoti-Kheiry, M. Solaimanian, and T. Qiu, “Characterization of High RAP/RAS Asphalt Mixtures Using Resonant Column Tests,” *Journal of Materials in Civil Engineering*, vol. 28, no. 11, Nov. 2016, doi: 10.1061/(asce)mt.1943-5533.0001668.
- [22] F. Moreno-Navarro and M. C. Rubio-Gámez, “A Review of Fatigue Damage In Bituminous Mixtures: Understanding the Phenomenon from A New Perspective,” *Construction and Building Materials*, vol. 113. Elsevier Ltd, pp. 927–938, Jun. 15, 2016. doi: 10.1016/j.conbuildmat.2016.03.126.
- [23] H. Di Benedetto, C. de La Roche, H. Baaj, A. Pronk, and R. Lundström, “Fatigue of Bituminous Mixtures,” *Materials and Structures*, vol. 37, pp. 202-216, April 2004, doi: 10.1007/bf02481620.
- [24] A. Soltani and D. A. Anderson, “New Test Protocol to Measure Fatigue Damage in Asphalt Mixtures,” *Road Materials and Pavement Design*, vol. 6, no. 4, pp. 485–514, Jan. 2005, doi: 10.1080/14680629.2005.9690017.
- [25] S. Mangiafico, L. F. A. L. Babadopulos, C. Sauzéat, and H. Di Benedetto, “Nonlinearity of Bituminous Mixtures,” *Mechanics of Time-Dependent Materials*, vol. 22, no. 1, pp. 29–49, 2018, doi: 10.1007/s11043-017-9350-3.
- [26] J. F. Masson, P. Collins, and G. Polomark, “Steric Hardening and the Ordering of Asphaltenes in Bitumen,” *Energy and Fuels*, vol. 19, no. 1, pp. 120–122, Jan. 2005, doi: 10.1021/ef0498667.
- [27] A. A. Tayebali, G. M. Rowe, and J. B. Sousa, *Fatigue response of asphalt-aggregate mixtures*, Strategic Highway Research Program National Research Council, Washington, DC, 1994.
- [28] W. Van Dijk and W. VISSER, “Energy Approach to Fatigue for Pavement Design,” *Journal of the Association of Asphalt Paving Technology*, vol. 46, pp. 1-40, 1977.
- [29] K. Ghazi and S. Aroon, “A Distinctive Fatigue Failure Criterion,” *Journal of the AAPT*, vol. 73, pp. 585-622, 2004.

- [30] S. Shen, "Dissipated Energy Concepts for HMA Performance: Fatigue and Healing," Ph.D. dissertation, Department of Civil and Environmental Engineering, University of Illinois at Urbana-Champaign Urbana, Illinois, 2006.
- [31] C. L. Tayebali, A. A., Deacon, J.A., Coplantz, J.S., and Monismith, "Modeling Fatigue Response of Asphalt-Aggregate Mixtures," *Proceedings of Associations of Asphalt Paving Technologists*, vol. 62, pp. 385–421, 1993.
- [32] S. H. Carpenter, K. A. Ghuzlan, and S. Shen, "Fatigue Endurance Limit for Highway and Airport Pavements," in *Transportation Research Record*, National Research Council, 2003, pp. 131–138. doi: 10.3141/1832-16.
- [33] H. Di Benedetto, A. A. Soltani, and P. Chaverot, "Fatigue Damage for Bituminous Mixtures: A Pertinent Approach," *Journal of the Association of Asphalt Paving Technologists*, vol. 65, 1996. <https://trid.trb.org/view/487704> (accessed Sep. 12, 2020).
- [34] H. Baaj, H. Di Benedetto, and P. Chaverot, "Effect of binder characteristics on fatigue of asphalt pavement using an intrinsic damage approach," *Road Materials and Pavement Design*, 2005, doi: 10.1080/14680629.2005.9690003.
- [35] S. W. Park, Y. R. Kim, and R. A. Schapery, "A Viscoelastic Continuum Damage Model and Its Application to Uniaxial Behavior of Asphalt Concrete," *Mechanics of Materials*, vol. 24, no. 4, pp. 241–255, 1996, doi: 10.1016/S0167-6636(96)00042-7.
- [36] R. A. Schapery, "A Theory of Mechanical Behavior of Elastic Media With Growing Damage and Other Changes in Structure," *Journal of the Mechanics and Physics of Solids*, vol. 38, no. 2, pp. 215–253, Jan. 1990, doi: 10.1016/0022-5096(90)90035-3.
- [37] R. A. Schapery, "Correspondence Principles and A Generalized J Integral for Large Deformation and Fracture Analysis of Viscoelastic Media," *International Journal of Fracture*, vol. 25, no. 3, pp. 195–223, 1984, doi: 10.1007/BF01140837.
- [38] Y. Kim, H. Lee, and D. Little, "Fatigue characterization of asphalt concrete using viscoelasticity and continuum damage theory," *Journal of the Association of Asphalt Paving Technologists*, vol. 66, 1997.
- [39] M. E. Kutay, N. Gibson, and J. Youtcheff, "Conventional and viscoelastic continuum damage (VECD) - Based fatigue analysis of polymer modified asphalt pavements," *Asphalt Paving*

Technology: Association of Asphalt Paving Technologists-Proceedings of the Technical Sessions, vol. 77, pp. 395–433, 2008.

- [40] P. S. Pell, “Fatigue Of Asphalt Pavement Mixes,” International Conference on the Structural Design of Asphalt Pavements, Michigan, Aug. 1967.
- [41] A. García, J. Norambuena-Contreras, M. Bueno, and M. N. Partl, “Single and Multiple Healing of Porous and Dense Asphalt Concrete,” *Journal of Intelligent Material Systems and Structures*, vol. 26, no. 4, pp. 425–433, 2015, doi: 10.1177/1045389X14529029.
- [42] D. Sun, G. Sun, X. Zhu, A. Guarin, B. Li, Z. Dai, J. Ling, “A Comprehensive Review on Self-Healing of Asphalt Materials: Mechanism, Model, Characterization And Enhancement,” *Advances in Colloid and Interface Science*, vol. 256, pp. 65-93, 2018, doi: 10.1016/j.cis.2018.05.003.
- [43] D. Sun, G. Sun, X. Zhu, Q. Pang, F. Yu, and T. Lin, “Identification of Wetting And Molecular Diffusion Stages during Self-Healing Process of Asphalt Binder via Fluorescence Microscope,” *Construction and Building Materials*, vol. 132, pp. 230–239, 2017, doi: 10.1016/j.conbuildmat.2016.11.137.
- [44] X. Wang, S. Shen, H. Huang, and Z. Zhang, “Quantitative Assessment of the Pavement Modulus and Surface Crack using the Rayleigh Wave Dispersion Curve,” *Transportation Research Record*, vol. 2674, no. 5, pp. 259–269, 2020, doi: 10.1177/0361198120913856.
- [45] T. Saarenketo and T. Scullion, “Road Evaluation with Ground Penetrating Radar,” *Journal of Applied Geophysics*, vol. 43, no. 2–4, pp. 119–138, Mar. 2000, doi: 10.1016/S0926-9851(99)00052-X.
- [46] S. Lagüela, M. Solla, I. Puente, and F. J. Prego, “Joint Use of GPR, IRT and TLS Techniques for the Integral Damage Detection In Paving,” *Construction and Building Materials*, vol. 174, pp. 749–760, Jun. 2018, doi: 10.1016/j.conbuildmat.2018.04.159.
- [47] L. Edwards and H. P. Bell, “Comparative evaluation of nondestructive devices for measuring pavement thickness in the field,” *International Journal of Pavement Research and Technology*, vol. 9, no. 2, pp. 102–111, Mar. 2016, doi: 10.1016/J.IJPRT.2016.03.001.

- [48] D. Mounier, H. di Benedetto, and C. Sauzéat, “Determination of bituminous mixtures linear properties using ultrasonic wave propagation,” *Construction and Building Materials*, vol. 36, pp. 638–647, 2012, doi: 10.1016/j.conbuildmat.2012.04.136.
- [49] S. Abo-Qudais and A. Suleiman, “Monitoring fatigue damage and crack healing by ultrasound wave velocity,” *Nondestructive Testing and Evaluation*, vol. 20, no. 2, pp. 125–145, 2005, doi: 10.1080/10589750500206774.
- [50] B. Birgisson, R. Roque, and G. C. Page, “Ultrasonic Pulse Wave Velocity Test for Monitoring Changes in Hot-Mix Asphalt Mixture Integrity from Exposure to Moisture,” *Transportation Research Record*, no. 1832, pp. 173–181, 2003, doi: 10.3141/1832-21.
- [51] H. Di Benedetto, C. Sauzéat, J. Sohm, H. Di, and B.-C. Sauzéat, “Stiffness of Bituminous Mixtures Using Ultrasonic Wave Propagation,” *Road Materials and Pavement Design*, vol. 10, no. 4, pp. 789–814, Jan. 2011, doi: 10.1080/14680629.2009.9690227.
- [52] Y. Yildirim, “Polymer modified asphalt binders,” *Construction and Building Materials*, vol. 21, no. 1, pp. 66–72, Jan. 2007, doi: 10.1016/j.conbuildmat.2005.07.007.
- [53] C. P. Valkering, W. C. Vonk, and C. D. Whiteoak, “Improved Asphalt Properties Using SBS Modified Bitumens,” in *Shell Bitumen Rev. 66.*, 1992, pp. 9–11.
- [54] Y. Becker, M. P. Méndez, and Y. Rodríguez, “Polymer Modified Asphalt.” *Vision Technologica*, vol.9, pp. 39-50, 2001.
- [55] F. Xiao, S. Amirkhani, H. Wang, and P. Hao, “Rheological Property Investigations for Polymer and Polyphosphoric Acid Modified Asphalt Binders at High Temperatures,” *Construction and Building Materials*, vol. 64, pp. 316–323, Aug. 2014, doi: 10.1016/j.conbuildmat.2014.04.082.
- [56] M. Sabouri, D. Mirzaeian, and A. Moniri, “Effectiveness of Linear Amplitude Sweep (LAS) asphalt binder test in predicting asphalt mixtures fatigue performance,” *Construction and Building Materials*, vol. 171, pp. 281–290, May 2018, doi: 10.1016/j.conbuildmat.2018.03.146.
- [57] S. C. Huang and H. di Benedetto, “Damage Healing in Asphalt Pavements: Theory, Mechanisms, Measurement, and Modeling,” in *Advances in asphalt materials: Road and pavement construction*. Cambridge: Woodhead, 2015, pp. 205-242, doi: 10.1016/C2014-0-02666-4.

- [58] M. Aurilio, P. Tavassoti, M. Elwardany, and H. Baaj, "Impact of Styrene-Butadiene-Styrene (SBS) Content on Asphalt Binder's Fatigue Resistance at Various Aging Levels Using Viscoelastic Continuum Damage And Fracture Mechanics," *Construction and Building Materials*, vol. 305, Oct. 2021, doi: 10.1016/j.conbuildmat.2021.124627.
- [59] F. Zhou *et al.*, "Draft final report of NCHRP 9-57:Experimental Design for Field Validation of Laboratory Tests to Assess Cracking Resistance of Asphalt Mixtures," Jan. 2016.
- [60] H. Chen, Y. Zhang, and H. U. Bahia, "The Role of Binders in Mixture Cracking Resistance Measured by IDEAL-CT Test," *International Journal of Fatigue*, vol. 142, Jan. 2021, doi: 10.1016/J.IJFATIGUE.2020.105947.
- [61] A. Seitllari, I. Boz, J. Habbouche, and S. D. Diefenderfer, "Assessment of Cracking Performance Indices of Asphalt Mixtures at Intermediate Temperatures," *International Journal of Pavement Engineering*, vol. 23, no. 1, pp. 70–79, 2022, doi: 10.1080/10298436.2020.1730838.
- [62] "Standard Test Method for Determination of Cracking Tolerance Index of Asphalt Mixture Using the Indirect Tensile Cracking Test at Intermediate Temperature", doi: 10.1520/D8225-19.
- [63] J. R. Medina, B. S. Underwood, and M. Mamlouk, "Estimation of asphalt concrete modulus using the ultrasonic pulse velocity test," *Journal of Transportation Engineering Part B: Pavements*, vol. 144, no. 2, pp. 1–9, 2018, doi: 10.1061/JPEODX.0000036.
- [64] P. Tavassoti-Kheiry, I. Boz, X. Chen, and M. Solaimanian, "Application of Ultrasonic Pulse Velocity Testing of Asphalt Concrete Mixtures to Improve the Prediction Accuracy of Dynamic Modulus Master Curve," *Airfield and Highway Pavements 2017: Testing and Characterization of Bound and Unbound Pavement Materials - Proceedings of the International Conference on Highway Pavements and Airfield Technology 2017*, vol. 2017-Augus, pp. 152–164, 2017, doi: 10.1061/9780784480939.014.
- [65] A. Basu and A. Aydin, "Evaluation of Ultrasonic Testing in Rock Material Characterization," 2006. [Online]. Available: www.astm.org

- [66] S. Popovics and J. S. Popovics, “Critique of the ultrasonic pulse velocity method for testing concrete,” *Nondestructive Testing of Concrete Elements and Structures*, pp. 94–103, 1992, doi: 10.1016/S0963-8695(97)88958-X.
- [67] M. Aurilio and H. Baaj, “Predicting HMA Fatigue Using the Double Edge Notched Tension Test and Multiple Stress Creep Recovery Test” in *Canadian Technical Asphalt Association Conference*, Halifax, Ontario, 2017, pp. 267-290.
- [68] Z. P. Bazant and P. C. Prat, “Effect of Temperature and Humidity on Fracture Energy of Concrete,” *ACI Material Journal*, vol. 85, no. 4, pp. 262–271, 1988.
- [69] C. Liu, “Elastic Constants Determination and Deformation Observation Using Brazilian Disk Geometry,” *Experimental Mechanics*, vol. 50, no. 7, pp. 1025–1039, Aug. 2010, doi: 10.1007/s11340-009-9281-2.
- [70] F. Kaseer, F. Yin, E. Arámbula-Mercado, A. Epps Martin, J. S. Daniel, and S. Salari, “Development of An Index to Evaluate the Cracking Potential of Asphalt Mixtures using the Semi-Circular Bending Test,” *Construction and Building Materials*, vol. 167, pp. 286–298, Apr. 2018, doi: 10.1016/j.conbuildmat.2018.02.014.
- [71] Y. Zhu, E. v. Dave, R. Rahbar-Rastegar, J. S. Daniel, and A. Zofka, “Comprehensive evaluation of low-temperature fracture indices for asphalt mixtures,” *Road Materials and Pavement Design*, vol. 18, no. S4, pp. 467–490, Nov. 2017, doi:10.1080/14680629.2017.1389085.
- [72] J. C. Carret, H. di Benedetto, and C. Sauzéat, “Characterization of Asphalt Mixes Behaviour From Dynamic Tests and Comparison with Conventional Cyclic Tension-Compression Tests,” *Applied Sciences (Switzerland)*, vol. 8, no. 11, 2018, doi: 10.3390/app8112117.
- [73] G. H. Kaufmann and G. E. Galizzi, “Phase Measurement in Temporal Speckle Pattern Interferometry: Comparison Between the Phase-Shifting and The Fourier Transform Methods,” *Applied Optics*, vol. 41, no. 34, pp. 7254–7263, Dec. 2002, doi: 10.1364/AO.41.007254.
- [74] M. Aurilio, A. Qabur, M. A. S. Candidate, P. Mikhailenko, H. Baaj, and N. W. Mcleod, “Comparing the Fatigue Performance of HMA Samples with PMA to their Multiple Stress Creep Recovery and Double Notched Tension Test Properties,” in *Canadian Technical Asphalt Association Conference*, Regina, Ontario, 2018, pp. 385-410. 2018.

- [75] P. Wiciak, “Quality Assessment of Composite Materials using Ultrasonic Non-Destructive Testing Methods,” Ph.D. dissertation, Department of Civil and Environmental Engineering, University of Waterloo, Ontario, 2020.
- [76] E. C. Leong, S. H. Yeo, and H. Rahardjo, “Measurement of wave velocities and attenuation using an ultrasonic test system,” *Canadian Geotechnical Journal*, vol. 41, no. 5, pp. 844–860, Oct. 2004, doi: 10.1139/T04-041.
- [77] P. Bazin and J. Saunier, “Deformability, Fatigue and Healing Properties of Asphalt Mixes,” Second International Conference on Design of Asphalt Pavements, Ann Arbor, Mich., 1967.
- [78] R. Aurilio, M. Aurilio, and H. Baaj, “High-Performance Pavements: A Focus on Self-healing Asphalt Technologies,” in *Canadian Technical Asphalt Association Conference*, Virtual, 2020, pp. 127-155.
- [79] R. P. Wool and K. M. O’Connor, “A Theory Crack Healing in Polymers,” *Journal of Applied Physics*, vol. 52, no. 10, pp. 5953-5963, Jun. 1998, doi: 10.1063/1.328526.
- [80] A. Bhasin, R. Bommavaram, K. Vasconcelos, and D. N. Little, “A Framework to Quantify the Effect of Healing in Bituminous Materials using Material Properties,” *Road Materials and Pavement Design*, vol. 9, pp. 219–242, Jan. 2011, doi: 10.1080/14680629.2008.9690167.
- [81] R. L. Lytton, “Characterizing Asphalt Pavements for Performance,” Civil Engineering Department, Texas A&M University System, TX, Research Record 1723, PP 5-18, 2000
- [82] Y. R. Kim, D. N. Little, and F. C. Benson, “Chemical and Mechanical Evaluation on Healing Mechanism of Asphalt Concrete (with Discussion),” *Journal of the Association of Asphalt Paving Technologists*, vol. 59, 1990.
- [83] L. Zhou, W. Huang, Y. Zhang, Q. Lv, C. Yan, and Y. Jiao, “Evaluation of the adhesion and healing properties of modified asphalt binders,” *Construction and Building Materials*, vol. 251, Aug. 2020, doi: 10.1016/j.conbuildmat.2020.119026.
- [84] G. Leegwater, A. Taboković, O. Baglieri, F. Hammoum, and H. Baaj, “Terms and Definitions on Crack-Healing and Restoration of Mechanical Properties in Bituminous Materials,” *RILEM Bookseries*, vol. 27, pp. 47–53, 2022, doi: 10.1007/978-3-030-46455-4_6/figures/2.

- [85] R. Roque and W. G. Buttlar, "Development of a measurement and analysis system to accurately determine asphalt concrete properties using the indirect tensile mode," *Asphalt Paving Technology: Association of Asphalt Paving Technologists-Proceedings of the Technical Sessions*, vol. 61, pp. 304–332, 1992.
- [86] R. Brewster, T. Collins, and A. M. Sandberg, "NCHRP Report 530 – Evaluation of Indirect Tensile Test (IDT) Procedures for Low-Temperature Performance of Hot Mix Asphalt," 2003.
- [87] I. Daubechies, J. Lu, and H. T. Wu, "Synchrosqueezed Wavelet Transforms: An Empirical Mode Decomposition-Like Tool," *Applied Computational Harmonic Analysis*, vol. 30, no. 2, pp. 243–261, Mar. 2011, doi: 10.1016/j.acha.2010.08.002.
- [88] S. Amani, A. Kavussi, and M. M. Karimi, "Effects of aging level on induced heating-healing properties of asphalt mixes," *Construction and Building Materials*, vol. 263, p. 120105, Dec. 2020, doi: 10.1016/j.conbuildmat.2020.120105.
- [89] C. Wang, Y. Chen, and W. Cao, "A Chemo-Rheological Approach to The Healing Characteristics of Asphalt Binders Under Short- and Long-Term Oxidative Aging," *Construction and Building Materials*, vol. 221, pp. 553–561, Oct. 2019, doi: 10.1016/J.CONBUILDMAT.2019.06.115.
- [90] H. Baaj, H. Di Benedetto, and P. Chaverot, "Effect of Binder Characteristics on Fatigue of Asphalt Pavement Using An Intrinsic Damage Approach," *Road Materials and Pavement Design*, vol. 6, no. 2, pp. 147–174, 2005, doi: 10.1080/14680629.2005.9690003.
- [91] S. Mangiafico, L. F. A. L. Babadopulos, C. Sauzéat, and H. di Benedetto, "Nonlinearity of Bituminous Mixtures," *Mechanics of Time-Dependent Materials*, vol. 22, no. 1, pp. 29–49, Feb. 2018, doi: 10.1007/s11043-017-9350-3.
- [92] H. A. Barnes, "Scopus - Document details - Thixotropy - A review," *J. Non-Newtonian Fluid Mechanics*, vol. 70, pp. 1-33, 1997.
- [93] L. Shan, Y. Tan, S. Underwood, and Y. R. Kim, "Application of Thixotropy to Analyze Fatigue and Healing Characteristics of Asphalt Binder," *Transportation Research Record: Journal of the Transportation Research Board*, vol. 2179, no. 1, pp. 85–92, Jan. 2010, doi: 10.3141/2179-10.

- [94] P. Collins, J. F. Masson, and G. Polomark, "Ordering and Steric-Hardening in SBS-Modified Bitumen," *Energy and Fuels*, vol. 20, no. 3, pp. 1266–1268, May 2006, doi: 10.1021/ef050403q.
- [95] A. Soltani and D. A. Anderson, "New test protocol to measure fatigue damage in asphalt mixtures," *Road Materials and Pavement Design*, vol. 6, no. 4, pp. 485–514, 2005, doi: 10.1080/14680629.2005.9690017.
- [96] J. C. Sontomarina, D. Fratta, and J. Wiley, "Frequency Domain Analysis of Systems," in *Discrete Signals and Inverse Problems: An Introduction for Engineers and Scientists*, Chichester: John Wiley & Sons Ltd, The Atrium, 2005, pp. 103-172
- [97] S. Dai, F. Wuttke, and J. C. Santamarina, "Coda Wave Analysis to Monitor Processes in Soils," *Journal of Geotechnical and Geoenvironmental Engineering*, vol. 139, no. 9, pp. 1504–1511, Sep. 2013, doi: 10.1061/(asce)gt.1943-5606.0000872.
- [98] M. Dinov, R. Lorenz, G. Scott, D. J. Sharp, E. D. Fagerholm, and R. Leech, "Novel Modeling of Task Vs. Rest Brain State Predictability Using A Dynamic Time Warping Spectrum: Comparisons and Contrasts with Other Standard Measures of Brain Dynamics," *Frontiers in Computational Neuroscience*, vol. 10, May 2016, doi: 10.3389/fncom.2016.00046.
- [99] H. Sakoe and S. Chiba, "Dynamic Programming Algorithm Optimization for Spoken Word Recognition," *IEEE Transaction on Acoustics, Speech, and Signal Processing*, vol. 26, no. 1, pp. 43–49, 1978, doi: 10.1109/TASSP.1978.1163055.

